DETERMINISTIC METHODS FOR MULTI-CONTROL FUEL LOADING OPTIMIZATION

by

Fariz B. Abdul Rahman

A dissertation submitted in partial fulfillment
of the requirements for the degree of
Doctor of Philosophy
(Nuclear Engineering and Radiological Sciences)
in The University of Michigan
2015

Doctoral Committee:

Professor John C. Lee, Chair
Professor Thomas J. Downar
Fausto Franceschini, Westinghouse Electric Company
Professor William R. Martin
Professor Romesh Saigal

In the name of Allah, Most Gracious, Most Merciful.

for Aliyah, to Alisha, Elias and the coming one

Your love, support and belief in me gave me strength.

for Pa and Ma

For always being there for me and being the best parents.

for Faina

For being the best sis growing up with.

for all my family relatives

For your well wishes and prayers.

and for everyone who has touched my life

I dedicate this dissertation to all of you.

ACKNOWLEDGEMENTS

First and foremost, I praise and thank Allah for all His blessings. Indeed I would not be capable of any of this if not for Him.

I would like to thank my advisor Professor John Lee for his direction, guidance and support throughout my graduate studies. I am very grateful for all your time and effort that you have so generously shared with me, and the knowledge that you have imparted on me. And thank you Theresa Lee for all your support.

I am very thankful to the dissertation committee members, including Professor Thomas Downar, Dr. Fausto Franceschini, Professor Bill Martin and Professor Romesh Saigal. You have all been very insightful with your suggestions and feedback. One could not ask for a better dissertation committee than the one I had.

I would also like to thank the staffs in the NERS department who have encouraged and supported me, most notably Peggy Gramer and Caroline Joaquin. You are both just fantastic.

Finally I would like to thank my wife Aliyah for all her support directly and indirectly in my work. You are always there for me as a source of love and encouragement, through thick and thin, and I am ever so grateful. And to my children Alisha and Elias, thanks so much for being understanding when daddy was busy and missing, and taking good care of mommy and your little brother on the way. And thank you Pa and Ma for your nurturing support and duas for the success in my education.

TABLE OF CONTENTS

LIST OF FIGURES

Figure

LIST OF TABLES

Table

ABSTRACT

Deterministic Methods for Multi-Control Fuel Loading Optimization

by

Fariz B. Abdul Rahman

Chair: John C. Lee

We have developed a multi-control fuel loading optimization code for pressurized water reactors based on deterministic methods. The objective is to flatten the fuel burnup profile, which maximizes overall energy production. The optimal control problem is formulated using the method of Lagrange multipliers and the direct adjoining approach for treatment of the inequality power peaking constraint. The optimality conditions are derived for a multi-dimensional multi-group optimal control problem via calculus of variations. Due to the Hamiltonian having a linear control, our optimal control problem is solved using the gradient method to minimize the Hamiltonian and a Newton step formulation to obtain the optimal control. We are able to satisfy the power peaking constraint during depletion with the control at beginning of cycle (BOC) by building the proper burnup path forward in time and utilizing the adjoint burnup to propagate the information back to the BOC. Our test results show that we are able to achieve our objective and satisfy the power peaking constraint during depletion using either the fissile enrichment or burnable poison as the control. Our fuel loading designs show an increase of 7.8 equivalent full power days (EFPDs) in cycle length compared with 517.4 EFPDs for the AP600 first cycle.

CHAPTER I

Introduction

1.1 Fuel Management in Light Water Reactors (LWRs)

Fuel management is a branch of nuclear engineering that seeks fuel loading designs for producing full power within adequate safety margins [1]. Various decisions on different levels are made by engineers in designing a fuel loading. In general, fuel management involves making excore and incore decisions. Described in very simple terms, excore fuel management involves decisions on what fuel assemblies are fabricated and incore fuel management decides where to put those fuel assemblies in the core.

The focus of our study will be in the area of incore fuel management, where we seek to design fuel assembly arrangements in the core that promote a flat fuel burnup profile at the end of cycle (EOC). This design provides the maximum cycle length subject to the constraint on the maximum discharge burnup. The general scheme for designing fuel assemblies in the core is usually divided into two stages: (1) placement of fresh and shuffled/burnt fuel, and (2) placement of burnable poison (BP).

Sufficient fuel needs to be added to the core to meet the cycle length requirements for operation, which is dictated by excore decisions to meet the electric grid power demand. The role of the BP is to control the excess reactivity at the beginning of cycle (BOC) and ensure a sufficiently negative moderator temperature coefficient

of reactivity. The placement of BPs in our study will only be considered at BOC, which is the case for pressurized water reactor (PWR) operations. Due to the large absorption cross sections associated with BPs, large power fluctuations could occur during the reactor operation causing power imbalance. The higher fluence in the regions of peak power will lead to an increased BP depletion. This will result in a power peak to that region later in the cycle until sufficient fuel is depleted. The power distribution will then be shifted to other regions in the core, continuing the cycle of power imbalance or fluctuations throughout the core.

Due to major concerns over safety and reliability, a strict constraint is placed on the maximum power density, which is expressed in term of the power peaking factor during the reactor operation. As a result, the goal of the engineer is to shape the power distributions throughout the core cycle and stay within the safety limits, by properly loading fresh and burnt fuel together with BPs at the BOC in an optimal manner. This represents the main objective of fuel loading optimization in our study. Other constraints that need to be considered include discharge fuel burnup limits, fuel enrichment and BP maximum limits, and the reactor power limit. Some of these constraints represent active constraints to the optimization problem, which means the objective function cannot be further improved without violating the active constraints. Existence of active constraints further complicates the optimization problem, even with the assistance of automated optimization capability.

1.2 The Fuel Loading Optimization Problem

If we consider the fuel loading optimization as a combinatorial problem where a number of x fuel assemblies are permuted in n locations in the core, the size of the decision space that needs to be considered becomes more apparent. For an inventory of 24 possible fuel assemblies (combinations of fissile enrichment and BP) that can be selected and placed in a reactor core with 145 fuel assembly locations, there would

be 24^{145} possible permutations to consider. In practice, a flat power distribution is desirable for maximizing fuel burnup within safety margins. Thus we can employ a $1/8^{\text{th}}$ symmetry fuel design, which significantly reduces the number of n fuel assembly locations in the core, bringing down the possible permutations to 24^8, or 110 billion fuel loading designs. This decision space is only indicative of a possible optimization problem and can grow exponentially if we account for more than 24 fuel assembly variations, which happens very easily when we consider various possible fuel enrichment, BP quantity and boron content in BPs. Adding another dimensionality to the problem from 2-D to 3-D will also exponentially increase the decision space.

The fuel loading optimization problem is also a highly nonlinear problem, with high-dimensionality, a large number of feasible solutions, and disconnected feasible regions in the search space [2]. Function evaluations are computationally expensive due to partial differential equations appearing over time and three dimensional space. System variables range from time-dependent variables to a combination of space- and time-dependent variables, and it is possible that system variables are a vector themselves, with each element a vector of time and/or space (like group fluxes). In addition, certain characteristics of a nuclear reactor operations complicate the optimization problem, such as control variables only appearing at the start of operations, as in the operation of PWRs. This challenge is unique to the nuclear optimization problem that is not found in other engineering field. Other attributes of the optimization problem are handling of mixed integer and continuous decision variables, multiobjective and lack of derivative information concerning objective functions and constraints in regard to decision variables [3].

1.3 LWR Optimization Methodologies

In practice, nuclear engineers still rely heavily on knowledge-based systems to select an optimal fuel loading. Based on a library of fuel loading performances that

have been used or tested in the past, the most optimal loading is selected which best satisfies the system constraint and requirement at that time. The obvious advantage of doing this is the predictability of the fuel loading performance, which can be applied to similar situations that it had been applied in the past. However this leaves a lot of room to explore for a better fuel loading, which is the goal of developing automated optimization schemes.

In the last four decades, nuclear engineers have tackled the fuel loading optimization problem with various strategies, employing mathematical models and computers to assist in traversing the vast decision space in search of optimal solutions. Over the years, automated optimization scheme has helped engineers find better fuel loading patterns and explore new loading designs, especially with the rapid improvement of computing power. The methodologies that have been applied can be divided into two main categories, one employing deterministic methods and the other employing stochastic methods. Both these methods are in use today and each have its own advantages and disadvantages.

A deterministic method obtain results from the analytical solution of a series of conditions. It can determine the input and output model of a system conclusively. Thus results can be analyzed intuitively to understand the physical behavior of the system and the optimization scheme. Simulation run times are relatively short, which makes it possible to undertake large optimization problems with high dimensionality and numerous variables. Deterministic methods tend to rely heavily on the initial guess and their solutions are highly sensitive to system perturbations, making convergence to an optimal solution challenging. A stochastic method employs a large number of simulations to randomly establish the cause and effect relationship of a system. Unlike deterministic methods, it is possible that a unique input lead to a different output, which makes the stochastic method better suited to quantify uncertainty due to varying inputs. In general, the stochastic method has very good

convergence fidelity and can be applied easily to most optimization problems without much mathematical nuances. The main drawback of this method is the large amount of computation resource that is consumed and its heavier reliance on heuristics to search for the optimal solution. With the continued growth of computing speeds reaching the realm of petaflops (10^{15} flops) now in supercomputing, stochastic methods have become the preferred method with numerous methods developed such as simulated annealing [2, 4–6], genetic algorithm [7–9], tabu search [10] and neural networks [11–14]. However the decision space still seems vast, even with the use of supercomputers and we expect it to grow larger as computational speed increases due to increasing expectations of better modelling of optimization problems, better capability of handling more variables and perhaps wanting more constraints on the optimal control problem. These are a few reasons why deterministic methods are still very relevant today.

Deterministic methods have been devised decades back since Goertzel [15] in 1956 determined analytically that it was necessary to have a flat thermal flux in the core region to obtain a minimum critical mass in a thermal reactor with a finite reflector. Goertzel used multi-group diffusion theory to derive an integral equation for the spatial variation of mass distribution of fuel material which would lead to such a flat flux. Many other papers that followed treated the optimization of fuel and burnable loading in the reactor as an optimal control problem and benefited from Pontryagin's Maximum Principle developed in 1962 for optimal control theory. In 1970, Axford [16] formulated a BOC optimal control problem with Pontragin's Maximum Principle to determine the fuel loading in a three-region slab reactor with maximum thermal power. He formulated the neccessary conditions of optimality with calculus of variation and applied a power peaking inequality constraint in the form of two equality constraints. He was able to obtain analytical results for the problem using two-group neutron diffusion equations. Goldschmidt and Quenon [17] also devised

a similar optimal control problem by finding the fuel loading with bounded controls for a two-region slab reactor model. They applied a phase-space method to find the solution to the one-group diffusion equation. A more realistic reactor model for an EOC optimal control problem was presented by Wade and Terney [18]. Using Pontryagin's Maximum Principle approach and applying the power peaking inequality constraint as a penalty function, they developed an iterative approach to consistently improve the performance of the objective function. They used a one-group spatially nodalized reactor model with the nodal material bucklings acting as the control in the problem. The objective of their optimization was to minimize the time integral of squared deviations of system states from a target distribution.

Another popular method of optimizing the reactor operation is based on minimizing the power peaking by maintaining a consistent set of EOC power distribution and the distribution of the infinite multiplication factor k_∞ with BP throughout the lifetime proposed by Haling [19] and Crowther [20]. Although the overall core reactivity is maintained with the effective multiplication factor k_{eff}=1, there is still considerable local changes in k_∞ due to loss of reactivity due to fuel burnup. This causes changes in the power shape and the power peaking factor, which can be optimized by adhering to a consistent power shape through active control. This technique is more applicable in boiling water reactors (BWRs) where control rods are actively being moved throughout the lifetime of the core. In PWR applications, Chao et al. [21] further developed the backward diffusion theory from Crowther's study for a more general loading pattern optimization. Crowther had solved the two-group, one-dimensional diffusion equation backwards to obtain the optimal axial BP for BWR based on the desired power shape. Chao extended his method by using the backward diffusion theory to obtain the desired reactivity distributions and perform a loading pattern search by matching the available fuel assemblies to the desired reactivity.

Several more recent papers have developed deterministic methods that apply Pon-

tryagin's Maximum Principle to a PWR cycle length extension problem subject to a power peaking inequality constraint. Drumm and Lee [22] used the penalty method [23] to account for the power peaking inequality constraint on a one-group one-dimensional diffusion equation problem. They found the optimal control for BP using the necessary optimality conditions together with the method of conjugate gradients [24] to minimize the Hamiltonian in the problem. Their study proved successful in extending the cycle length but ineffective in satisfying the power peaking inequality constraint throughout the reactor lifetime with the control determined at BOC.

In an attempt to apply the inequality constraint more strictly on the optimal control problem, Wu [25] and Sorenson [26] used the method of directly adjoining the inequality constraint to the Hamiltonian developed by Jacobson [27]. This method creates constrained and unconstrained regions in the core to determine the control that will simultaneously optimize the Hamiltonian and satisfy the inequality power peaking constraint. They used Pontryagin's Maximum Principle approach to arrive at the necessary optimality conditions and applied the conjugate gradient method as an iterative solution to search for the optimal control. They, however, faced difficulty handling the Lagrange multipliers resulting from the direct adjoining method and were not able to satisfy the power peaking constraint during depletion with a control at BOC. So they added other means of treating the power peaking constraint during the depletion that involved some empirical data and heuristics. As a result, they were able to control the power peaking constraint during depletion at the expense of optimizing the objective function and restricting the decision space through empirical and heuristic applications.

1.4 Statement of Objective and Thesis Organization

We have chosen a primary goal of our study to develop an improved methodology of determining the control at BOC that satisfies the power peaking factor throughout

the lifetime of the core without sacrificing the optimization of the objective function. This remains a big challenge in fuel loading design, especially using deterministic methods. We are encouraged with the results obtained using the direct adjoining method to incorporate the inequality power peaking constraint. The method guarantees the satisfaction of the inequality constraint for a steady-state problem and integrates well with the optimization problem. So one of our objectives in the study is to further develop the method of direct adjoining for a depletion problem where the control exists at BOC. Implied in this goal is to further develop our understanding of the jump conditions and the selection of constrained and unconstrained regions as a result of the direct adjoining method. These issues are non-trivial and have gained very little attention in past investigations for an optimal control problem. So we aim to provide further insights and propose new ways to address these issues.

Another main objective of this study is to organically find optimal fuel loading designs based on the necessary optimality conditions that will be derived using the method of Lagrange multipliers and calculus of variations. This is a similar approach to using Pontryagin's Maximum Principle in optimal control problems. We avoid using any heuristics or other methodologies that may interfere with the solution of the necessary optimality conditions, which allows us to achieve the most optimal solution that the optimization scheme is capable of producing. We will also employ general fuel loading designs for our initial loading selection to avoid any bias due to or from a desirable known fuel loading design. The final goal of this study is to present a multi-control fuel loading design based on the solution of our optimization methodology that is comparable in performance to published results of the AP600 first cycle loading [28]. For the purpose of benchmarking and practical use of our solution, our optimal multi-control fuel loading design is matched to the closest assembly types similarly used in the AP600, and simulated in the Westinghouse APA code package [29].

It is worth mentioning here that a large amount of effort was invested in our attempt to develop a second-order optimization method by applying Newton's method on the set of first-order optimality conditions. The aim was to use the second-order equations to iteratively approach the optimal solutions and provide a means of obtaining the control from the second-order control equation. Unfortunately the equations did not converge correctly due to the fact that it is necessary to take a control variation on the microscopic cross sections to obtain the control variable. Attempts to use the second-order control equation differently to solve other state or adjoint variables were also futile. So we had to abandon this approach and use the control optimality condition as a gradient in our current approach. We were, however, able to make use of one of the second order equations to enable us to simultaneously optimize the control and the eigenvalue of the diffusion equation. This has significantly improved the convergence of the control length iterations within the gradient method when finding the optimal controls.

In Chapter 2 we formulate our optimal control problem and derive the necessary optimality conditions using the method of Lagrange multipliers and calculus of variation for a multi-dimensional space-time dependent problem subject to an inequality constraint that is applied with the direct adjoining method. We also formulate our approach for finding the optimal control solutions and the sequence of solving the set of optimality conditions. In Chapter 3 we provide our numerical implementation of the formulations derived in Chapter 2 in our optimization code DMCO, and perform verifications on our numerical methods. We will also provide further discussion on the implementation of our iterative scheme. In Chapter 4 we present our results for four test cases to highlight the capabilities of our optimization code and produce a multi-control fuel loading design based on our original work. Finally in Chapter 5 we summarize our work and provide recommendations for future work.

CHAPTER II

Formulation of Optimal Control Problem in PWRs

The optimal control problem in PWRs is made up of four main constraints that represent the neutron transport equation, power normalization equation, fuel burnup equation, and the power peaking constraint. The neutron transport equation is approximated by the neutron diffusion equation in our study, representing a set of coupled partial differential equations in space and time. The group fluxes are normalized in the problem with the power normalization equation, which is in the form of an integral over space. The cross sections are dependent on burnup and the controls selected in fuel assemblies, which are fissile U^{235} number densities and BP number densities. The fuel burnup is calculated at the end of every time step with the burnup equation to generate a new cross section set for the next time step. The final constraint represents the maximum allowable power density of the fuel, which limits the fuel temperature from exceeding the fuel melting temperature. The power density for each fuel assembly is normalized to the core-averaged power density to represent the power peaking factor, which must stay at all times and at all assembly locations below the power peaking limit. In this chapter we formulate our optimal control problem in an approach similar to Pontryagin's Maximum Principle using the method of Lagrange multipliers and calculus of variations with a direct adjoining approach of the inequality constraint.

Pontryagin's Maximum Principle is used in optimal control theory to find the best control for a dynamic system in the presence of equality constraints. It represents a special case of the Euler-Lagrange equation from calculus of variation. For our optimal control problem, we will extend Pontryagin's Maximum Principle approach to a problem where state variables are defined in both time and space in the presence of inequality constraints in addition to equality constraints. We will re-derive our optimality conditions using the general method of Lagrange multipliers and calculus of variation, in a similar way one can take to derive the Euler-Lagrange equations in Pontryagin's Maximum Principle approach.

Equality Constraint Formulation: The method of Lagrange multipliers is a well-known method for finding the local minimum or maximum (in general extremum) of a function subject to equality constraints. It is used with calculus of variations to produce a system of equations that represent the optimality condition of the problem. It is very useful for solving problems with complex formulations and multiple constraints that does not render a closed form solution for the function being extremized. Through this approach it is possible to find the optimum solution without the need to explicitly represent the conditions and use them to eliminate extra variables. This is well-suited to handle our optimal control problem with equality constraints appearing in the form of partial differential equations mixed with an integral form of constraints. For the treatment of our inequality constraint, the Lagrange method is compatible with a few methodologies which can either incorporate the inequality constraint directly or indirectly into the problem.

Inequality Constraint Formulation: In the direct approach, the optimal trajectory is viewed as being composed of constrained regions, where the inequality constraint is active and unconstrained regions where the inequality constraint is inactive. In general, the constrained regions could represent a point or finite volume in the core, and the number and sequence of the constrained and unconstrained regions are pre-

assumed [30]. The existence of constrained and unconstrained regions introduce discontinuities in the optimality conditions at the constrained boundaries. Bryson [31] first applied the inequality constraint to Pontryagin's formulation of the optimal control problem by recognizing that the inequality constraint or one of its derivatives depend explicitly on the control variable. Later Jacobson [27] improved on Bryson's work by directly appending the inequality constraint to the optimal control problem using a generalized Kuhn-Tucker (KT) theorem formulated by Leunberger [32]. Jacobson showed that the optimal trajectory across the constrained boundaries where discontinuities occur is better represented in a consistent manner.

In the indirect approach, the optimal trajectory is viewed as a single unconstrained arc, which eliminates any discontinuities in the optimality conditions. The inequality constraint is applied to the unconstrained problem by adding a penalty function or barrier term to the problem. The popular methods using this approach include the Interior Point Method and the Barrier Method. The general approach of both methods is to convert the constrained problem into a sequence of unconstrained problems by adding a penalty term to the optimal control problem. The unconstrained problem is then successively solved by varying values of a parameter multiplying the penalty term so that the optimal trajectory stays within the feasible region of the problem.

The advantage of the indirect method over the direct method is that the constrained and unconstrained regions do not need to be predetermined and the variables do not suffer any discontinuities. However for the application to our optimal control problem where the fuel assembly boundaries represent a fixed boundary location, the direct method becomes more suitable as the constrained and unconstrained regions can be defined within the boundaries of fuel assemblies. Furthermore, the power peaking constraint is strictly applied in the direct adjoining method and any sub-optimal results could potentially be used as a solution.

The direct adjoining method suggests that the inequality constraint is satisfied by

the selection of the control variable in the constrained region. This is accomplished by calculating the control in this region directly from the inequality constraint equation. The control for the unconstrained region is determined from the control optimality condition obtained via the calculus of variation, which serves the purpose of optimizing the problem. This dual process of selecting the control in the constrained and unconstrained regions separately assures that we are able to satisfy the inequality constraint together with the optimization of the problem simultaneously.

A Linear Control in Hamiltonian: A special class of our optimal control problem in PWRs is that the control variable appears linearly in the Hamiltonian. This follows from the selection of the possible controls representing either the macroscopic cross sections or number densities of U^{235} or BP, which appears linearly in all the constraint equations. The consequence of this is the first-order variation of the Hamiltonian with respect to the control variable in the unconstrained region will result in the control variable dropping out of the equation. We are left with the control optimality condition without a control variable in it, which makes it infeasible to explicitly determine the control variable from the equation. In the constrained region, the problem is slightly different as only the control for BP is not present in the inequality constraint. So we examine the strategy for finding the control in the unconstrained and constrained region separately.

Control formulation in the unconstrained region: A significant amount of effort was put into applying the control optimality condition differently to solve the system of equations from the necessary optimality conditions. Attempts were made to use the control equation to solve for other state variables or adjoint variables instead of the control variable, which requires the use of other equations in the system representation to solve for the other unknown variables. Unfortunately our study concluded that the type of system of equations that make up our optimality condition does not provide a meaningful solution when used in the unconventional way. The

conventional method of solving the system of equations is to use the adjoint equation to solve for the adjoint variables, the constraint equations to solve for the state variables and the control equation to solve for the control variable. To circumvent the problem of the missing control variable in the control equation, there are two known approaches that have been applied in the past. The control equation could be used as a switching function to determine the bang-bang control that will minimize the Hamiltonian. Alternatively, the control equation could be used as a gradient to minimize the Hamiltonian.

The bang-bang control method is applicable to optimal control problems with a linear control in the Hamiltonian. The control equation which is devoid of the control variable is used as a switching function to determine the extreme value of the control. If the switching function assumes a negative value, then the maximum allowable value of the control is selected. Likewise if the switching function is positive, the minimum control is selected.

To use the control equation as a gradient to find the control, we apply a necessary condition of Pontryagin's Maximum Principle which states that the Hamiltonian H must be minimized over the set of all permissible control u such that:

$$H[x^*(t), u^*(t), \lambda^*(t), t] \leq H[x^*(t), u, \lambda^*(t), t], \tag{2.1}$$

where $x^*(t)$, $u^*(t)$, and $\lambda^*(t)$ represent the optimal solution for the state variable, control variable and the adjoint variable, respectively. Therefore, at the stationary point of the state and adjoint variables, the optimal control will yield the minimum value of the Hamiltonian compared to other control values. So we could use the gradient dH/du to find the control that minimizes the Hamiltonian at the stationary point of the state and adjoint variables.

Our study shows that application of the bang-bang method to determine the

control is effective for an analytical problem. However, when applied to an iterative numerical approach, the optimal control problem faces convergence issues. This can be attributed to a large change in control from iteration to iteration due to the selection method of bang-bang control that chooses either the upper or lower limit of control. Therefore the approach of using the control equation as a gradient to minimize the Hamiltonian is better suited for our numerical approach, which shows better convergence.

Control formulation in the constrained region: It is possible to obtain the control from the inequality constraint by taking the spatial variation of the inequality constraint until the control emerges [25, 26, 31]. Since the inequality constraint equation which is active in space must vanish in the constrained region, it follows that the spatial derivatives of the inequality constraint equation must also vanish. When this method is applied to our optimal control problem where the diffusion equation constraint is an eigenvalue equation with second-order partial derivatives, the control would emerge after taking two spatial derivatives of the inequality constraint. The resulting condition for determining the control in the constrained region is equivalent to the requirement of flat flux. This method is effective for finding the control if the optimal solution of the eigenvalue of the problem is known. This is possible in an analytical problem, but not effective in an iterative approach where the optimal solution of the eigenvalue is unknown.

Therefore, we provide in our study a novel way of using Newton's method to provide a path to determine the control in the constrained region together with the optimal eigenvalue solution of the diffusion equation simultaneously. The basic idea involves taking a Newton step on the diffusion equation and the inequality constraint equation, which provides two equations to solve for the optimal control and the optimal eigenvalue together. This will allow the eigenvalue to vary and enable our optimization scheme to optimize the eigenvalue solution iteratively if it is selected as

an objective to our optimal control problem. The reader is referred to Appendix A for a quick overview of Newton's method and how it is applied in our study.

In this chapter, the necessary optimality conditions for the optimal control problem in PWRs will be formulated with the method of Lagrange multipliers and the direct method of adjoining the inequality constraint. We will build an iterative scheme by using the control optimality condition as a gradient to find the control in the unconstrained region and by applying Newton's method to obtain the control in the constrained region. We will begin with a general formulation for an arbitrary optimization problem to present the basic ideas of our methodology, and then later apply the formulation to our PWR optimal control problem for a steady-state or BOC problem, followed by the full depletion problem.

2.1 Method of Lagrange Multipliers

An optimization problem typically consists of an objective function, equality and inequality constraints, and boundary conditions. For our general notational purposes, we define the objective function J as a function of the state variables x and control variables u:

$$J(x, u) = f[x(r, t), u(r, t)]. \tag{2.2}$$

Note that, in general, the vector variable x and scalar variable u are functions of the spatial variable r and time t. For notational convenience, the spatial and temporal variables will be suppressed here onwards except where necessary. Vector and matrix representations will also be suppressed consistent with recent literature in control theory. Instead we will mention explicitly when introducing a variable if it is a vector or matrix. The equality constraints g and inequality constraints S are also defined as functions of the state variables x and control variables u, subject to constraint c:

$$g(x, u) = c, \tag{2.3}$$

$$S(x, u) \leq 0. \tag{2.4}$$

To incorporate the objective function together with the equality and inequality constraint in an optimization problem, the augmented objective function H is formulated by appending the constraint equations with Lagrange multipliers λ and η to the objective function:

$$H(x, u, \lambda, \eta) = J(x, u) + \lambda^T h(x, u) + \eta^T S, \tag{2.5}$$
$$\text{with} \quad h(x, u) \equiv g(x, u) - c.$$

Since the Lagrange multipliers could be vectors, we have added the transpose notations. Thus, the objective of our optimization task is to minimize the Hamiltonian H.

Finding the extrema to Eq. (2.5) via calculus of variation will yield the optimal solution that minimizes the objective function subject to the constraints. This means that if $J(x_0, u_0)$ is a minimum of $J(x, u)$ for the original constrained problem, then there exists λ_0 and η_0 such that (x_0,u_0,λ_0,η_0) is a stationary point, where the partial derivatives of H are zero. However, not all stationary points yield a solution to the original problem. Hence the method of Lagrange multipliers yields the necessary condition for optimality to the constrained problem.

When constructing the augmented objective function in Eq. (2.5), we applied the direct adjoining method and appended the inequality constraint directly to the equation with Lagrange multipliers, in a similar fashion as the equality constraints. Because the nature of equality and inequality constraints are different, it is only

possible to do this with an additional constraint placed on the Lagrange multiplier of the inequality constraint:

$$\begin{aligned} \eta(r) = 0 \quad &\text{when} \quad S < 0 \\ \geq 0 \quad &\text{when} \quad S = 0 \end{aligned} \tag{2.6}$$

This condition is known as the Karush-Kuhn-Tucker (KKT) condition where η is some non-negative scalar. By the conditions in Eq. (2.6), we are assured that the product $\eta^T S$ will not add unwanted contributions to the augmented objective function in Eq. (2.5), thereby satisfying the concept of the augmented functional. Jacobson [27] proved this condition by use of a generalized Kuhn-Tucker (KT) theorem.

2.2 Optimality Conditions using Calculus of Variations

Next to solve the optimal control problem, we use calculus of variations to arrive at the necessary optimality conditions by taking the partial derivative of Eq. (2.5) with respect to all the variables and setting them to zero. This is akin to finding the extrema of a function by finding the gradient of the function and setting it to zero. The solution would yield either the maximum or minimum point of that function. The difference here is that we are extremizing functionals in Eq. (2.5), which are mappings from a set of functions to real numbers, rather than just functions. The necessary optimality conditions are written in the system of equations below:

$$\frac{\partial H}{\partial x} = \frac{\partial J}{\partial x} + \lambda^T \frac{\partial h}{\partial x} + \eta^T \frac{\partial S}{\partial x} = 0 \tag{2.7a}$$

$$\frac{\partial H}{\partial u} = \frac{\partial J}{\partial u} + \lambda^T \frac{\partial h}{\partial u} + \eta^T \frac{\partial S}{\partial x} = 0 \tag{2.7b}$$

$$\frac{\partial H}{\partial \lambda} = h = 0 \tag{2.7c}$$

$$\frac{\partial H}{\partial \eta} = S = 0. \tag{2.7d}$$

Equation (2.7a) is the adjoint equation and is used to find the values of the Lagrange multipliers. This is why the Lagrange multipliers are sometimes referred to as the adjoint variables. It suffices to say here that some of the Lagrange multipliers suffer a discontinuity due to the non-negative nature of the Lagrange multiplier η as defined in Eq. (2.6). This jump term will be derived explicitly in Section 2.4.2 when we formulate our actual optimal control problem. Equation (2.7b) is the control optimality condition that yields the value of the control variable. Equations (2.7c) and (2.7d) represent the equality and inequality constraints that need to be satisfied in the problem, yielding the values of the state variables.

The role of the Lagrange multipliers can be understood in a different light by examining the adjoint equation (2.7a) at the optimal point. Dropping the inequality constraint term to simplify our explanation without any loss of generality, we see that we are trying to equate the gradients of J and h by a multiplier λ at the optimal solution of x and u.

$$\nabla J(x^{opt}, u^{opt}) = -\lambda^T \nabla h(x^{opt}, u^{opt}) \tag{2.8}$$

In our multi-variable problem, the gradients of J and h are each a normal vector to a curve in two dimensions. The magnitude of the normal vector is not important since any multiple of the gradient is also a normal vector and will satisfy Eq. (2.8). So the unknown constant Lagrange multiplier λ is necessary because the magnitude of the two gradients may be different and it facilitates the solution for the optimal point.

2.3 Objective Functions

Before we begin the formulation of our optimal control problems, we define the type of objective functions we intend to use for our study. In the steady-state problem, we select the objective to maximize the reactivity in the core which is best represented

by maximizing the effective multiplication factor k:

$$J_1 = -k. \tag{2.9}$$

The negative sign is needed to turn our minimization problem into a maximization problem. This objective is in line with our overall objective to extend the cycle length of the reactor.

For the depletion problem, we select the objective for a flat burnup profile at the EOC which reflects the overall objective of our study to achieve a maximum discharge fuel burnup:

$$J_2 = \int_V dr \left[E(r,\tau) - \overline{E}(\tau)\right]^2, \tag{2.10}$$

where $\overline{E}(\tau)$ is the average fuel burnup in the core at EOC, $t = \tau$:

$$\overline{E}(\tau) = \frac{1}{V}\int_V drE(r,\tau). \tag{2.11}$$

2.4 Formulation of the Steady-State Optimal Control Problem

We will begin with the formulation for the steady-state optimal control problem in PWRs by considering the problem in two-dimensional space. The purpose of not considering time variation in the optimal control problem for now is to provide the derivation of the optimality conditions in the most succinct manner given the complexity in some of our equations. In this manner, we will also be able to show the explicit equations and methodology that are used to optimize the steady-state problem in Chapter 4. In the following section, we will then provide the formulation for a time-dependent optimal control problem.

Before continuing to formulate the optimal control problem by the method of

Table 2.1: Description of variables

State Variable	**Description**
$\phi(x, y, t)$	Group flux
$k(t)$	Multiplication factor
$Q(x, y, t)$	Power density
$E(x, y, t)$	Fuel burnup
Control Variable	**Description**
$u(x, y)$	Cross section or number density
Adjoint Variable	**Description**
$\phi^+(x, y, t)$	Adjoint group flux
$Q^+(t)$	Adjoint power density
$E^+(x, y, t)$	Adjoint burnup
$\eta^+(x, y, t)$	Adjoint peaking factor
Variable Functions	**Description**
$D(u, E)$	Diffusion coefficient
$\Sigma_a(u, E)$	Absorption cross section
$\Sigma_r(u, E)$	Removal cross section
$\nu\Sigma_f(u, E)$	Nu fission cross section
$\kappa\Sigma_f(u, E)$	Kappa fission cross section

Lagrange multipliers, we introduce all the variables that will be used in our study in Table 2.1 so that the reader can follow the derivation, especially during the process of taking partial derivatives with respect to the state and control variables. For our two-group formulation, only the variables ϕ and ϕ^+ in Table 2.1 are vectors. The control variable u is a scalar representing one of the two possible control option in our study, which is either the fissile U^{235} number density or the BP number density.

During our formulation of the steady-state problem, we will not show the time variable for notational convenience. Here onwards, we will use the variable x as a space variable in our two-dimensional notations and will no longer refer to x as we did in Section 2.1 as a state variable. Instead we will use explicit representation of all state variables in customary notations that is used in nuclear reactor terminologies.

The form of the objective function that we employ in the steady-state optimal

control problem is simply the effective multiplication factor k from Eq. (2.9):

$$J_1 = -k. \tag{2.12}$$

The first equality constraint represents the neutron diffusion equation in two energy-group form:

$$\begin{pmatrix} -\nabla \cdot D_1 \nabla + \Sigma_{\mathrm{a1}} + \Sigma_r & 0 \\ -\Sigma_r & -\nabla \cdot D_2 \nabla + \Sigma_{\mathrm{a2}} \end{pmatrix} \begin{pmatrix} \phi_1 \\ \phi_2 \end{pmatrix} = \frac{1}{k} \begin{pmatrix} \nu\Sigma_{\mathrm{f1}} & \nu\Sigma_{\mathrm{f2}} \\ 0 & 0 \end{pmatrix} \begin{pmatrix} \phi_1 \\ \phi_2 \end{pmatrix}. \tag{2.13}$$

For the purpose of presenting the equations in succinct form, Eq. (2.13) is re-written in simpler operator form by combining the loss and production matrices into a single matrix operator L:

$$L\phi = \begin{pmatrix} \nabla \cdot D_1 \nabla - \Sigma_{\mathrm{a1}} - \Sigma_r + \frac{\nu\Sigma_{f1}}{k} & \frac{\nu\Sigma_{f2}}{k} \\ \Sigma_r & \nabla \cdot D_2 \nabla - \Sigma_{\mathrm{a2}} \end{pmatrix} \begin{pmatrix} \phi_1 \\ \phi_2 \end{pmatrix} = 0. \tag{2.14}$$

The operator L represents a matrix operating on the flux vector ϕ containing the state variable k and variable functions dependent on the control u and burnup E. Also keep in mind that the operator L contains second order differential operators when we later take the first order variation to find the optimality conditions. The formulation using operator form will also be useful for representing the neutron diffusion equations in one or two energy group form.

The second equality constraint in our optimal control problem is the normalization condition for power density $p(x, y)$, which determines the magnitude of the flux in the reactor:

$$Q(X^{'},Y^{'}) = \int_0^{X'}\int_0^{Y'} dx\,dy\,p(x,y) = \int_0^{X'}\int_0^{Y'} dx\,dy\,(\kappa\Sigma_{\mathrm{f1}}\phi_1 + \kappa\Sigma_{\mathrm{f2}}\phi_2), \tag{2.15}$$

where Q is the state variable that represents the power within regions of $(0, X')$ and $(0, Y')$. Thus the total power P_{tot} in a reactor of dimensions X and Y is represented by the boundary condition:

$$Q(X,Y) = P_{tot}. \tag{2.16}$$

Converting the power normalization equation to a partial differential form and representing the variables in vector form

$$\kappa\Sigma_f\phi \equiv \begin{pmatrix} \kappa\Sigma_{f1} & \kappa\Sigma_{f2} \end{pmatrix} \begin{pmatrix} \phi_1 \\ \phi_2 \end{pmatrix}, \tag{2.17}$$

we simplify Eq. (2.15) to:

$$\kappa\Sigma_f\phi(x,y) - \frac{\partial^2 Q(x,y)}{\partial x \partial y} = 0. \tag{2.18}$$

Finally our inequality constraint represents the power peaking constraint in the reactor core and is represented as:

$$S(x,y) \equiv \frac{\kappa\Sigma_f\phi(x,y)}{p_{\mathrm{ave}}} - p_{\max} \leq 0, \tag{2.19}$$

where p_{ave} is the average power density in the core and p_{max} is the desired power peaking factor limit in the core.

We are now ready to combine our objective function and constraints in the aug-

mented objective function by the method of Lagrange multipliers:

$$H = -k + \int_X \int_Y dx\, dy \left[{\phi^+}^T L\phi + Q^+ \left(\kappa \Sigma_f \phi - \frac{\partial^2 Q}{\partial x \partial y} \right) + \eta^+ S \right], \tag{2.20}$$

where we have added transpose notation for the adjoint flux ϕ^+ because it is a vector.

We use the function H to represent our augmented objective function which is also the Hamiltonian of our optimal control problem, analogous to the Hamiltonian defined in Pontryagin's Maximum Principle formulation. The KKT condition for adjoining the inequality constraint to the augmented objective function now states that $\langle \eta^+, S \rangle = 0$ is a sufficient condition. The inner product bracket here represents the integral over space. Similarly as before, we arrive at the boundary condition for the Lagrange multiplier for the inequality constraint as:

$$\begin{aligned} \eta^+(x,y) = 0 \quad &\text{when} \quad S(x,y) < 0 \\ \geq 0 \quad &\text{when} \quad S(x,y) = 0. \end{aligned} \tag{2.21}$$

Using the augmented objective function H in Eq. (2.20), we proceed to find the optimality conditions which represent the first order variation with respect to the state and control variables via calculus of variation. We begin by taking the variation on all the state and control variables only, as taking the variation of the adjoint variables will only yield back our original constraint equation. This is evident in our general formulation from equations (2.7c) and (2.7d):

$$\delta H = -\delta k + \int_X \int_Y dxdy \left\{ {\phi^+}^T \delta \left(L\phi \right) + Q^+ \left[\delta \left(\kappa \Sigma_f \phi \right) - \frac{\partial^2 \delta Q}{\partial x \partial y} \right] + \eta^+ \delta S \right\}. \tag{2.22}$$

Next we expand the inequality constraint S and distribute the variation in $L\phi$:

$$\delta H = -\delta k + \int_X \int_Y dxdy \left\{ \phi^{+T} \left[\delta L\phi + L\delta\phi \right] + Q^+ \left[\delta \left(\kappa \Sigma_f \phi \right) - \frac{\partial^2 \delta Q}{\partial x \partial y} \right] + \eta^+ \frac{\delta \left(\kappa \Sigma_f \phi \right)}{p_{ave}} \right\} \tag{2.23}$$

Collecting the terms that have the same multipliers $\delta(\kappa\Sigma_f\phi)$, we get:

$$\delta H = -\delta k + \int_X \int_Y dxdy \left\{ \phi^{+T} L\delta\phi + \phi^{+T} \delta L\phi + \left(Q^+ + \frac{\eta^+}{p_{ave}} \right) \delta \left(\kappa \Sigma_f \phi \right) - Q^+ \frac{\partial^2 \delta Q}{\partial x \partial y} \right\}. \tag{2.24}$$

This equation can be further simplified if we use integration by parts on the derivative terms that involve variations on $\delta\phi$ and δQ and invoke the definition of adjoint operators:

$$\int_X \int_Y dxdy \ \phi^{+T} L\delta\phi = \int_X \int_Y dxdy \ \left(L^+ \phi^+ \right)^T \ \delta\phi \tag{2.25}$$

$$\int_X \int_Y dxdy \ Q^+ \frac{\partial^2 \delta Q}{\partial x \partial y} = \int_X \int_Y dxdy \ \frac{\partial^2 Q^+}{\partial x \partial y} \ \delta Q, \tag{2.26}$$

where the perturbations $\delta\phi$ and δQ at the limits are zero since they are fixed by boundary conditions. By applying equations (2.25) and (2.26) to the augmented objective function and selecting an objective function J that is a function of state variable k only, which is the case for our steady-state objective function, we get:

$$\begin{aligned} &\delta H = \\ &-\delta k + \int_X \int_Y dxdy \left\{ \left(L^+ \phi^+ \right)^T \delta\phi + \phi^{+T} \delta L\phi + \left(Q^+ + \frac{\eta^+}{p_{ave}} \right) \delta \left(\kappa \Sigma_f \phi \right) - \frac{\partial^2 Q^+}{\partial x \partial y} \delta Q \right\} \end{aligned} \tag{2.27}$$

where

$$\delta L = \frac{\partial L}{\partial k} \delta k + \frac{\partial L}{\partial u} \delta u$$

$$\delta \left(\kappa \Sigma_f \phi \right) = \frac{\partial \kappa \Sigma_f}{\partial u} \delta u \phi + \kappa \Sigma_f \delta \phi.$$

Next we collect the variation terms that are alike. The objective function has been brought into the volume integral to collect the δk term. We are able to factor out the δu variable by virtue that it is a scalar variable. We arrive at the following final form of the augmented objective function:

$$\delta H = \int_X \int_Y dxdy \left\{ \begin{array}{l} \left[(L^+\phi^+)^T + \left(Q^+ + \frac{\eta^+}{p_{ave}} \right) \kappa\Sigma_f \right] \delta\phi + \left[\phi^{+T} \frac{\partial L}{\partial k}\phi - \frac{1}{V} \right] \delta k \\ -\frac{\partial^2 Q^+}{\partial x \partial y}\delta Q + \left[\phi^{+T} \frac{\partial L}{\partial u}\phi + \left(Q^+ + \frac{\eta^+}{p_{ave}} \right) \frac{\partial \kappa\Sigma_f}{\partial u}\phi \right] \delta u \end{array} \right\} = 0. \tag{2.28}$$

With the first order variation of the augmented objective function H reduced to the form in Eq. (2.28), the Lagrange multipliers can now be determined to satisfy δH=0. This is accomplished by choosing the Lagrange multipliers ϕ^+, Q^+, and η^+ such that the integrals involving $\delta\phi$, δu, δQ, and δk vanish.

2.4.1 First Order Optimality Conditions for Steady-State Problem

The first integral in Eq. (2.28) represents the adjoint equation that determines the value of the Lagrange multipliers by forcing the integrals involving $\delta\phi$ to vanish:

$$\int_X \int_Y dxdy \left[\left(L^+\phi^+ \right)^T + \left(Q^+ + \frac{\eta^+}{p_{\text{ave}}} \right) \kappa\Sigma_f \right] \delta\phi = 0. \tag{2.29}$$

Since $\delta\phi$ is dependent on space variables, we require the integrand attached to $\delta\phi$ to vanish as the sufficient condition for Eq. (2.29):

$$\left(L^+\phi^+ \right)^T + \left(Q^+ + \frac{\eta^+}{p_{\text{ave}}} \right) \kappa\Sigma_f = 0. \tag{2.30}$$

The adjoint equation in (2.30) is known as the Euler-Lagrange equation in Pontryagin's Maximum Principle approach which takes the form of an inhomogeneous adjoint equation. It is very similar to the homogenous equation form of the neutron diffusion equation with adjoint operators and the addition of a source term, which refers to the

terms that does not include ϕ^+. We see this more clearly by re-arranging Eq. (2.30) and defining a representative variable S^+ for the source terms:

$$\left(L^+\phi^+\right)^T = -\left(Q^+ + \frac{\eta^+}{p_{\text{ave}}}\right)\kappa\Sigma_f \equiv S^+. \tag{2.31}$$

This type of equation has an additional requirement for finding the solution to ϕ^+. It is an orthogonality condition [33, 34] also known as the Fredholm Alternative, which states that the adjoint source S^+ must be orthogonal to the homogenous flux solution:

$$\left\langle \phi, S^+ \right\rangle = 0 \tag{2.32}$$

where the homogeneous flux ϕ comes from the solution of Eq. (2.14):

$$L\phi = 0. \tag{2.33}$$

The next optimality condition requires the integral involving δQ to vanish:

$$-\int_X \int_Y dxdy \; \frac{\partial^2 Q^+}{\partial x \partial y}\delta Q = 0. \tag{2.34}$$

Since δQ is space-dependent, a sufficient condition for this equation is to set the integrand attached to δQ term to zero.

$$\frac{\partial^2 Q^+(x,y)}{\partial x \partial y} = 0. \tag{2.35}$$

This optimality condition only describes that the Lagrange multiplier Q^+ is constant in space and does not yield a full solution for Q^+. The next optimality condition involving δk takes a different form because δk is not space-dependent. Therefore it sits outside the space integral and the stationary condition for δk is obtained by setting the spatial integral to zero:

$$\left[\int_X \int_Y dxdy \left(\phi^{+T} \frac{\partial L}{\partial k}\phi - \frac{1}{V}\right)\right] \delta k = 0 \tag{2.36}$$

$$\Rightarrow \int_X \int_Y dxdy \left(\phi^{+T} \frac{\partial L}{\partial k}\phi\right) = \frac{1}{V}. \tag{2.37}$$

Because Eq. (2.37) is subject to an integral over space, it is used as a normalization condition to find the magnitude of ϕ^+. Note that it has a term $1/V$ that came from the objective function k. The final optimality condition represents the control optimality condition for the integral involving δu:

$$\int_X \int_Y dxdy \left[\phi^{+T} \frac{\partial L}{\partial u}\phi + \left(Q^+ + \frac{\eta^+}{p_{\text{ave}}}\right) \frac{\partial \kappa \Sigma_f}{\partial u}\phi\right] \delta u = 0. \tag{2.38}$$

Since the control variable is a function of space, a sufficient condition is to set the integrand attached to δu to zero:

$$\phi^{+T} \frac{\partial L}{\partial u}\phi + \left(Q^+ + \frac{\eta^+}{p_{\text{ave}}}\right) \frac{\partial \kappa \Sigma_f}{\partial u}\phi = 0. \tag{2.39}$$

2.4.2 Jump Conditions

As a result of the method of direct adjoining the inequality constraint, junctions will exist between the boundary of a constrained and unconstrained region that may cause Lagrange multipliers to be discontinuous due to the non-negativity property of η^+ defined in Eq. (2.21). Since the inequality constraint S is active only in space, we would also expect the discontinuity to occur in the spatial Lagrange multipliers, in particular, the Lagrange multipliers that are adjoint to the state variable ϕ from the inequality constraint. The handling of the jump condition here would apply the same way for a time-dependent problem since the jump does not occur over the time variable.

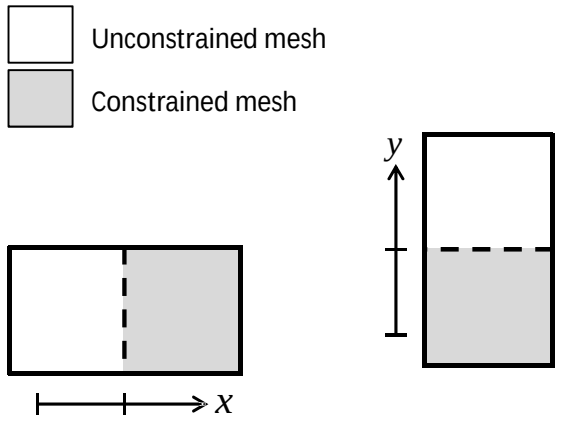

Figure 2.1: Two possible orientation of the junction

Even though our formulation of the control problem is in two dimensions, the jump condition can only be evaluated in one dimension because the junction is essentially an infinitesimal line between an unconstrained and constrained region. We refer to Figure 2.1 and examine two possible cases in our two-dimensional problem. If the junction occurs between two meshes located side by side, the jump exists in the x-axis. Likewise if the junction occurs between two meshes one on top of the other, then the jump exists in the y-axis.

We begin by integrating the Euler-Lagrange equation (2.31) over a junction boundary in the x-axis because we are expecting a discontinuity in a Lagrange multiplier. Since the adjoint flux is physically a continuous function, we expect the discontinuity to appear in the leakage term that has a second order derivative of the adjoint flux. We will also expect a discontinuity in η^+ due to the KKT conditon. Other terms that are continuous will drop out of the integral over the junction boundary x_i:

$$-\int_{x_i^-}^{x_i^+} dx \left(\nabla \cdot D\nabla\phi^+\right) = \int_{x_i^-}^{x_i^+} dx \frac{\eta^+}{p_{ave}} \kappa\Sigma_f. \tag{2.40}$$

Expressing η^+ in terms of a temporary variable η^*:

$$\eta^+ = \frac{d\eta^*}{dx} \tag{2.41}$$

where η^* is a nondecreasing function that assures η^+ is always non-negative to satisfy the KKT condition, Eq. (2.40) becomes:

$$-\int_{x_i^-}^{x_i^+} dx \left(\nabla \cdot D\nabla\phi^+\right) = \int_{x_i^-}^{x_i^+} dx \frac{d\eta^*}{dx} \frac{\kappa\Sigma_f}{p_{ave}}. \tag{2.42}$$

Then we can simply perform the integration and obtain:

$$-\left[D\nabla\phi^+(x_i^+) - D\nabla\phi^+(x_i^-)\right] = \frac{\eta^*(x_i^+) - \eta^*(x_i^-)}{p_{ave}} \kappa\Sigma_f. \tag{2.43}$$

By defining the jump parameter as

$$\mu(x_i) \equiv \eta^*(x_i^+) - \eta^*(x_i^-) \geq 0, \tag{2.44}$$

we obtain the jump condition that will appear in the Euler-Lagrange equation in the derivative of the adjoint flux, which is simply the adjoint current J^+:

$$\left[J^+(x_i^+) - J^+(x_i^-)\right] = \frac{\mu(x_i)}{p_{ave}} \kappa\Sigma_f \tag{2.45}$$

where

$$J^+ = -D\nabla\phi^+. \tag{2.46}$$

The jump parameter μ is non-negative in Eq. (2.45) because η^* was defined as a nondecreasing function in Eq. (2.41).

2.4.3 Control Formulation

By the method of directly adjoining the inequality constraint to the Hamiltonian, we have constrained and unconstrained regions that require different formulations of the control. In the unconstrained region, the control will be determined from the control optimality condition of Eq. (2.39). Due to a special case of our optimal control problem that has a linear control in the Hamiltonian, the control variable does not appear in Eq. (2.39). Hence, this does not allow us to find an explicit solution of the control from this equation that will satisfy the optimality condition. Instead we use the gradient method of Drumm and Lee [22] and Eq. (2.39) as a gradient $\partial H/\partial u$ to obtain a search direction. This is accomplished by first computing the gradient based on the initial control u_i:

$$q = \frac{\partial H(u_i)}{\partial u} = \phi^{+T}\frac{\partial L}{\partial u}\phi + \left(Q^{+} + \frac{\eta^{+}}{p_{ave}}\right)\frac{\partial \kappa \Sigma_f}{\partial u}\phi \tag{2.47}$$

and choosing the search direction to be the negative gradient direction:

$$s = -q. \tag{2.48}$$

Then an optimal control length ϵ^* is chosen such that the Hamiltonian is minimized:

$$min\ H(u_i + \epsilon s) = H(u_i + \epsilon^* s) \tag{2.49}$$

through an iterative bi-sectional scheme that tests different values of control length ϵ, yielding the optimal control u^* in the unconstrained region as:

$$u^* = u_i + \epsilon^* s. \tag{2.50}$$

For control formulation in the constrained region, the control must be obtained

from the inequality constraint equation S that is active in that region. This requires the inequality constraint S of Eq. (2.19) to vanish on the constrained region:

$$S(x,y) = \frac{\kappa\Sigma_f\phi(x,y)}{p_{ave}} - p_{\max} = 0. \tag{2.51}$$

Since the function S which is active in space must vanish in the constrained region, it follows that the spatial derivatives of S must also vanish:

$$\nabla^i S = 0 \tag{2.52}$$

where i represents the i^{th} spatial derivative. So we look for the first spatial derivative of S in which the control emerges to extract the control in the constrained region [31]. This condition assures that the power peaking constraint is always met and yields a flat power distribution p_{max} in the constrained regions. Taking the first derivative of S yields:

$$\nabla S = \kappa\Sigma_f\nabla\phi = 0 \tag{2.53}$$

which does not yield the control. So we take another spatial derivative of S to get:

$$\nabla\cdot\nabla S = \kappa\Sigma_f\nabla\cdot\nabla\phi = 0 \tag{2.54}$$

and continue to expand the vectors $\kappa\Sigma_f$ and ϕ to obtain an explicit representation of the control in the two-group notation:

$$\nabla\cdot\nabla S = \kappa\Sigma_{f1}\frac{\left(\Sigma_{a1}+\Sigma_r-\nu\Sigma_{f1}/k\right)\phi_1 - \nu\Sigma_{f2}\phi_2/k}{D_1} + \kappa\Sigma_{f2}\frac{\Sigma_{a2}\phi_2-\Sigma_r\phi_1}{D_2} = 0. \tag{2.55}$$

To simplify Eq. (2.55), we obtain the flux ratio of ϕ_1/ϕ_2 from the thermal diffusion equation by making an approximation that the thermal leakage term is negligible

compared to Σ_{a2}:

$$\left(-\nabla \cdot D_2 \nabla + \Sigma_{a2}\right) \phi_2 \approx \Sigma_{a2}\phi_2 = \Sigma_r \phi_1 \tag{2.56a}$$

$$\Rightarrow \frac{\phi_1}{\phi_2} \approx \frac{\Sigma_{a2}}{\Sigma_r}. \tag{2.56b}$$

Then we are left with a simplified expression of the second spatial derivative of the inequality constraint as:

$$\nabla^2 S = \left(\Sigma_{a1} + \Sigma_r - \frac{\nu\Sigma_{f1}}{k}\right)\frac{\Sigma_{a2}}{\Sigma_r} - \frac{\nu\Sigma_{f2}}{k} = 0. \tag{2.57}$$

Equation (2.57) provides an explicit representation of the control variables contained in the cross sections Σ_f and Σ_a for both energy groups, and we see that it is dependent on the eigenvalue k. Since we have ignored the leakage terms to arrive at Eq. (2.57), the eigenvalue k is simply the infinite multiplication factor k_∞. This is equivalent to the flat flux condition which is the result of a flat power distribution p_{max} in the constrained region. Due to the nature of eigenvalue equations that derive the eigenvector and eigenvalue simultaneously in the solution, we are not able to obtain an optimal solution of the control variable in Eq. (2.57) without knowing the optimal solution of the eigenvalue beforehand. To address this problem, we seek two equations to solve for the two unknowns u and k in terms of the incremental values δu and δk that we obtain by using Newton's method. In part 1, we perform a Newton step on the diffusion equation from Eq. (2.14) and apply the Fredholm Alternative to obtain δk in terms of δu. In part 2, we perform a Newton step on the second spatial derivative of the inequality constraint equation (2.57) to obtain another equation in terms of δk and δu. Then the two equations are combined to find the solutions to δu in the constrained region and δk.

Part 1: Newton step on $L\phi = 0$. By taking a Newton step on the diffusion equa-

tion (2.14), we get:

$$L\delta\phi = -\delta L\phi = \frac{\nu\Sigma_f}{k^2}\phi\delta k - \frac{\partial L}{\partial u}\phi\delta u \tag{2.58}$$

where the residual of the diffusion equation in this Newton step is zero since we solve the diffusion equation exactly. Since this equation has an inhomogeneous source term, it must satisfy the Fredholm alternative condition, which states:

$$\left\langle \phi_h^+, \frac{\nu\Sigma_f}{k^2}\phi\delta k - \frac{\partial L}{\partial u}\phi\delta u \right\rangle = 0 \tag{2.59}$$

where the homogeneous adjoint flux ϕ_h^+ comes from the solution of:

$$L^+\phi_h^+ = 0. \tag{2.60}$$

Since the integral in Eq. (2.59) is summed over all regions, we need to separate it into integrals over constrained regions Γ and unconstrained regions $\overline{\Gamma}$ so that we can find an explicit representation of the control in the constrained region. The control in the unconstrained region $\delta u^{\overline{\Gamma}}$ is already known at this point because it can be determined beforehand using the gradient method. So from Eq. (2.59) we have:

$$\delta k \left\langle \phi_h^+, \frac{\nu\Sigma_f}{k^2}\phi \right\rangle - \left\langle \phi_h^+, \frac{\partial L}{\partial u}\phi\delta u^{\Gamma} \right\rangle_{\Gamma} - \left\langle \phi_h^+, \frac{\partial L}{\partial u}\phi\delta u^{\overline{\Gamma}} \right\rangle_{\overline{\Gamma}} = 0. \tag{2.61}$$

Then we arrive at the first equation relating the unknowns δu^{Γ} and δk by:

$$I_1\delta k = \left\langle \phi_h^+, \frac{\partial L}{\partial u}\phi\delta u^{\Gamma} \right\rangle_{\Gamma} + I_2, \tag{2.62}$$

where $\quad I_1 = \left\langle \phi_h^+, \frac{\nu\Sigma_f}{k^2}\phi \right\rangle = \left\langle \begin{pmatrix} \phi_{1h}^+ \\ \phi_{2h}^+ \end{pmatrix}, \begin{pmatrix} \frac{\nu\Sigma_{f1}}{k^2} & \frac{\nu\Sigma_{f2}}{k^2} \\ 0 & 0 \end{pmatrix} \begin{pmatrix} \phi_1 \\ \phi_2 \end{pmatrix} \right\rangle,$

$$I_2 = \left\langle \phi_h^+, \frac{\partial L}{\partial u}\phi\delta u^{\overline{\Gamma}} \right\rangle_{\overline{\Gamma}} = \left\langle \begin{pmatrix} \phi_{1h}^+ \\ \phi_{2h}^+ \end{pmatrix}, \begin{pmatrix} -\frac{\partial\Sigma_{a1}}{\partial u} - \frac{\partial\Sigma_r}{\partial u} + \frac{1}{k}\frac{\partial\nu\Sigma_{f1}}{\partial u} & \frac{1}{k}\frac{\partial\nu\Sigma_{f2}}{\partial u} \\ \frac{\partial\Sigma_r}{\partial u} & -\frac{\partial\Sigma_{a2}}{\partial u} \end{pmatrix} \begin{pmatrix} \phi_1 \\ \phi_2 \end{pmatrix} \delta u^{\overline{\Gamma}} \right\rangle_{\overline{\Gamma}}.$$

Note that the perturbation of the diffusion coefficient in L in Eq. (2.62) is ignored because it is very small and negligible.

Part 2: Newton step on $\nabla^2 S = 0$. We return to the second spatial derivative of the inequality constraint in Eq. (2.57) and take a Newton step on it:

$$\begin{aligned}
&\frac{1}{k}\frac{\partial\nu\Sigma_{f1}}{\partial u}\Sigma_{a2}\delta u + \frac{\nu\Sigma_{f1}}{k}\frac{\partial\Sigma_{a2}}{\partial u}\delta u - \frac{\nu\Sigma_{f1}}{k^2}\Sigma_{a2}\delta k + \frac{1}{k}\frac{\partial\nu\Sigma_{f2}}{\partial u}\Sigma_r\delta u \\
&+ \frac{\nu\Sigma_{f2}}{k}\frac{\partial\Sigma_r}{\partial u}\delta u - \frac{\nu\Sigma_{f2}}{k^2}\Sigma_r\delta k - \frac{\partial\Sigma_{a2}}{\partial u}\left(\Sigma_{a1}+\Sigma_r\right)\delta u - \Sigma_{a2}\left(\frac{\partial\Sigma_{a1}}{\partial u} + \frac{\partial\Sigma_r}{\partial u}\right)\delta u \\
&= -\left[\frac{\nu\Sigma_{f1}}{k}\Sigma_{a2} + \frac{\nu\Sigma_{f2}}{k}\Sigma_r - \Sigma_{a2}\left(\Sigma_{a1}+\Sigma_r\right)\right] \qquad \text{on} \quad \Gamma,
\end{aligned}$$

where we explicitly represent the δu variable as δu^{Γ}, and collect the δu^{Γ} and δk terms to arrive at:

$$\delta u^{\Gamma} = \frac{-a_3 + a_2\delta k}{a_1}, \tag{2.63}$$

$$\begin{aligned}
\text{with} \qquad a_1 &= \frac{1}{k}\frac{\partial\nu\Sigma_{f1}}{\partial u}\Sigma_{a2} + \frac{\nu\Sigma_{f1}}{k}\frac{\partial\Sigma_{a2}}{\partial u} + \frac{1}{k}\frac{\partial\nu\Sigma_{f2}}{\partial u}\Sigma_r + \frac{\nu\Sigma_{f2}}{k}\frac{\partial\Sigma_r}{\partial u} \\
&\quad - \frac{\partial\Sigma_{a2}}{\partial u}\left(\Sigma_{a1}+\Sigma_r\right) - \Sigma_{a2}\left(\frac{\partial\Sigma_{a1}}{\partial u} + \frac{\partial\Sigma_r}{\partial u}\right), \\
a_2 &= \frac{1}{k^2}\left(\nu\Sigma_{f1}\Sigma_{a2} + \nu\Sigma_{f2}\Sigma_r\right), \\
a_3 &= \frac{\nu\Sigma_{f1}}{k}\Sigma_{a2} + \frac{\nu\Sigma_{f2}}{k}\Sigma_r - \Sigma_{a2}\left(\Sigma_{a1}+\Sigma_r\right).
\end{aligned}$$

Combining Parts 1 and 2: We combine Eqs. (2.62) and (2.63) by inserting the expression for δu^{Γ} from Eq. (2.63) into Eq. (2.62) to get:

$$I_1 \delta k = \left\langle \phi_h^+, \frac{\partial L}{\partial u} \phi \left(\frac{-a_3 + a_2 \delta k}{a_1} \right) \right\rangle_\Gamma + I_2,$$

and solve for the optimal δk as:

$$\delta k = \left(- \left\langle \phi_h^+, \frac{\partial L}{\partial u} \phi \frac{a_3}{a_1} \right\rangle_\Gamma + I_2 \right) / \left(I_1 - \left\langle \phi_h^+, \frac{\partial L}{\partial u} \phi \frac{a_2}{a_1} \right\rangle_\Gamma \right). \tag{2.64}$$

Then we obtain the optimal control δu^Γ from Eq. (2.63) with the optimal δk.

2.4.4 Sequence to Solve the Steady-State Optimality Conditions

With the formulation of all the optimality conditions required to find the solution to the steady-state optimal control problem in PWRs completed, we present a flowchart in Figure 2.2 of the sequence that we use to solve the optimality conditions iteratively.

1. We begin with an estimate of the control variable and solve the constraint equations of the neutron diffusion equation (2.14) and the power normalization equation (2.18). Thus we obtain the state variables ϕ and k.

2. Next we solve the inhomogeneous adjoint equation (2.31) with the jump condition (2.45) to obtain the adjoint variables ϕ^+ and Q^+. Then we apply the normalization equation (2.37) on ϕ^+ to complete our solution of the state and adjoint variables up to this point based on the initial estimate of the control.

3. We proceed now to use the calculated state and adjoint variables to obtain the control variable from Eq. (2.50) by using the control equation as a gradient in the unconstrained region, and from Eq. (2.63) by using Newton's method in the constrained region.

4. The newly calculated control is then checked with the initial control estimate for convergence, and the iteration is repeated until the control u converges.

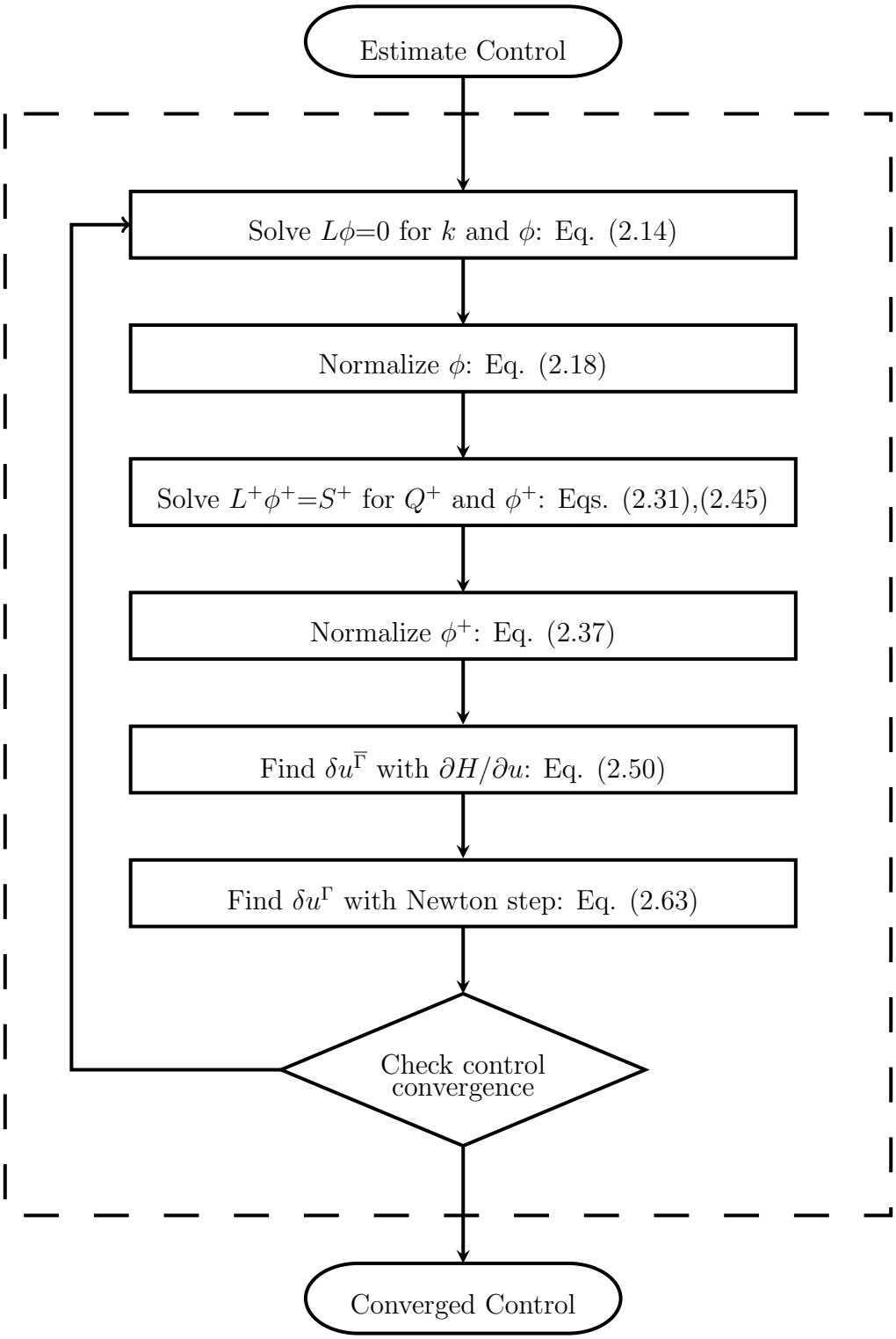

Figure 2.2: Flowchart for steady-state optimal control problem

2.5 Formulation of the Depletion Optimal Control Problem

Now that we have developed the formulation of the optimality condition for a steady-state problem, we are ready to move into the full formulation of our optimal control problem for a depletion problem. The methodology for deriving the optimality conditions for the depletion problem will be very similar to the steady-state problem with the added dimension of time and an additional equality constraint from the fuel burnup equation. Instead of reformulating all the equations as we did in the steady-state formulation, only the equations that are different and new in the depletion formulation will be shown.

The objective function that we are interested in is evaluating the objective at the terminal time τ for the depletion case introduced in Eq. (2.10):

$$J_2(\tau) = \int_X \int_Y dxdy \left[E(x,y,\tau) - \overline{E}(\tau)\right]^2. \tag{2.65}$$

The constraint equations we had in the steady-state problem remain the same with the addition of the fuel burnup equation where we introduce the state variable E which is a function of space and time:

$$\frac{\partial E(x,y,t)}{\partial t} = \frac{\kappa\Sigma_f\phi(x,y,t)}{\rho} = \frac{p(x,y,t)}{\rho}, \tag{2.66}$$

where ρ is the mass density of the homogenized fuel in the core and $p(x,y,t)$ was introduced in Eq. (2.15). This equation is used to calculate the fuel burnup for the time step Δt:

$$E(x,y,t+\Delta t) = E(x,y,t) + \frac{p(x,y,t)}{\rho}\Delta t. \tag{2.67}$$

With these changes, we build the new augmented objective function for the de-

pletion problem in time domain:

$$H(\tau) = \int_X \int_Y dxdy \left[E(x,y,\tau) - \overline{E}(\tau)\right]^2 + \int_\tau dt \left\{ \int_X \int_Y dxdy \right.$$
$$\left. \left[\phi^{+^T} L\phi + Q^+ \left(\kappa\Sigma_f \phi - \frac{\partial^2 Q}{\partial x \partial y} \right) + E^+ \left(\frac{\kappa\Sigma_f \phi}{\rho} - \frac{\partial E}{\partial t} \right) + \eta^+ S \right] \right\}, \quad (2.68)$$

which replaces the objective $-k$ by the new flat burnup objective (2.65) and adds the burnup equation (2.66) in the steady-state augmented objective function of Eq. (2.20) . We also note that every system parameter is now time-dependent although they may not be shown explicitly in the formulation for notational convenience. By applying calculus of variation on the new augmented objective function, we develop the equation in a similar way as in the steady-state problem by first taking the variation on all the state and control variables:

$$\begin{aligned} \delta H(\tau) = & \int_X \int_Y dxdy \left[2\left(E(x,y,\tau) - \overline{E}(\tau)\right)\right] \delta E(x,y,\tau) \\ & + \int_\tau dt \int_X \int_Y dxdy \left[\begin{array}{l} \phi^{+^T} \delta\left(L\phi\right) + Q^+ \left[\delta\left(\kappa\Sigma_f\phi\right) - \frac{\partial^2 \delta Q}{\partial x \partial y}\right] \\ + E^+ \left[\frac{\delta\left(\kappa\Sigma_f\phi\right)}{\rho} - \frac{\partial \delta E}{\partial t}\right] + \eta^+ \left[\frac{\delta\left(\kappa\Sigma_f\phi\right)}{p_{ave}}\right] \end{array} \right]. \end{aligned} \quad (2.69)$$

In the same way we performed integration by parts on the derivative terms involving $\delta\phi$ and δQ to simplify the steady-state augmented objective function in Eq. (2.24), we do the same to the adjoint burnup $\delta E(x,y,t)$ term:

$$\begin{aligned} & \int_\tau dt \int_X \int_Y dxdy \left[E^+(x,y,t) \frac{\partial \delta E(x,y,t)}{\partial t} \right] \\ = & \int_X \int_Y dxdy \left[E^+(x,y,t)\delta E(x,y,t)|_0^\tau - \int_\tau \frac{\partial E^+(x,y,t)}{\partial t} \delta E(x,y,t) \right] \\ = & \int_X \int_Y dxdy \left[E^+(x,y,\tau)\delta E(x,y,\tau) - \int_\tau \frac{\partial E^+(x,y,t)}{\partial t} \delta E(x,y,t) \right] \end{aligned} \quad (2.70)$$

where the variation $\delta E(x,y,0)$ is zero as we restrict perturbations in the BOC fuel burnup distribution which is either fixed from the previous cycle or zero for a fresh fuel loading. Applying Eq. (2.70) to the augmented objective function and selecting an objective function that is a function of the burnup variable E for our depletion problem, we get:

$$\begin{aligned}\delta H(\tau) = & \int_X \int_Y dxdy \left[2\left(E(x,y,\tau) - \overline{E}(\tau)\right) - E^+(x,y,\tau)\right] \delta E(x,y,\tau) \\ & + \int_\tau dt \int_X \int_Y dxdy \left[\begin{array}{l} \left(L^+\phi^+\right)^T \delta\phi + \phi^{+T} \delta L \phi + \left(Q^+ + \frac{E^+}{\rho} + \frac{\eta^+}{p_{ave}}\right) \delta\left(\kappa\Sigma_f\phi\right) \\ -\frac{\partial^2 Q^+}{\partial x \partial y}\delta Q + \frac{\partial E^+}{\partial t}\delta E \end{array}\right]\end{aligned} \tag{2.71}$$

where

$$\delta L = \frac{\partial L}{\partial k}\delta k + \frac{\partial L}{\partial u}\delta u$$

$$\delta\left(\kappa\Sigma_f\phi\right) = \frac{\partial \kappa\Sigma_f}{\partial u}\delta u\phi + \kappa\Sigma_f\delta\phi.$$

Two additional terms involving E^+ and $\partial E^+/\partial t$ are noted, compared with Eq. (2.27). Next we expand the remaining variation terms δL and $\delta(\kappa\Sigma_f\phi)$ and collect the variation terms that are alike to arrive at the final form of the augmented objective

function:

$$
\begin{aligned}
\delta H(\tau) = & \int_X \int_Y dxdy \left[2\left(E(x,y,\tau) - \overline{E}(\tau)\right) - E^+(x,y,\tau)\right] \delta E(x,y,\tau) \\
& + \int_\tau dt \int_X \int_Y dxdy \left[\left\{\left(L^+\phi^+\right)^T + \left(Q^+ + \frac{E^+}{\rho} + \frac{\eta^+}{p_{ave}}\right)\kappa\Sigma_f\right\}\delta\phi\right] \\
& - \int_\tau dt \int_X \int_Y dxdy \left[\left(\frac{\partial^2 Q^+}{\partial x \partial y}\right)\delta Q\right] + \int_\tau dt \int_X \int_Y dxdy \left[{\phi^+}^T \frac{\partial L}{\partial k}\phi\delta k\right] \\
& + \int_\tau dt \int_X \int_Y dxdy \left[\left\{{\phi^+}^T \frac{\partial L}{\partial u}\phi + \left(Q^+ + \frac{E^+}{\rho} + \frac{\eta^+}{p_{ave}}\right)\frac{\partial \kappa\Sigma_f}{\partial u}\phi\right\}\delta u\right] \qquad (2.72) \\
& + \int_\tau dt \int_X \int_Y dxdy \left[\left\{\frac{\partial E^+}{\partial t} + {\phi^+}^T \frac{\partial L}{\partial E}\phi + \left(Q^+ + \frac{E^+}{\rho} + \frac{\eta^+}{p_{ave}}\right)\frac{\partial \kappa\Sigma_f}{\partial E}\phi\right\}\delta E\right] \\
& \equiv I_1 + I_2 + I_3 + I_4 + I_5 + I_6 = 0
\end{aligned}
$$

2.5.1 First Order Optimality Conditions for the Depletion Problem

Comparing the augmented objective function in Eq. (2.72) with the steady-state augmented objective function in Eq. (2.28), we have a new terminal condition in integral I_1, additional time integrals for the remaining integrals I_2 - I_6, additional terms E^+/ρ in I_2 and I_5, and an additional adjoint burnup equation in I_6. The additional time integrals over the same spatial integrals that were evaluated in the steady-state problem does not change any of the optimality conditions, except the control optimality condition in I_5.

The optimality for the terminal condition at $t = \tau$ in I_1 requires:

$$
\int_X \int_Y dxdy \left[2\left(E(x,y,\tau) - \overline{E}(\tau)\right) - E^+(x,y,\tau)\right] \delta E(x,y,\tau) = 0, \qquad (2.73)
$$

which is satisfied by setting to zero the integrand attached to $\delta E(\tau)$. This condition

gives us the distribution of the adjoint burnup E^+ at $t = \tau$:

$$E^+(x, y, \tau) = 2\left[E(x, y, \tau) - \overline{E}(\tau)\right]. \tag{2.74}$$

In the Euler-Lagrange equation obtained from I_2 in Eq. (2.72), the optimality condition is the same as the steady-state problem at every time step t with the addition of the adjoint burnup term E^+/ρ:

$$\left(L^+\phi^+\right)^T + \left(Q^+ + \frac{E^+}{\rho} + \frac{\eta^+}{p_{\text{ave}}}\right)\kappa\Sigma_f = 0. \tag{2.75}$$

Optimality conditions obtained from I_3 and I_4 are also the same as the steady-state problem at every time step t:

$$\frac{\partial^2 Q^+}{\partial x \partial y} = 0 \tag{2.76}$$

$$\int_X \int_Y dxdy \left[\phi^{+T}\frac{\partial L}{\partial k}\phi\right] = 0, \tag{2.77}$$

with the difference that we do not have the term $1/V$ in Eq. (2.77) as we did in Eq. (2.37). This is because the objective function in this depletion problem is the flat burnup profile and not the multiplication factor k. This optimality condition is satisfied no longer by normalizing the magnitude of ϕ^+ since the integral in Eq. (2.77) is zero. Instead this optimality condition is naturally satisfied during the solution of the Euler-Lagrange equation for ϕ^+ when the fundamental mode contamination removal is performed, as will be discussed in Section 3.2.3.

Integral I_5 needs to be evaluated differently because δu is only a function of space and not time in our PWR problem where the control only exist at the BOC. This causes δu to sit outside the time integral:

$$\int_X \int_Y dxdy \left\{ \int_\tau dt \left[\phi^{+T} \frac{\partial L}{\partial u} \phi + \left(Q^+ + \frac{E^+}{\rho} + \frac{\eta^+}{p_{\text{ave}}} \right) \frac{\partial \kappa \Sigma_f}{\partial u} \phi \right] \right\} \delta u = 0. \tag{2.78}$$

Thus, the sufficient condition for this optimality condition is to set the time integral to zero:

$$\int_\tau dt \left[\phi^{+T} \frac{\partial L}{\partial u} \phi + \left(Q^+ + \frac{E^+}{\rho} + \frac{\eta^+}{p_{\text{ave}}} \right) \frac{\partial \kappa \Sigma_f}{\partial u} \phi \right] = 0. \tag{2.79}$$

Finally for the integral involving δE in I_6,

$$\int_\tau dt \int_X \int_Y dxdy \left[\left\{ \frac{\partial E^+}{\partial t} + \phi^{+T} \frac{\partial L}{\partial E} \phi + \left(Q^+ + \frac{E^+}{\rho} + \frac{\eta^+}{p_{\text{ave}}} \right) \frac{\partial \kappa \Sigma_f}{\partial E} \phi \right\} \delta E \right] \tag{2.80}$$

setting the integrand attached to δE to zero yields the optimality condition for determining the incremental E^+ distribution after every time step:

$$\frac{\partial E^+}{\partial t} + \phi^{+T} \frac{\partial L}{\partial E} \phi + \left(Q^+ + \frac{E^+}{\rho} + \frac{\eta^+}{p_{\text{ave}}} \right) \frac{\partial \kappa \Sigma_f}{\partial E} \phi = 0. \tag{2.81}$$

2.5.2 Sequence to Solve the Depletion Optimality Conditions

The main challenge in the depletion problem is satisfying the peaking factor constraint for every burnup step with the initial control defined at the BOC. The formulation that we have developed so far using the direct adjoining method to satisfy the power peaking constraint requires the control in the constrained region to be determined at every burnup step to satisfy the inequality constraint. Since this is not a possibility in our PWR optimal control problem, we need to devise a method that could determine the control that is needed somewhere in the middle of the cycle, and trace its required depletion path back to the BOC where the control exists. To achieve a mechanism with this feature, we explored using the adjoint burnup variable

since it holds information of the fuel burnup and naturally progresses reverse in time from EOC to BOC.

1. We begin the iterative approach for the depletion problem by solving the forward depletion equations in quasi-steady-state fashion. During the depletion steps, we develop a desirable fuel burnup path that satisfies the power peaking constraint on every depletion step. This is accomplished by applying the steady-state optimal control problem as described in Figure 2.2 whenever a power peaking violation occurred in that time step. To proceed to the next time step, the burnup is calculated based on the modified control and fluxes with Eq. (2.67) so that we develop a burnup distribution over the cycle that conforms to the power peaking requirement. By doing so, we have effectively turned a depletion problem into a series of steady-state problems with burnup calculations performed between burnup steps.

2. With the desirable burnup path calculated from the forward depletion calculations, we proceed to solve the adjoint depletion calculations performed backwards in time. The EOC burnup information from the forward depletion mode is used at the start of the EOC step in the adjoint depletion mode in the calculation of the adjoint burnup E^+ from Eq. (2.74). The adjoint burnup E^+ is updated after every adjoint burnup step marching backwards in time with Eq. (2.81) and transfers the information of the desired burnup path over time to the adjoint flux variable ϕ^+ until the run reaches the BOC step on its final adjoint step.

3. The control for the next iteration is determined by combining δu from the BOC control recommendation from the forward depletion run if any, and the suggested δu control from the gradient $\partial H/\partial u$ obtained after the adjoint depletion run. This will combine the control recommendations to satisfy power peaking at

the BOC and during the depletion, where at both times the objective function is being optimized.

4. This completes one full iteration on the system of equations from the optimality conditions and is repeated until the control converges. The iterative solution for the depletion optimal control problem is summarized in Figure 2.3.

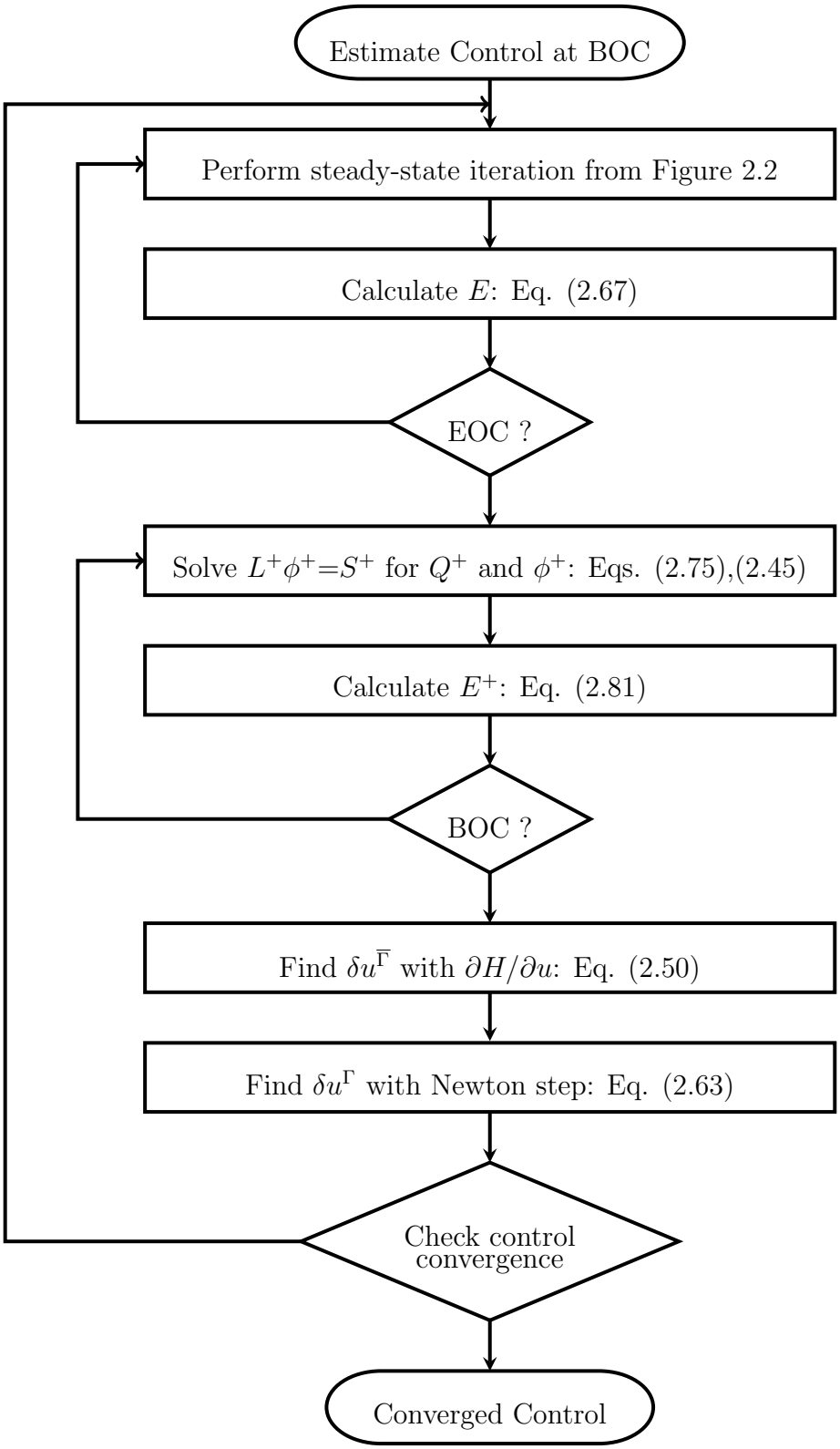

Figure 2.3: Flowchart for depletion optimal control problem

CHAPTER III

Numerical Implementation of Our Methodology

In this chapter we show the numerical implementation of the optimality conditions in the DMCO code based on the formulations in Chapter 2 for a two-group two-dimensional reactor. The DMCO code, short for Deterministic Multi-Control Optimization, is an optimization package that we have developed to perform the optimization routines with a built-in neutron diffusion equation solver called UM2DB. It is capable of automating the optimization routines for various combinations of 1-D, 2-D, one-group, two-group, BOC and full cycle optimization using either fissile U^{235} number densities or BP number densities controls. It runs on the Windows platform using batch command scripting and Fortran 95. It is lightweight enough to run on a personal desktop or laptop with average runtimes of 13 minutes for one full depletion control optimization in 2-D and two-group formulation.

The UM2DB code is a modified version of the 2DB code originally developed for fast reactor applications [35]. It is capable of solving the PWR global depletion equations using diffusion theory for a two-group two-dimensional problem. We have made a few enhancements to the code to perform thermal feedback modeling, critical boron search and solution for an inhomogeneous adjoint diffusion equation. The code is used as a calculator within DMCO which is capable of solving the optimality conditions iteratively in an automated fashion. The cross section library that we

employ in DMCO is generated by the CASMO-4 lattice physics code [36]. The library provides macroscopic cross sections to the system equations based on the selected controls, fuel burnup and critical boron concentration.

We begin our numerical formulation by performing a mesh-centered finite-differencing scheme on the forward and adjoint equations representing our optimality conditions. Then we describe how the discretized equations are solved iteratively in DMCO, including our iterative method of selecting the junction distribution in the core. We also provide in this chapter the verification results of the numerical forward and adjoint equations that we have formulated. We perform a benchmarking of the AP600 first cycle in our code to verify the discretized forward equations as well as the accuracy of our cross section libraries and the thermal feedback modeling. The results are compared to the published results in the AP600 Standard Safety Analysis Report (SSAR) [28] as well as results obtained from another global code package APA which is developed by Westinghouse. For verification of the discretized adjoint equations, we first solve a simplified analytical problem. We then solve the same problem in DMCO in an iterative approach and verify the results we obtain for the solution of the adjoint variables.

3.1 Numerical Solution of the Forward Equations

The set of forward equations are the equality constraints in our optimal control problem which includes the two-group two-dimensional neutron diffusion equation (2.13), the power normalization equation (2.18) and the burnup equation (2.66). To solve these equations over the lifetime of the core, the operating cycle is divided into finite number of time intervals with increasing time intervals. Shorter time intervals are used near BOC to evaluate the effects of xenon poisoning on the optimal control problem. Over each of these time steps, the neutron diffusion equation and the power normalization equation are solved in quasi-static fashion, where we have assumed

that the system is varying very slowly over the time interval that we can treat it as a static system. Two-group macroscopic cross sections generated from the CASMO-4 lattice physics code are applied to each fuel assembly based on the fuel burnup of the assembly. The macroscopic cross sections are also modified to account for thermal feedback from Doppler broadening and moderator density feedback, as well as critical boron concentration in the reactor. At the end of each time interval, the burnup equation is solved to update the fuel burnup in each fuel assembly so that the macroscopic cross sections can be generated for the next time step. This process is repeated until we have proceeded from BOC to EOC.

The reactor core is divided into a finite number of mesh intervals in the x-axis and y-axis over the fuel regions and the reflector regions of the core. Each fuel assembly is made up of a 6 x 6 mesh array, representing a 21.6cm x 21.6cm fuel assembly dimension. The z-axis or axial dimension of the reactor core is approximated by use of a transverse buckling parameter that accounts for the neutron leakage in that direction. This is generally a good approximation if the reactor core has a uniform axial distribution, which is the case for the AP600 reactor core that we are using as our test case. Therefore all our formulations and numerical calculations are performed in two-dimension with a unit height in the axial direction.

3.1.1 Forward Finite-Difference Equations

We proceed to discretize our forward equations using a mesh-centered finite-differencing scheme that is used in DMCO by first re-writing the neutron diffusion equation in terms of the neutron current J to help us discretize the leakage term:

$$\nabla \cdot J_1 + (\Sigma_{a1} + \Sigma_r)\,\phi_1 = \frac{\nu\Sigma_{f1}\phi_1 + \nu\Sigma_{f2}\phi_2}{k}, \tag{3.1a}$$

$$\nabla \cdot J_2 + \Sigma_{a2}\phi_2 = \Sigma_r\phi_1. \tag{3.1b}$$

To simplify the derivation of our finite-difference equation for both energy groups, we will derive a general form using the following representation:

$$\nabla \cdot J + \Sigma\phi = F\phi \tag{3.2}$$

where $F\phi$ is the fission source term for group 1 and the removal term for group 2.

We present a schematic of a single mesh at index 0 surrounded by its four adjacent neighboring meshes in Figure 3.1 for the purpose of illustrating our finite-differencing scheme where the flux ϕ_i is defined at the center of volume V_i, i=0,1,2,3,4. To discretize Eq. (3.2), we integrate these equations over the mesh volume i:

$$\int_{x_i-\frac{\Delta x}{2}}^{x_i+\frac{\Delta x}{2}} \int_{y_i-\frac{\Delta y}{2}}^{y_i+\frac{\Delta y}{2}} dxdy\,(\nabla \cdot J + \Sigma\phi) = \int_{x_i-\frac{\Delta x}{2}}^{x_i+\frac{\Delta x}{2}} \int_{y_i-\frac{\Delta y}{2}}^{y_i+\frac{\Delta y}{2}} dxdyF\phi \tag{3.3}$$

where we have dropped the integral over the axial z direction because we represent the reactor with unit thickness.

We transform the leakage term from a volume integral to a surface integral using the divergence theorem which states:

$$\int_V dV\,(\nabla \cdot J) = \int_S dA\,(J \cdot \hat{n}) \tag{3.4}$$

where $\hat{n}$ represents the outward-pointing unit normal vector on the surface. We represent the surface integral in Eq. (3.4) as the sum of four current values J_k multiplied by the respective surface area A_k with unit thickness:

$$\int_S dA\,(J \cdot \hat{n}) = \sum_{k=1}^{4} J_k A_k. \tag{3.5}$$

Discretization of the remaining terms in Eq. (3.3) yields in a straightforward

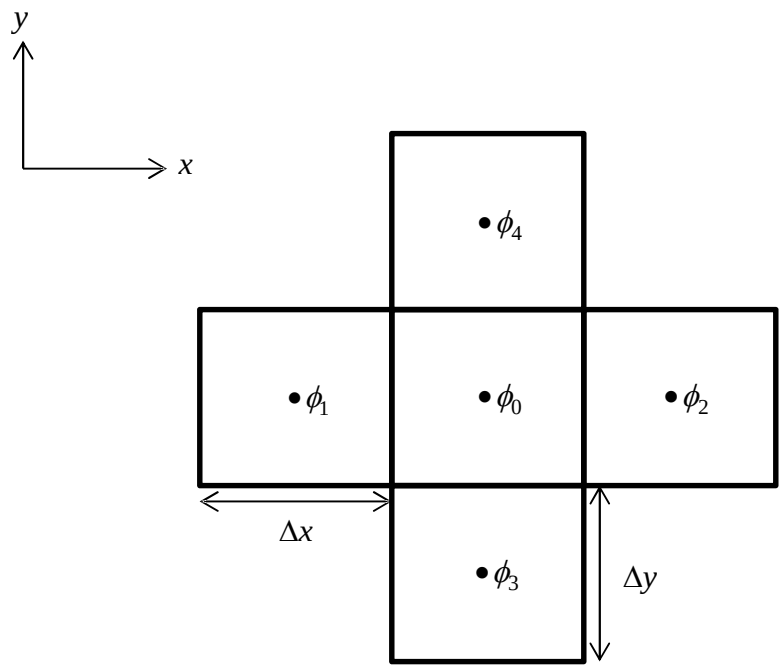

Figure 3.1: Schematic of mesh i and adjacent meshes

manner the mesh center value of the terms multiplied by the volume of the mesh V_0 with unit thickness:

$$\int_{x_i-\frac{\Delta x}{2}}^{x_i+\frac{\Delta x}{2}} \int_{y_i-\frac{\Delta y}{2}}^{y_i+\frac{\Delta y}{2}} dxdy\Sigma\phi = \Sigma_0\phi_0 V_0 \tag{3.6}$$

and

$$\int_{x_i-\frac{\Delta x}{2}}^{x_i+\frac{\Delta x}{2}} \int_{y_i-\frac{\Delta y}{2}}^{y_i+\frac{\Delta y}{2}} dxdyF\phi = F_0\phi_0 V_0. \tag{3.7}$$

Thus we obtain our general form of the discretized neutron diffusion equation in terms of current J_k as:

$$\sum_{k=1}^{4} J_k A_k + \Sigma_0\phi_0 V_0 = F_0\phi_0 V_0. \tag{3.8}$$

Next we re-write Eq. (3.8) in terms of flux using the discretized form of the current which is continuous over the mesh boundary between mesh 0 and mesh 1 in Figure

3.1:

$$J_1 = \frac{D_0(\phi_0 - \phi_{1/2})}{\Delta x_0/2} = \frac{D_1(\phi_{1/2} - \phi_1)}{\Delta x_1/2} \tag{3.9}$$

where $\phi_{1/2}$ is the boundary flux between mesh 0 and mesh 1 and calculated as:

$$\phi_{1/2} = \frac{D_1\phi_1\Delta x_0 + D_0\phi_0\Delta x_1}{D_1\Delta x_0 + D_0\Delta x_1}. \tag{3.10}$$

Inserting Eq. (3.10) into Eq. (3.9), we get:

$$J_1 = \frac{2D_0D_1(\phi_0 - \phi_1)}{D_1\Delta x_0 + D_0\Delta x_1}. \tag{3.11}$$

We can generalize the current in Eq. (3.11) for any one of the mesh boundaries A_k as:

$$J_k = \frac{2D_0D_k(\phi_0 - \phi_k)}{D_k\Delta x_0 + D_0\Delta x_k}. \tag{3.12}$$

Then Eq. (3.3) becomes:

$$\sum_{k=1}^{4} \frac{2D_0D_k(\phi_0 - \phi_k)}{D_k\Delta x_0 + D_0\Delta x_k} A_k + \Sigma_0\phi_0V_0 = F_0\phi_0V_0 \tag{3.13}$$

and written in a concise form as:

$$\sum_{k=1}^{4} c_k(\phi_0 - \phi_k) + \Sigma_0\phi_0V_0 = F_0\phi_0V_0 \tag{3.14}$$

where

$$c_k \equiv \frac{2D_0D_k}{D_k\Delta x_0 + D_0\Delta x_k} A_k. \tag{3.15}$$

Finally we can re-write the discretized equation (3.14) for a generalized mesh at (i,j) to arrive at the final discretized form of the forward neutron diffusion equation as:

$$a_{ij}\phi_{i-1,j} + b_{ij}\phi_{ij} + c_{ij}\phi_{i+1,j} + d_{ij}\phi_{i,j-1} + e_{ij}\phi_{i,j+1} = F_{ij}\phi_{ij} \tag{3.16}$$

where:

$$a_{ij} = -c_1, \quad b_{ij} = \sum_{k=1}^{4} c_k + \Sigma_0 V_0, \quad c_{ij} = -c_2, \quad d_{ij} = -c_3, \quad e_{ij} = -c_4$$

$$\phi_{ij} = \phi_0, \quad \phi_{i-1,j} = \phi_1, \quad \phi_{i+1,j} = \phi_2, \quad \phi_{i,j-1} = \phi_3, \quad \phi_{i,j+1} = \phi_4, \quad F_{ij}\phi_{ij} = F_0\phi_0 V_0.$$

Equation (3.16) can be simply represented in the matrix form for each group:

$$M\phi = F\phi \tag{3.17}$$

where F contains the multiplication factor k in the first group.

Matrix M representing the loss terms is shown in Figure 3.2 consisting of a 5-band matrix with the diagonal terms representing the absorption terms and leakage for the center volume, and the off-diagonals terms representing the leakage in the four possible directions in the x-axis and the y-axis. The production term F is a matrix and the fluxes ϕ are column vectors. In our numerical implementation in DMCO, the UM2DB code is used to solve the eigenvalue problem iteratively using the standard power iteration [37].

Next we are ready to normalize the flux with the power normalization equation in Eq. (2.18) by summing the power in the reactor core and adjusting the flux magnitude by a coefficient α such that the total power is satisfied:

$$\alpha \sum_{i=1}^{I} \sum_{j=1}^{J} \kappa\Sigma_{fij}\phi_{ij}V_{ij} = P_{tot} \tag{3.18}$$

where I and J represents the total number of meshes i and j in the core. Finally the last forward equation is solved by calculating the burnup of each fuel assembly according to Eq. (2.67) in the discretized form for the time step Δt:

$$\Delta E_{ij} = \frac{\kappa\Sigma_{fij}\phi_{ij}V_{ij}}{\rho} \cdot \Delta t. \tag{3.19}$$

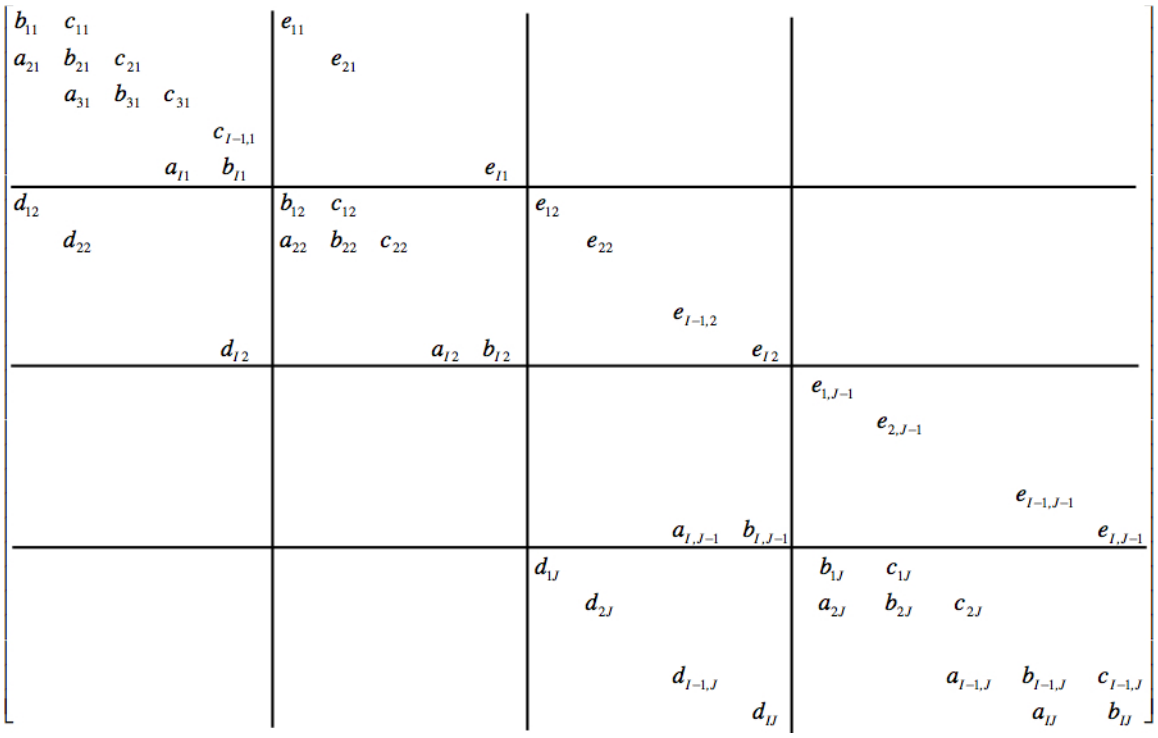

Figure 3.2: 5-band matrix M

3.2 Numerical Solution of the Euler-Lagrange Equations

We next show the numerical formulations of the Euler-Lagrange equations to find solutions for our adjoint variables. We first recognize that the Euler-Lagrange equation is an inhomogeneous adjoint diffusion equation, which means that it has a source term and requires a different solver than the eigenvalue solver we used for the forward neutron diffusion equation. The DMCO code builds the adjoint source terms and provides the proper cross sections to the UM2DB code, which solves the fixed source problem in the adjoint mode. The cross sections in the operator L^+ are the same cross sections used in the forward neutron diffusion equations with the difference that they are arranged reverse in time and are transposed. The source term contains four different adjoint variables, namely the inequality Lagrange multiplier η^+, adjoint power Q^+, adjoint burnup E^+ and the jump parameter μ. All these four adjoint variables need to be determined at every time step before solving for the adjoint flux

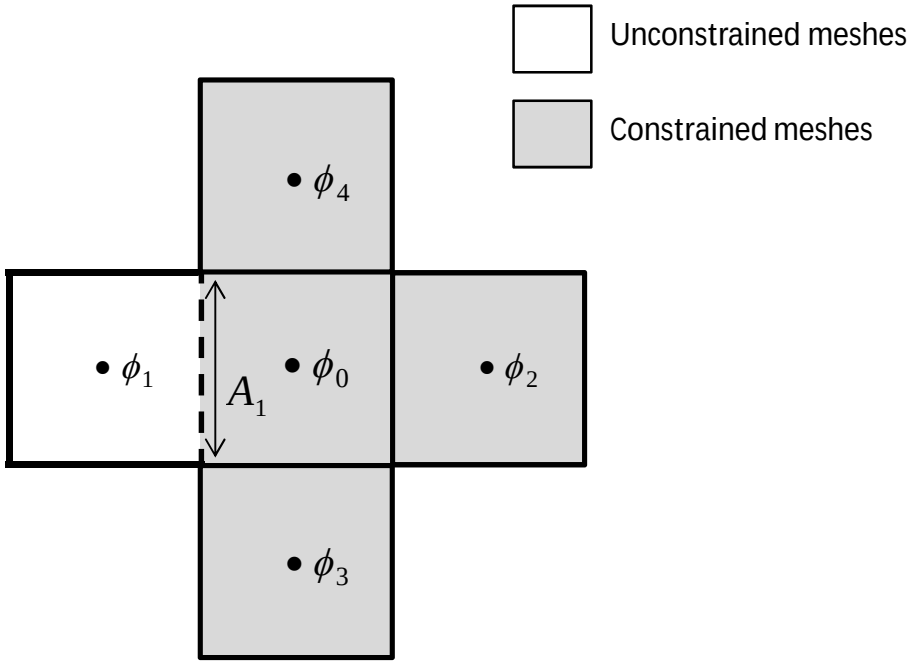

Figure 3.3: Schematic of mesh i with a junction boundary

ϕ^+ and moving on to the next time step. Due to the nature of adjoint equations in a time-dependent problem, the adjoint variables are determined in reverse order of time, from the EOC to the BOC.

The main challenge in obtaining a finite-differencing solution of the Euler-Lagrange equation is handling the jump parameters correctly, which originates from the leakage term L^+ at a junction as determined in Section 2.4.2. Otherwise the finite-differencing of the Euler-Lagrange equation is essentially the same form as the forward neutron diffusion equations without the presence of any junctions, which as we recall is the boundary between a constrained and unconstrained region. So to provide a meaningful derivation here with the jump parameters, we consider a mesh that has a junction boundary with one of its neighboring mesh as in Figure 3.3.

3.2.1 Euler-Lagrange Finite-Difference Equations

We begin formulating the numerical adjoint equations in the same way we did with the forward neutron diffusion equations by expanding the L^+ operator and re-writing the Euler-Lagrange equations (2.75) in terms of the adjoint current J^+:

$$\nabla \cdot J_1^+ + (\Sigma_{a1} + \Sigma_r)\,\phi_1^+ = \frac{\nu\Sigma_{f1}\phi_1^+}{k} + \Sigma_r\phi_2^+ + \left(Q^+ + \frac{E^+}{\rho} + \frac{\eta^+}{p_{\text{ave}}}\right)\kappa\Sigma_{f1}, \tag{3.20a}$$

$$\nabla \cdot J_2^+ + \Sigma_{a2}\phi_2^+ = \frac{\nu\Sigma_{f2}\phi_1^+}{k} + \left(Q^+ + \frac{E^+}{\rho} + \frac{\eta^+}{p_{\text{ave}}}\right)\kappa\Sigma_{f2}. \tag{3.20b}$$

We proceed by casting the two-group inhomogeneous Euler-Lagrange equations into a generalized form:

$$\nabla \cdot J^+ + \Sigma^+\phi^+ = F^+\phi^+ + S^+ \tag{3.21}$$

where we have represented the inhomogeneous adjoint source terms in Eqs. (3.20a) and (3.20b) as S^+. To discretize Eq. (3.21), we integrate the equations across the mesh volume i with unit thickness in the z direction:

$$\int_{x_i-\frac{\Delta x}{2}}^{x_i+\frac{\Delta x}{2}}\int_{y_i-\frac{\Delta y}{2}}^{y_i+\frac{\Delta y}{2}} dxdy\left(\nabla \cdot J^+ + \Sigma^+\phi^+\right) = \int_{x_i-\frac{\Delta x}{2}}^{x_i+\frac{\Delta x}{2}}\int_{y_i-\frac{\Delta y}{2}}^{y_i+\frac{\Delta y}{2}} dxdy\left(F^+\phi^+ + S^+\right). \tag{3.22}$$

Applying the divergence theorem of Eq. (3.4) to the leakage term and integrating the remaining terms the same way we did with the forward neutron diffusion equation, we get:

$$\sum_{k=1}^{4} J_k^+ A_k + \Sigma_0^+\phi_0^+ V_0 = F_0^+\phi_0^+ V_0 + S_0^+ V_0. \tag{3.23}$$

We proceed to re-write the discretized Euler-Lagrange equation in terms of flux using the discretized form of the current which unlike in the forward neutron diffusion equation, is not continuous over all its mesh boundaries. As was derived in Sec 2.4.2,

a jump occurs in the adjoint current J^+ when it is evaluated over a junction at x_i:

$$J^+(x_i^-) = J^+(x_i^+) - \frac{\mu(x_i)}{p_{ave}}\kappa\Sigma_f. \tag{3.24}$$

Applying this jump condition to the junction between mesh 0 and mesh 1 in Figure 3.3 where the current J_1^+ takes the role of current $J^+(x_i^-)$ in Eq. (3.24), we get:

$$J_1^+ = \frac{D_1(\phi_{1/2}^+ - \phi_1^+)}{\Delta x_0/2} - \frac{\mu_1}{p_{ave}}\kappa\Sigma_{f0} \tag{3.25}$$

where $\phi_{1/2}^+$ is the boundary adjoint flux between mesh 0 and mesh 1 and calculated as:

$$\phi_{1/2}^+ = \frac{D_1\phi_1^+\Delta x_0 + D_0\phi_0^+\Delta x_1}{D_1\Delta x_0 + D_0\Delta x_1}. \tag{3.26}$$

We have chosen the notation scheme to represent the current of mesh $J_k^+ = J^+ \cdot \hat{n}$ as the inward-facing current $J^+(x_i^-)$ on each of the mesh boundaries. This would imply that if the junction occurs on a different side of the mesh in Figure 3.3, the sign of the jump term in Eq. (3.25) would still be the same. Inserting Eq. (3.26) into Eq. (3.25), we get:

$$J_1^+ = \frac{2D_0D_1(\phi_0^+ - \phi_1^+)}{D_1\Delta x_0 + D_0\Delta x_1} - \frac{\mu_1}{p_{ave}}\kappa\Sigma_{f0}. \tag{3.27}$$

We can now add this current term containing the jump parameter with the remaining current terms for mesh 0 to represent the discretized leakage term as:

$$\sum_{k=1}^{4} J_k^+ A_k = \sum_{k=1}^{4} c_k(\phi_0^+ - \phi_k^+) - \frac{\mu_1}{p_{ave}}\kappa\Sigma_{f0}A_1. \tag{3.28}$$

We can easily extend this exercise for a mesh that contains more than one junction boundary by simply adding more jump terms to the leakage term for every additional junction boundary. So in general for a mesh with M junction boundaries,

the discretized leakage term is:

$$\sum_{k=1}^{4} J_k^+ A_k = \sum_{k=1}^{4} c_k(\phi_0^+ - \phi_k^+) - \sum_{m=1}^{M} \frac{\mu_m}{p_{ave}} \kappa\Sigma_{f0} A_m. \tag{3.29}$$

Then we arrive at an expression of the discretized Euler-Lagrange equations for a mesh with M junctions as:

$$\sum_{k=1}^{4} c_k(\phi_0^+ - \phi_k^+) + \Sigma_0^+ \phi_0^+ V_0 = F_0^+ \phi_0^+ V_0 + S_0^+ V_0 + \sum_{m=1}^{M} \frac{\mu_m}{p_{ave}} \kappa\Sigma_{f0} A_m \tag{3.30}$$

where we have placed the jump term on the right hand side of Eq. (3.30).

3.2.2 Inhomogeneous Adjoint Source Terms

If we update the inhomogeneous adjoint source terms in Eq. (3.21) to include the jump terms, then Eq. (3.30) can be simplified to:

$$\sum_{k=1}^{4} c_k(\phi_0^+ - \phi_k^+) + \Sigma_0^+ \phi_0^+ V_0 = F_0^+ \phi_0^+ V_0 + S_0^+ V_0 \tag{3.31}$$

where:

$$S_0^+ V_0 = \left(Q^+ + \frac{E_0^+}{\rho} + \frac{\eta_0^+}{p_{\text{ave}}} \right) \kappa\Sigma_{f0} V_0 + \sum_{m=1}^{M} \frac{\mu_m}{p_{ave}} \kappa\Sigma_{f0} A_m. \tag{3.32}$$

Next, we proceed to build the inhomogeneous adjoint source terms in Eq. (3.32) for each energy group by finding the values of the adjoint variables in the following order:

1. inequality Lagrange multiplier η^+,
2. adjoint burnup E^+,
3. adjoint power Q^+, and
4. jump parameters μ.

The jump parameters are actually a by-product of the inequality Lagrange multiplier η^+, but are treated as a separate variable because it is determined from posteriori knowledge [30].

3.2.2.1 Inequality Lagrange Multiplier

The inequality Lagrange multiplier η^+ is partially determined by the KKT condition in Eq. (2.21) which says that it is zero in unconstrained regions and non-negative in constrained regions. To obtain a representation in the constrained region, the control optimality condition from Eq. (2.79) can be used to get:

$$\eta_{ij}^+ = -p_{\text{ave}} \left[\frac{\phi_{ij}^{+T} \frac{\partial L}{\partial u} \phi_{ij}}{\frac{\partial \kappa \Sigma_{fij}}{\partial u} \phi_{ij}} + \left(Q^+ + \frac{E_{ij}^+}{\rho} \right) \right]. \tag{3.33}$$

3.2.2.2 Adjoint Burnup

The adjoint burnup E^+ is determined from the terminal condition in Eq. (2.74) and its incremental value at the end of each time step by Eq. (2.81). Because adjoint equations are solved backwards in time, the initial value of adjoint burnup is obtained from the EOC burnup variable E for each mesh (i, j) as:

$$E_{ij}^+(\tau) = E_{ij}(\tau) - \overline{E}(\tau). \tag{3.34}$$

Then at the end of each adjoint step, an incremental change of the adjoint burnup is calculated using the converged adjoint flux ϕ^+ and the determined values of Q^+, initial E^+ and η^+ of that time step by:

$$\Delta E_{ij}^+ = - \left[\phi_{ij}^{+T} \frac{\partial L}{\partial E} \phi_{ij} + \left(Q^+ + \frac{E_{ij}^+}{\rho} + \frac{\eta_{ij}^+}{p_{\text{ave}}} \right) \frac{\partial \kappa \Sigma_{fij}}{\partial E} \phi_{ij} \right] \Delta t. \tag{3.35}$$

The partial derivatives of the cross sections were calculated from the forward run when the cross sections and burnup variable E were determined at each time step.

3.2.2.3 Adjoint Power

The adjoint power is only partially described from the optimality condition in Eq. (2.76) which indicates that the adjoint power is a constant value. We are able to obtain an expression for the adjoint power by using the Fredholm Alternative condition that is required for the solution of the inhomogeneous Euler-Lagrange equation and inserting the adjoint source term S^+ from Eq. (3.32) into Eq. (2.32). Then using the solution of η from Eq. (3.33), we obtain an expression of Q^+ in terms of the jump parameter μ:

$$Q^+ = -\frac{\sum_{i=1}^{I}\sum_{j=1}^{J}\left(E_{ij}^+ + \frac{\eta_{ij}}{p_{ave}}\right)p_{ij}V_{ij} + \sum_{m=1}^{M_{ij}}\frac{\mu_m}{p_{ave}}\kappa\Sigma_{fij}A_m}{\sum_{i=1}^{I}\sum_{j=1}^{J}p_{ij}V_{ij}} \tag{3.36}$$

where

$$p_{ij} = \kappa\Sigma_{fij}\phi_{ij}. \tag{3.37}$$

3.2.2.4 Jump Parameter

The jump parameters μ have a unique position in our adjoint solution because its optimal value can only be determined after an initial solution for the adjoint flux ϕ^+ is found. However since we need to assign a value for the jump parameters μ to find a solution for the adjoint flux ϕ^+ in the first place, we need to iteratively solve for its optimal value. So we begin by initially making a guess for the jump parameters μ, solve for the adjoint flux ϕ^+, and then find the optimal jump parameters from another optimality condition.

To locate the optimality condition that can be used to find the value of the jump parameters, we must first understand the role of the jump parameters within the Euler-Lagrange equations. For this purpose, we can take a closer look at the adjoint power equation in Eq. (3.36). It becomes clear in this equation that the jump parameters μ will directly affect the magnitude of Q^+ since it is located in the numerator.

Since μ is a non-negative number by its definition in Eq. (2.44), its value will only increase or decrease the magnitude of the adjoint power, and not change its sign. Since the adjoint power is a constant value determined through Fredholm Alternative, it acts as the eigenvalue for the Euler-Lagrange equation. So modifying the jump parameters will only modify the magnitude of the adjoint power, and consequently modify the magnitude of the adjoint flux solution.

So the most appropriate optimality condition to use for finding the optimal jump parameters is the normalization optimality condition:

$$\int_X \int_Y dxdy \left({\phi^+}^T \frac{\partial L}{\partial k} \phi \right) = \frac{\partial J}{\partial k}. \tag{3.38}$$

In the case where the objective function J does not contain the state variable k, then the optimal junction parameters cannot be determined from this equation, which is the case for the EOC objective function representing a flat burnup. In this scenario, the jump magnitude then becomes irrelevant because the magnitude of the adjoint flux ϕ^+ is inconsequential to the determination of the optimal control. This is because the adjoint flux information is only used in the unconstrained region where we are interested in the gradient $\partial H/\partial u$, and not its magnitude, to find the optimal control. The gradient $\partial H/\partial u$ is paired with a control length used within an iterative scheme to determine the most optimal control that minimizes the Hamiltonian, as discussed with Eq. (2.49).

3.2.3 Solving the Euler-Lagrange Finite-Difference Equations Iteratively

The discretized Euler-Lagrange equation (3.31) can be re-written for a generalized mesh at (i, j) to arrive at the following discretized form:

$$a_{ij}\phi^+_{i-1,j} + b_{ij}\phi^+_{ij} + c_{ij}\phi^+_{i+1,j} + d_{ij}\phi^+_{i,j-1} + e_{ij}\phi^+_{i,j+1} = F^+_{ij}\phi^+_{ij} + S^+_{ij} \tag{3.39}$$

where a_{ij} through e_{ij} are the same as in Eq. (3.16) with $M^+ = M$ and

$$F^+_{ij}\phi^+_{ij} = F^+_0\phi^+_0 V_0, \quad S^+_{ij} = S^+_0 V_0.$$

Then the matrix form of Eq. (3.39) is:

$$M^+\phi^+ = F^+\phi^+ + S^+ \tag{3.40}$$

where the loss term M^+ is the same as the 5-band matrix M in Figure 3.2 since it only contains the diagonal terms in L^+, the production term F^+ is a matrix containing the adjoint production terms, and the adjoint flux ϕ^+ and inhomogeneous adjoint source S^+ are column vectors. To solve the matrix system in Eq. (3.39), the power-source iteration is used to incorporate the inhomogeneous adjoint source term and solve for the adjoint flux. For an initial adjoint flux guess of $\phi^+_0 = 0$, the evolution of the power-source iteration is given by:

$$\begin{aligned}
S^+ &= M^+\phi^+_{p1} \\
S^+ + F^+\phi^+_{p1} &= M^+\phi^+_{p2} \\
S^+ + F^+\phi^+_{p2} &= M^+\phi^+_{p3} \\
&\vdots \\
S^+ + F^+\phi^+_{p(n-1)} &= M^+\phi^+_{pn}
\end{aligned} \tag{3.41}$$

We have introduced a subscript p in Eq. (3.41) to denote that the adjoint flux solution that we are interested in is the particular solution. In theory, the particular solution should propagate through the power-source iteration if we begin with $\phi_0^+ = 0$ as the initial guess, but that is not always the case. Fundamental mode contamination could be introduced into the particular adjoint flux solution during the iterations such that the Fredholm alternative condition in Eq. (2.32) is no longer satisfied in the calculation of Q^+. A method that could be used to remove the fundamental mode contamination during the iteration as proposed by Oblow [38] is to define a contaminated solution ϕ_c^+ to be the solution of Eq. (3.41) and sweep out the contamination by using the Fredholm alternative condition during the power-source iteration. We recall that the Fredholm alternative condition from Eq. (2.32) states that:

$$\left\langle \phi, S^+ \right\rangle = 0 \tag{3.42}$$

where ϕ is the solution from Eq. (3.17):

$$M\phi = F\phi. \tag{3.43}$$

This Fredholm alternative condition cannot be used during the power-source iteration in the form that is in Eq. (3.42). So we find an expression for the Fredholm alternative condition in terms of ϕ_p^+ by using Eqs. (3.41), (3.42) and (3.43) together with the properties of adjoint operators:

$$\begin{aligned}
\left\langle \phi, S^+ \right\rangle = \left\langle \phi, M^+\phi_{p1}^+ \right\rangle = \left\langle \phi_{p1}^+, M\phi \right\rangle = \left\langle \phi_{p1}^+, F\phi \right\rangle = \left\langle \phi, F^+\phi_{p1}^+ \right\rangle = 0 \\
\left\langle \phi, F^+\phi_{p1}^+ \right\rangle = \left\langle \phi, M^+\phi_{p2}^+ \right\rangle = \left\langle \phi_{p2}^+, M\phi \right\rangle = \left\langle \phi_{p2}^+, F\phi \right\rangle = \left\langle \phi, F^+\phi_{p2}^+ \right\rangle = 0 \\
\left\langle \phi, F^+\phi_{p2}^+ \right\rangle = \left\langle \phi, M^+\phi_{p3}^+ \right\rangle = \left\langle \phi_{p3}^+, M\phi \right\rangle = \left\langle \phi_{p3}^+, F\phi \right\rangle = \left\langle \phi, F^+\phi_{p3}^+ \right\rangle = 0 \\
\vdots \quad \vdots \quad \vdots \quad \vdots \quad \vdots \\
\left\langle \phi, F^+\phi_{p(n-1)}^+ \right\rangle = \left\langle \phi, M^+\phi_{pn}^+ \right\rangle = \left\langle \phi_{pn}^+, M\phi \right\rangle = \left\langle \phi_{pn}^+, F\phi \right\rangle = \left\langle \phi, F^+\phi_{pn}^+ \right\rangle = 0.
\end{aligned} \tag{3.44}$$

Now we can implement the Fredholm alternative condition on the j^{th} iteration in the power-source iteration by satisfying:

$$\left\langle \phi, F^{+}\phi_{pj}^{+} \right\rangle = \left\langle \phi_{pj}^{+}, F\phi \right\rangle = \left\langle \phi_{pj}^{+}, \frac{\partial L}{\partial k}\phi \right\rangle = 0. \tag{3.45}$$

This equation will also satisfies the optimality condition in Eq. (2.77) for the depletion optimal control problem. By defining the contaminated adjoint flux solution during the power-source iteration as:

$$\phi_{cj}^{+} = \phi_{pj}^{+} + \alpha\phi_{h}^{+}, \tag{3.46}$$

and inserting it into Eq. (3.45), we obtain the value of α as:

$$\alpha = \frac{\left\langle \phi, F^{+}\phi_{cj}^{+} \right\rangle}{\left\langle \phi, F^{+}\phi_{h}^{+} \right\rangle}. \tag{3.47}$$

Then at the end of every power-source iteration, we can remove the fundamental mode contamination and satisfy the optimality condition (2.77) by performing the following calculation:

$$\phi_{pj}^{+} = \phi_{cj}^{+} - \frac{\left\langle \phi, F^{+}\phi_{cj}^{+} \right\rangle}{\left\langle \phi, F^{+}\phi_{h}^{+} \right\rangle}\phi_{h}^{+}. \tag{3.48}$$

3.3 Fuel Assembly Cross Sections

To perform the calculations for our optimal control problem, we prepare a cross section library for the fuel assemblies that will be used in our study. We have selected the AP600 reactor as our test reactor and CASMO-4 as the lattice physics code to generate our cross section library. CASMO-4 is a multi-group two-dimensional transport code using collision probability calculations developed by Studsvik. It is a production computer code which makes it user friendly and can be readily applied to geometries consisting of cylindrical fuel rods of varying composition in a square

pitch. This makes it a very good candidate for our test reactor.

The cross section generation with CASMO-4 was based on the AP600 reactor parameters such as the operating temperature, pressure and power density. The core is rated at 1933 MW thermal power with an active core height of 12 feet. Each fuel assembly is modeled with fuel rods, BP rods, instrument tubes and guide tubes that meet the specifications from the SSAR. The fuel assembly designs were based on the available fuel assembly arrangements in the SSAR and extended to include combinations of fissile enrichment of 2 wt%, 2.5 wt% and 3 wt% with the number of BP rods equal to 0, 4, 8, 9, 10, 12, 16 and 24. The BPs were assigned a natural boron content of 3.845 wt%. The purpose of our extended library is to provide more data points during the iterative numerical calculations and help the problem converge more smoothly. The fuel assemblies were depleted over fuel burnups of 0, 0.5, 1 through 20 MWD/kgHM in increments of 1.0 MWD/kgHM. Branch calculations were also performed for different critical boron concentrations between 0 and 1,300 ppm. All this makes up our four-dimensional cross section library based on fissile enrichment, number of BPs, fuel burnup and critical boron concentration.

3.3.1 Thermal Feedback Correction

For the treatment of thermal feedback in our fuel assembly cross sections, we apply a correction to the macroscopic cross sections after the power distribution has been determined during our solution of the neutron diffusion equations. We have chosen to represent the Doppler feedback and moderator density feedback in our calculations, representing the two main feedback effect in PWRs using methods applied in the Westinghouse ANC global code. For the Doppler model, we calculate the effects of Doppler on the fast absorption cross section by

$$\Sigma_{a1}(P) = \Sigma_{a1}(P=1) + \frac{a_1 P}{1 + a_2 P} - \frac{a_1}{1 + a_2}, \tag{3.49}$$

where P is the normalized power density and a_1 and a_2 are fitted parameters which are obtained from the ANC code.

For the moderator density feedback, the corrections are made based on the differences between the actual water density derived from the enthalpy rise from the reference values that were used during the cross section generation. We begin by finding the enthalpy rise in the channel based on the relative power and then calculating the average enthalphy, H. This allows us to calculate the water density using a quadratic fitting using steam tables:

$$\rho(H) = a + bH + cH^2 \tag{3.50}$$

where a, b and c are fitting parameters. Once we have the water densities, we can find the changes in the water and boron number densities as given by

$$\delta N^w = 0.03344 \cdot (l_c \cdot (\rho - \rho_{ref}) + l_r \rho), \quad \text{and} \tag{3.51a}$$

$$\delta N^B = 0.03344 \cdot (l_c + l_r) \cdot \rho \cdot f \cdot ppm \cdot [(B^{10})/19.78], \tag{3.51b}$$

where $B^{10} = 19.90$ represents the isotope content in natural boron, l_c is the liquid area per unit area of the cell, l_r is the correction to the wet fraction to account for BP rods, the factor 0.03344 is the conversion between atoms and grams for water (assuming the microscopic cross sections will be in barns), and the factor f=3.295x10^{-7} converts from parts per million to actual grams of B^{10}. Then the calculation for the modified absorption cross sections due to moderator density feedback is given by:

$$\Sigma_a = \Sigma_a + \delta N^w \sigma_a^w + \delta N^B \sigma_a^B. \tag{3.52}$$

3.4 Verification of Discretized Forward Equations and Cross Section Library

For verification of the discretized forward equations, cross section library generation and the thermal feedback modeling, we have benchmarked the first cycle fuel loading in the AP600 reactor using the information and results from the SSAR as well as results obtained from the APA code package. The APA package is the Westinghouse core design system comprising the ALPHA, PARAGON and ANC codes. PARAGON is the lattice physics code that generates the cross section libraries and ANC is the global code that runs the core simulations. ALPHA is the script that sets up the input files for PARAGON and communicates the appropriate data to ANC. The APA package is well suited to simulate PWR operations and its neutronic code employs a nodal expansion method for calculating core reactivity and assembly-wise data including power and burnup distributions.

Using the fuel loading design of the AP600 reactor from the SSAR, the eight fuel assembly designs that are used in the reactor were modeled with both CASMO-4 and PARAGON to generate the burnup-dependent fuel assembly cross sections. Due to the lack of information on the reflector details of the reactor in the SSAR, both in the radial and axial reflectors, we created our own model for the reflectors. The reflector models were based on a mixture of steel and water. We then applied the CASMO-4 cross section libraries to our DMCO code and solved the set of forward equations (neutron diffusion, power normalization and fuel burnup equations) for the first cycle of the reactor. Likewise we performed the core simulation with the ANC code using the PARAGON cross section libraries for the same first cycle run. We performed our benchmarking exercise by comparing the BOC relative power distribution in Figure 3.4 and the critical boron concentration as a function of fuel burnup in Figure 3.5.

The relative fuel assembly power distributions for the three cases show reasonable

0.949 1.013 0.902				
0.865 0.942 0.854	0.986 1.044 0.942			
1.038 1.090 0.998	0.932 0.999 0.930	1.053 1.092 1.017		
0.991 1.046 1.000	1.252 1.284 1.220	0.957 0.999 0.964	1.057 1.057 1.031	
1.130 1.141 1.115	0.996 1.027 1.016	1.080 1.076 1.062	0.944 0.937 0.962	1.260 1.174 1.255
1.024 1.015 1.047	1.143 1.107 1.143	1.058 1.035 1.083	0.955 0.897 0.950	0.771 0.720 0.784
1.127 1.099 1.135	0.974 0.977 1.028	1.006 0.959 1.004	0.673 0.632 0.679	

A B C	A : ANC, k = 1, CB = 962ppm B : SSAR, k = 1, CB = 1020ppm C : DMCO, k=1, CB = 917ppm

Figure 3.4: Relative power distribution benchmarking for AP600

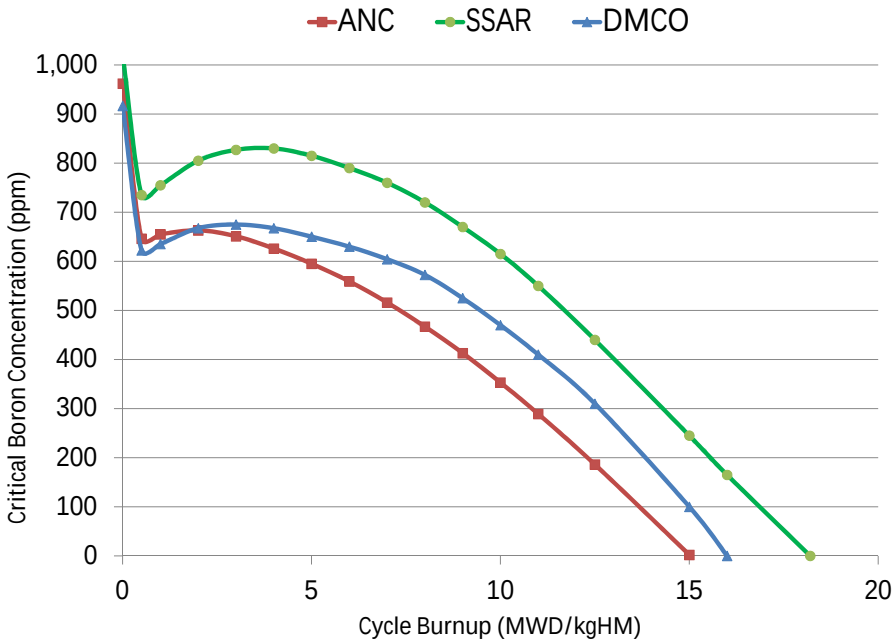

Figure 3.5: Critical boron concentration benchmarking for AP600

agreement, with the most distinct difference being the peak power assembly with relative power of 1.252 in the SSAR located near the mid-core is shifted to the periphery in the ANC and DMCO simulations. This is mainly attributed to the difference in the reflector cross sections used in the ANC and DMCO simulations, which apparently are different from those used in the SSAR calculation. Otherwise the maximum and minimum assembly power values from the DMCO and ANC cases agree within 5%, with larger differences observed from the SSAR results. The critical boron letdown curves over the fuel burnup also shows reasonable agreement between the DMCO and ANC results in Figure 3.5, but larger differences with that of the SSAR data, which appear to represent a more reactive core. With differences that could be attributed to the reflector cross sections and cross section data library among other reasons, we are satisfied enough to say that our discretized forward equations, cross section libraries and feedback model are within an acceptable tolerance level from the results obtained from SSAR and ANC.

3.5 Verification of Discretized Euler-Lagrange Equations

Next we wish to verify the discretized Euler-Lagrange equations and the supporting adjoint equations by benchmarking the results from our code with a simplified analytical problem that allows us to solve for the adjoint variables by hand. For this purpose, we employ a one-dimensional, one-group problem in the axial geometry z of the reactor without any reflectors. We choose the BP macroscopic cross section Σ_{BP} as the control and select the maximization of reactivity represented by the multiplication factor k as the objective function. We perform the optimization for the steady-state problem, which will simplify the equations without time dependence and the burnup variable in our equations. The reader is referred to Section 2.4 where the optimality conditions for this problem were formulated.

3.5.1 Simplified Analytical Problem in One-Group and 1-D

The simplified analytical problem formulation begins with the objective of the problem defined as

$$J = -k \tag{3.53}$$

where we seek to maximize the multiplication factor k with a negative sign introduced in the objective function. The problem is constrained by the one-group one-dimensional neutron diffusion equation

$$L\phi = D\frac{d^2\phi}{dz^2} - \Sigma^*\phi = 0 \tag{3.54}$$

where

$$\Sigma^* = \Sigma_a^0 + \Sigma_{BP} - \frac{\nu\Sigma_f}{k}. \tag{3.55}$$

For this analytical problem, we represent the control Σ_{BP} explicitly in the macroscopic absorption cross section Σ_a and lump the other absorption cross sections as Σ_a^0.

The problem is also constrained by the power normalization equation:

$$P_{tot} = \int_0^L dz\ \kappa\Sigma_f\phi \equiv L \tag{3.56}$$

and the power peaking inequality constraint:

$$S(z) = \frac{\kappa\Sigma_f\phi(z)}{p_{ave}} - p_{max} \leq 0. \tag{3.57}$$

By introducing the power density variable Q representing the sum of power over core height z:

$$Q(z) = \int_0^z dz'\ p(z') = \int_0^z dz'\ \kappa\Sigma_f\phi(z'), \tag{3.58}$$

the power normalization in Eq. (3.56) is converted into a first order differential

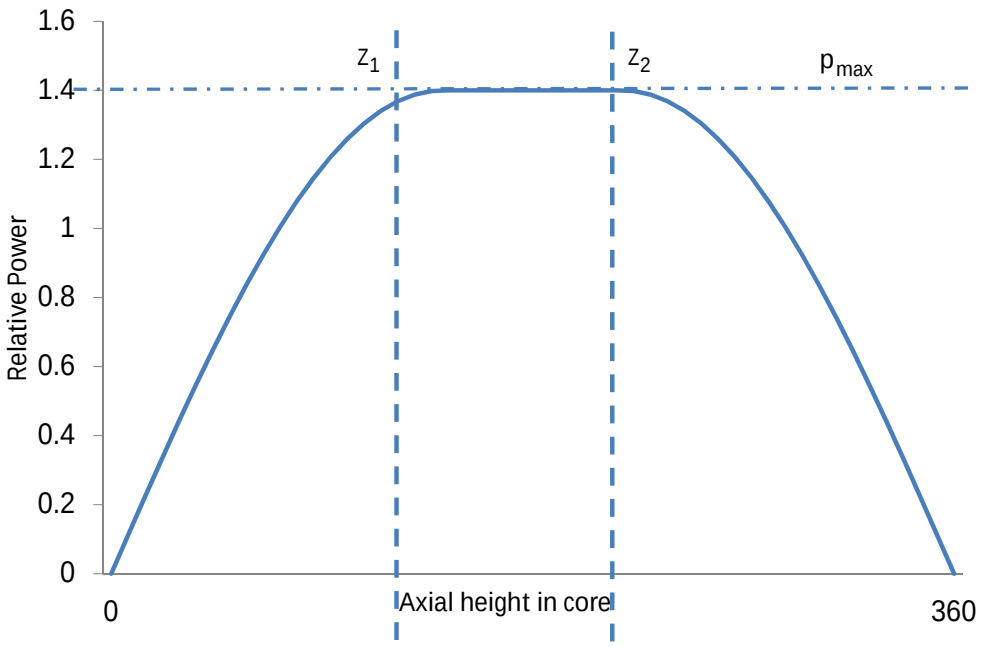

Figure 3.6: Optimal power trajectory for 1-D problem

equation:

$$\frac{dQ(z)}{dz} = \kappa\Sigma_f\phi(z). \tag{3.59}$$

3.5.1.1 Solution for the Forward Variables

We assume the optimal solution for the power trajectory that satisfies the power peaking inequality constraint of Eq. (3.57) has one constrained region in the middle of the core as depicted in Figure 3.6. The power is on the power peaking factor limit p_{max} between z_1 and z_2 which is the constrained region we define.

From the optimal power trajectory, we can obtain the analytical flux solution that satisfies the one-group one-dimensional neutron diffusion equation (3.54) as:

$$\begin{aligned}
\phi(z) &= \frac{p_{max}}{\kappa\Sigma_f} sinBz, && 0 \le z \le z_1 \\
\phi(z) &= \frac{p_{max}}{\kappa\Sigma_f}, && z_1 \le z \le L - z_1 \\
\phi(z) &= \frac{p_{max}}{\kappa\Sigma_f} sinB(L - z), && L - z_1 \le z \le L
\end{aligned} \tag{3.60}$$

where z_2 is $L - z_1$ by the symmetry of the problem and the optimal buckling B^2 is given by:

$$B^2 = \left(\frac{\pi}{2z_1}\right)^2 = -\frac{\Sigma^*}{D}. \tag{3.61}$$

Now that we have an analytical solution for the flux, we can use it in the power normalization equation to find the optimal z_1 location of the jump term:

$$2\int_0^{z_1} dz \frac{p_{max}}{\kappa\Sigma_f} sinBz + \int_{z_1}^{L-z_1} dz \frac{p_{max}}{\kappa\Sigma_f} = L. \tag{3.62}$$

Solving for z_1 yields the optimal jump location:

$$z_1 = \frac{L}{2 - \left(1 - \frac{2}{\pi}\right)} \left(1 - \frac{1}{p_{max}}\right). \tag{3.63}$$

3.5.1.2 Solution for the Adjoint Variables

Using the method of Lagrange multipliers as derived in Section 2.4, we arrive at the Hamiltonian for this steady-state optimal control problem in one-dimensional slab as:

$$H = -k + \int_0^L dz \left[\phi^+ L\phi + Q^+ \left(\kappa\Sigma_f\phi - \frac{dQ}{dz}\right) + \eta^+ S\right] \tag{3.64}$$

where we have dropped the transpose sign of ϕ^+ in Eq. (3.64) because it is no longer a vector of two-groups, but just a scalar function.

The resulting optimality conditions obtained via the calculus of variations are the same form as the optimality conditions derived in Section 2.4.1 for the steady-state problem except we express them here in one-dimensional slab as:

$$\int_0^L \phi^+ \left(\frac{\nu\Sigma_f}{k^2}\right) \phi = -1, \tag{3.65}$$

$$\frac{dH}{du} = -\phi^+\phi = 0. \tag{3.66}$$

The Euler-Lagrange equation is now written with the jump conditions represented as a delta function in the continuous form, which is equivalent to the jump conditions derived in the discretized Euler-Lagrange equations in Eq. (3.31):

$$-L^+\phi^+ = -D\frac{d^2\phi^+}{dz^2} + \Sigma^*\phi^+ = \left(Q^+ + \frac{\eta^+}{p_{\text{ave}}}\right)\kappa\Sigma_f + \mu_1\kappa\Sigma_f\delta(z-z_1) + \mu_2\kappa\Sigma_f\delta(z-z_2) \tag{3.67}$$

where the adjoint operator L^+ is just the same as the L operator for our one-group problem. We represent two jump terms in the Euler-Lagrange equation as part of our analytical solution which consists of one constrained region in the middle of the reactor.

For regions where the inequality constraint is active, Eq. (3.66) requires the optimal ϕ^+ to vanish only on the constrained region [39]:

$$\phi^+ = 0. \tag{3.68}$$

Then, the value of η^+ in the Euler-Lagrange equation is given by:

$$\begin{aligned} \eta^+(z) &= 0 && p(z) < p_{max}, \\ &= -Q^+ p_{ave} && p(z) = p_{max}. \end{aligned} \tag{3.69}$$

where the value of η^+ in the constrained region was obtained using Eqs. (3.33) and (3.68) with E^+=0 and ϕ^+=0 respectively. We provide here an analytical solution for the Euler-Lagrange equation, which is a general solution to the inhomogeneous diffusion equation:

$$\begin{aligned} &\phi^+(z) = -\frac{Q^+\kappa\Sigma_f}{\Sigma^*}\left[sinBz + cosBz + 1\right], && 0 \le z \le z_1 \\ &\phi^+(z) = 0, && z_1 \le z \le L - z_1 \\ &\phi^+(z) = -\frac{Q^+\kappa\Sigma_f}{\Sigma^*}\left[sinB(L-z) + cosB(L-z) + 1\right]. && L - z_1 \le z \le L \end{aligned} \tag{3.70}$$

The jump terms μ in the Euler-Lagrange equation does not appear in the piecewise solution of ϕ^+ in Eq. (3.70) explicitly, but through the proper values of Q^+ and B. We are able to solve for Q^+ analytically by using our analytical solution of ϕ and ϕ^+ in the normalization condition in Eq. (3.65) to yield:

$$Q^+ = \frac{D}{p_{max}\,(1/B^3 - z_1/B^2)}. \tag{3.71}$$

Finally, we obtain the value of μ by using the Fredholm Alternative condition of the Euler-Lagrange equation since it takes the form of an inhomogeneous diffusion equation, which states that:

$$< \phi, S^+ >= \int_0^L dz \left[\left(Q^+ + \frac{\eta^+}{p_{\text{ave}}} \right) \kappa\Sigma_f\phi + \mu_1\kappa\Sigma_f\phi\delta(z - z_1) + \mu_2\kappa\Sigma_f\phi\delta(z - z_2) \right] = 0. \tag{3.72}$$

Inserting η^+ from Eq. (3.69) and ϕ from Eq. (3.60) into Eq. (3.72), we find the jump parameter μ in terms of Q^+:

$$Q^+ = -\frac{\mu_1\kappa\Sigma_f\phi(z_1) + \mu_2\kappa\Sigma_f\phi(z_2)}{2\int_0^{z_1} dz\kappa\Sigma_f\phi} = -\frac{\mu\kappa\Sigma_f\phi(z_1)}{\int_0^{z_1} dz\kappa\Sigma_f\phi} = -\mu B \tag{3.73}$$

$$\Rightarrow \mu = -\frac{Q^+}{B} \tag{3.74}$$

where we represent one value for μ=μ_1=μ_2 as a result of the symmetry of the problem.

3.5.1.3 Solution for the Optimal Control

With the solution for the forward and adjoint variables known for our simplified analytical problem, we can find the optimal control solution in a similar way that was formulated in Section 2.4.3 when we described the control formulation of our direct adjoining method. The only difference is instead of using the gradient method in the unconstrained region, we apply the bang-bang control method, which is ideal for an

analytical solution. Recall that since the control is linear in the Hamiltonian, it does not appear in the control optimality condition (3.66) for us to derive its value from

$$\frac{dH}{du} = -\phi^{+}\phi. \tag{3.75}$$

Instead we use the control optimality condition as a switching function to assign bang-bang controls which will minimize the Hamiltonian. This is in agreement with the goal of minimizing our Hamiltonian defined in Eq. (3.64) and will facilitate the optimization of the objective function through the selection of the control in the unconstrained region. In bang-bang control problems, the optimal control is determined by the sign of the switching function:

$$\Sigma_{BP}^{\overline{\Gamma}} = \Sigma_{max}, \qquad -\phi^{+}\phi < 0 \tag{3.76}$$

$$\Sigma_{BP}^{\overline{\Gamma}} = \Sigma_{min}. \qquad -\phi^{+}\phi > 0 \tag{3.77}$$

In the constrained region, we use the inequality constraint equation (3.57) to obtain the control for the region. Since the control Σ_{BP} does not appear in the inequality constraint equation, we take the spatial derivative of the equation until the control variable appears. Taking the first spatial derivative yields:

$$\frac{dS}{dz} = \kappa\Sigma_f \frac{d\phi}{dz} = 0 \tag{3.78}$$

which fails to yield the control. So we take another spatial derivative and apply the neutron diffusion equation from Eq. (3.54) to yield:

$$\frac{d^2S}{dz^2} = \kappa\Sigma_f \frac{d^2\phi}{dz^2} = \kappa\Sigma_f \left(\frac{\Sigma^*\phi}{D}\right) = \frac{\kappa\Sigma_f\phi}{D}\left(\Sigma_a^0 + \Sigma_{BP} - \frac{\nu\Sigma_f}{k}\right) = 0. \tag{3.79}$$

Solving for the optimal control in the constrained region yields:

$$\Sigma_{BP}^{\Gamma} = \frac{\nu\Sigma_f}{k^{opt}} - \Sigma_a^0. \tag{3.80}$$

Equation (3.80) is simply the flat flux condition where the infinite multiplication factor k_∞ is the optimal effective multiplication factor k^{opt}. The condition of finding the control in the constrained region in Eq. (3.80) is dependent on knowing the optimal effective multiplication factor k^{opt}, which is also the objective function of the problem. We can solve for k^{opt} by using the optimal buckling equation (3.61) for the unconstrained region to get:

$$B^2 = \left(\frac{\pi}{2z_1}\right)^2 = -\frac{\Sigma^*}{D} = -\frac{\Sigma_a^0 + \Sigma_{BP}^{\overline{\Gamma}} - \nu\Sigma_f/k^{opt}}{D}. \tag{3.81}$$

Using the optimal control solution found for the unconstrained region via the bang-bang method, we obtain the optimal effective multiplication factor by:

$$k^{opt} = \frac{\nu\Sigma_f}{DB^2 + \Sigma_a^0 + \Sigma_{BP}^{\overline{\Gamma}}}. \tag{3.82}$$

3.5.2 Benchmarking Analytical and Numerical Solution

To quantify the analytical results and provide a benchmark for our numerical calculations of the Euler-Lagrange equations, we calculate the solution for the forward state and adjoint variables in the one-group one-dimensional optimal control problem with some representative values of the macroscopic cross sections. The total power will represent the total height in the core for the one-dimensional problem. The macroscopic cross section values and core parameters are included in Table 3.1. We summarize the results of the analytical model by plotting the analytical solution for the neutron flux, adjoint flux, switching function and control in Figures 3.7 and 3.8.

The results from the numerical implementation of our code shows a very good

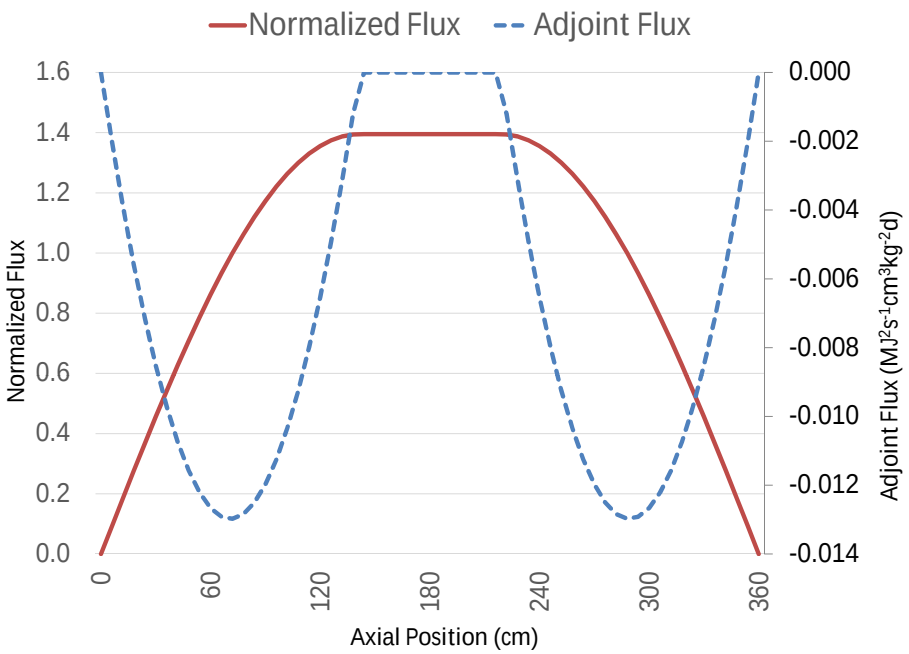

Figure 3.7: Analytical ϕ and ϕ^+ solution for 1-D

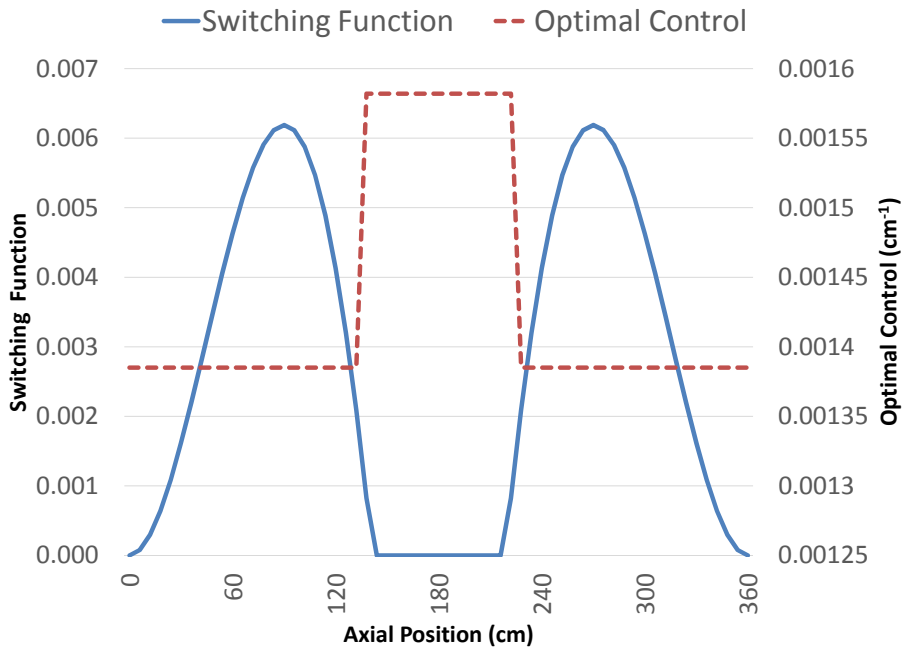

Figure 3.8: Analytical switching function and optimal control solution for 1-D

Table 3.1: Core parameters in one-group 1-D problem

Core Parameters
$D = 1.59\ cm$
$\Sigma_a^0 = 2.045 \times 10^{-2}\ cm^{-1}$
$\nu\Sigma_f = 2.471 \times 10^{-2}\ cm^{-1}$
$\Sigma_{max} = 1.761 \times 10^{-3}\ cm^{-1}$
$\Sigma_{min} = 1.385 \times 10^{-3}\ cm^{-1}$
$L = 360\ cm$
$P_{max} = 1.4$

Table 3.2: Benchmarking analytical and numerical solutions for 1-D

	Analytical Solution	**Numerical Solution**
Q^*	$-2.720 \times 10^{-6}\ cm^{-2}$	$-3.455 \times 10^{-6}\ cm^{-2}$
η	$2.720 \times 10^{-6}\ cm^{-2}$	$3.455 \times 10^{-6}\ cm^{-2}$
μ	$2.451 \times 10^{-4}\ cm^{-1}$	$2.707 \times 10^{-4}\ cm^{-1}$
z_1	141.5 cm	138 cm
z_2	218.5 cm	222 cm
J	k=1.122	k=1.119

agreement with the analytical results, which converged after 4 iterations. The main cause for the differences in the analytical and numerical results can be attributed to the location of the junction. Since we are using mesh sizes of 6.0 cm in our numerical finite-differencing scheme, we can only allocate the junction position in increments of 6.0 cm. The number of iterations it took were highly dependent on the selection method that was employed to determine the junction distributions, which will be discussed more in the next section. We summarize the benchmarking of the discretized Euler-Lagrange equations in this chapter by comparing the converged solution for the adjoint flux, adjoint power and jump parameters with the analytical solution in Figure 3.9 and Table 3.2.

3.6 Selection Method of Junction Distributions

With the method of directly adjoining the inequality constraint, the core will be divided into regions of constrained and unconstrained fuel assemblies. The constrained

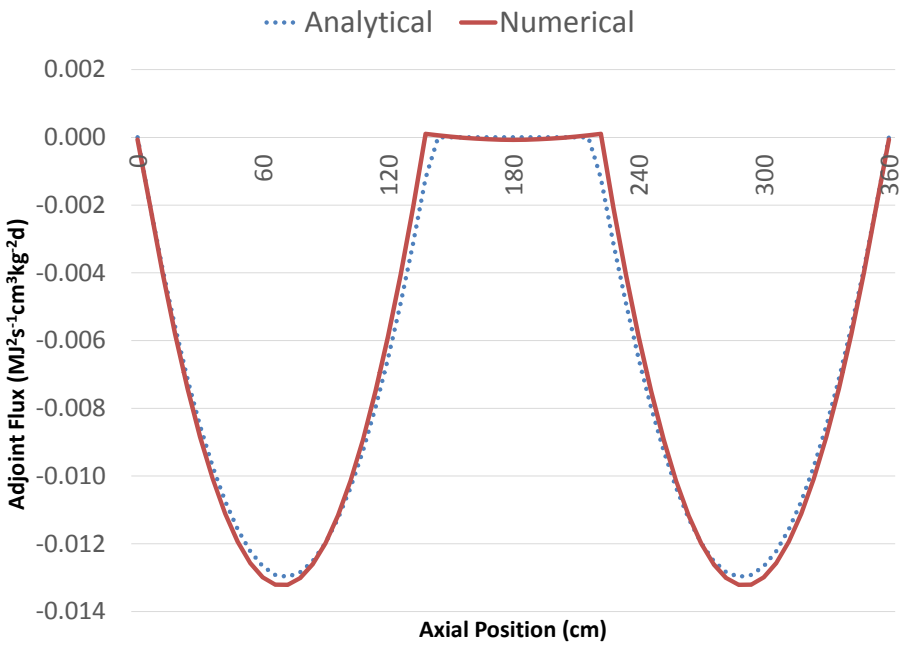

Figure 3.9: Benchmarking analytical and numerical adjoint flux for 1-D

regions represent the fuel assembly locations that will experience the maximum allowable power peaking values. These constrained regions could be distributed in many different ways, and they need to be determined before we begin to solve the Euler-Lagrange equations which require information on the junctions that occur at the boundaries between the constrained and unconstrained regions. This represents the outer loop around the optimization scheme we have devised in Chapters 2 and 3 because we do not have prior knowledge of the optimal junction distribution and need to rely on an iterative approach to find an acceptable junction distribution.

An important lesson we learn from the analytical solution is that the locations of the junctions is strongly coupled with the power peaking factor in the core. This is evident from the solution of the optimal junction locations z_1 in Eq. (3.63):

$$z_1 = \frac{L}{2 - \left(1 - \frac{2}{\pi}\right)} \left(1 - \frac{1}{p_{max}}\right).$$

We may interpret Eq. (3.63) differently by saying that given a location of the junction

z_1, we will obtain a unique value of p_{max} in the core. So the selection of a certain junction distribution will determine the maximum power peaking value in the core. This represents the criterion for stopping the outer loop iteration on the junction distribution which occurs when the junction distribution yields a maximum power peaking that is acceptable.

The method that we have adopted to determine the junction distribution iteratively is by defining constrained regions in the core that are above a determined fraction of the power peaking factor in the initial fuel loading of that iteration. This is a naturally good idea because we are defining constrained regions based on the highest power fuel assemblies in the core. We have found that a fraction between 85% to 95% of the power peaking factor in the initial fuel loading of that iteration yields a more predictable convergence pattern to the desired power peaking factor in the core. A smaller fraction than 85% may create larger changes in the junction distribution between iterations, that may cause convergence problem.

To illustrate this method, we use the example of finding the optimal z_1 location in a one-dimensional problem with a desired $p_{max} = 1.4$. Beginning with a flat distribution of the control in the core, the power peaking factor determined from the forward solution of the neutron diffusion equation is 1.65. Using the fraction of 95% on 1.65 gives 1.57. Thus we assign all the meshes with the relative power distribution ≥ 1.57 to the constrained region and the rest to the unconstrained region. Solving the Euler-Lagrange equation with this junction distribution and finding the new control suggestion, we obtain a new power peaking factor for the updated controls, which is 1.51. Since we have not achieved the desired power peaking factor of 1.4, we repeat the process with a new junction distribution obtained with the next power peaking limit of 95% from 1.51, which is 1.43. This exercise goes on until we finally arrive at the optimal z_1 location that yields the desired power peaking factor. The fraction used to obtain the power peaking limit can be varied by smaller amounts when we

approach the desired power peaking factor for a more accurate solution of the junction z_1.

CHAPTER IV

Results for Multi-Control Optimization in PWRs

We are now in a position to apply the numerical equations and iterative scheme that we developed in Chapters 2 and 3 on a few test cases representing two-group, two-dimensional problems over a full depletion cycle. In this chapter, we have applied the DMCO code to automate the optimization process and produce fuel loading designs that meet the power peaking factor constraint and have a flatter EOC fuel burnup profile so that the overall discharge burnup can be maximized. This promotes higher energy production with the same fuel loading and extends the fuel cycle. Initially, we tackle the challenge of satisfying the power peaking constraints throughout the cycle with only the control at BOC, which represents one of the bigger challenges in PWR optimal control problems. Giving this challenge its proper due attention, we use actual numerical results and explain how we approach to satisfy the power peaking constraint throughout the cycle.

- In Case A, we demonstrate how the power peaking factor is controlled in a quasi-steady state step.
- Then in Case B we demonstrate how we may control the power peaking factor during the cycle, by using the methodology of Case A in a depletion calculation.
- For the verification of our Case B results, we run Case C without power peaking factor control with the same initial control as in Case B.

To show the multi-control capability of the DMCO code, we perform Case A with number of BP rods as the control, and Cases B and C with fissile enrichment as the control. Next we present the test cases that were used to develop our final multi-control fuel loading design in two stages of control optimization.

- In Case D, we perform a BP control optimization by selecting a uniform fissile enrichment distribution in a general checkerboard pattern.
- Finally in Case E, we perform a fissile enrichment control optimization by using the optimal BP distribution from Case D. This case will represent our final multi-control fuel loading design featuring the optimal fissile enrichment and number of BP rods using our optimization code DMCO.

Cases D and E will be benchmarked with the first cycle AP600 performance by using the same average fissile enrichment in the core. The controls will be rounded off and grouped into a few fuel assembly types, that are comparable to the number of fuel assembly types used in the AP600 design.

4.1 Quasi-Steady State Power Peaking Control (Case A)

The quasi-steady state power peaking control refers to the ability of the DMCO code to satisfy the power peaking inequality constraint for any particular time step. Recalling that the depletion cycle is divided into intervals of time where each interval is treated as a quasi-steady state, we use the same calculational path that was described in the steady-state iteration in Figure 2.2. Here we will present a two-group two-dimensional test case and explain in detail how the power peaking constraint is satisfied iteratively on the quasi-steady state step.

For this test case, we begin with a uniform distribution of 2.2wt% fissile enrichment and eight BP rods in each fuel assembly. The control that will be employed for this test case is the BP number density, representing the number of BP rods in

each fuel assembly. We begin with a relative assembly power distribution in the core with a maximum value of 2.026 as shown in Figure 4.1. To select the junction distribution for this iteration, a fraction setting of 90% of the power peaking factor was selected as described in Section 3.6, which comes out to 1.823. Then the constrained regions are defined as the fuel assembly regions that are equal to or greater than this value, and the rest are defined as unconstrained regions. In this example, the central fuel assemblies will be selected as the constrained regions because that is where the maximum power distribution occurs. The junction distribution for this iteration is presented in Figure 4.2 where constrained regions are labeled as index 2 and unconstrained regions are labeled as 0.

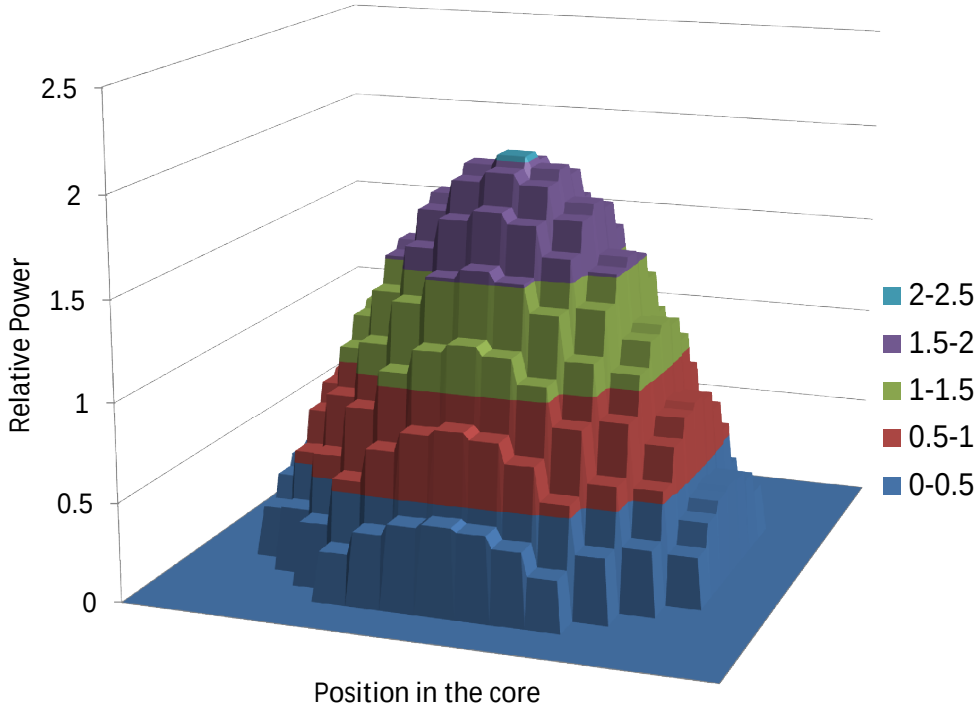

Figure 4.1: Initial relative power distribution for Case A

With the junction distributions defined as in Figure 4.2, the Euler-Lagrange equation is solved to obtain the solutions of the adjoint variables which are used to build the normalized search direction that is shown in Figure 4.3. The overall search direction provides information on how to insert or remove controls in the fuel assemblies

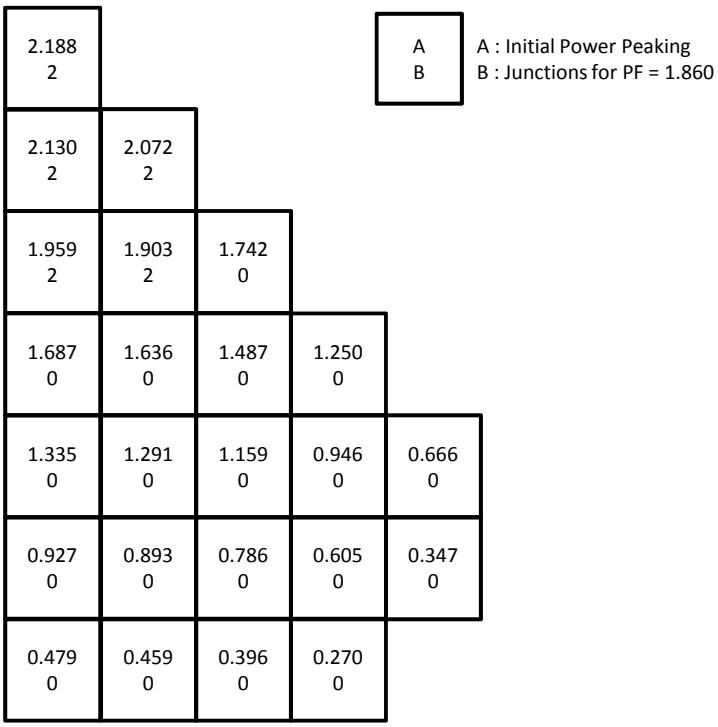

Figure 4.2: Junction selection on first iteration for Case A

that will minimize the Hamiltonian and optimize the objective function. Since we are using the objective of maximizing the reactivity for the steady-state problem, the search direction in Figure 4.3 suggests that we remove the BP rods in the periphery of the core, where the unconstrained regions are defined. Removing BP rods in those fuel assemblies will increase the reactivity in the core as it translates to less poison and higher neutron flux in the core. Since the search direction provides important information on the direction but not the magnitude of the control selection, a simple control length search is performed using the bi-section method according to Eq. (2.50) by testing a few control length values and choosing the one that best minimizes the objective function.

In the central part of the core where the constrained regions are located, the search direction is not used because the inequality constraint is active in that region. So the control is calculated from Eq. (2.63) that was formulated using Newton's

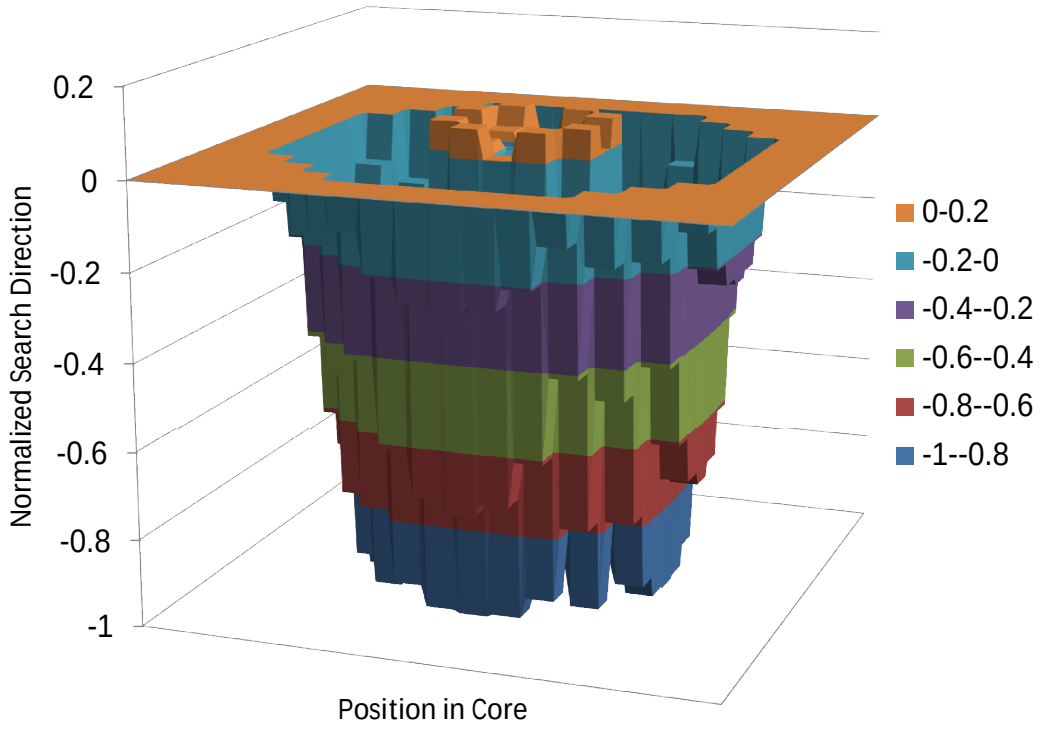

Figure 4.3: Normalized search direction on first iteration for Case A

method, essentially yielding the control that achieves a flat flux distribution in the constrained regions. The result of the optimal control suggestion in both constrained and unconstrained regions after the first iteration is presented in Figure 4.4. The term δu in the figure reflects the calculation of the control using the search direction in the unconstrained region, and the Newton step formulation in the constrained region.

Making the suggested changes to the control for this iteration and repeating the same procedure as explained here and summarized in Figure 2.2, we finally arrive at the optimal control distribution of the BP number density summarized in Figure 4.5. The final design shows that BP rods are removed from the periphery of the core and added to the middle of the core, promoting a flatter power distribution in the middle of the core with a peaking factor of 1.299 (Figure 4.6). We also see an improvement in the objective function k_{eff} from 1.115 to 1.119 from the initial control estimate. To a large degree, the improvement in the objective function is influenced by the magnitude of the control length selected in the unconstrained regions. A larger

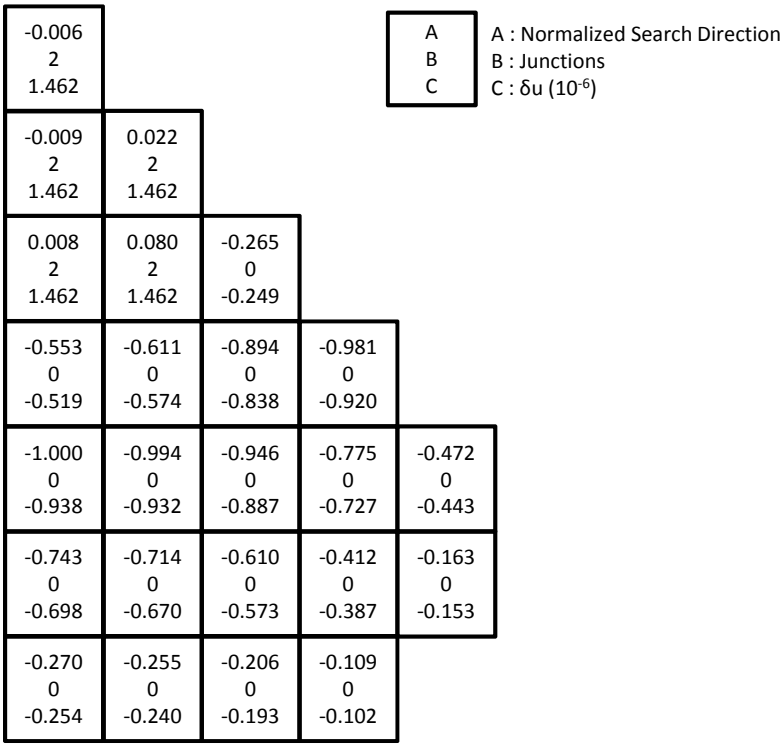

Figure 4.4: δu calculation on first iteration for Case A

control length generally reflects a larger improvement in minimizing the Hamiltonian and the objective function, but this has to be done in balance to satisfying the power peaking factor constraint in the constrained regions. Figure 4.7 shows the convergence of the power peaking factor in the core representing the progression of the junction selection during the iterations.

4.2 Power Peaking Control during Depletion (Cases B and C)

The next test case we present demonstrates how we may control the power peaking during depletion with the control variable at BOC. As we described in Section 2.5.2, we perform the quasi-steady state power peaking control during the forward depletion solution to build a desirable burnup path. Then this information is used in the adjoint depletion calculations which propagates back in time from EOC to BOC. Then we

6.218 7.479				
6.218 7.473	6.218 7.162			
6.218 7.044	6.218 6.575	6.218 6.466		
6.218 6.754	6.218 6.660	6.218 6.478	6.218 7.447	
6.218 6.939	6.218 6.926	6.218 3.127	6.218 3.256	6.218 4.185
6.218 3.666	6.218 3.661	6.218 3.718	6.218 4.390	6.218 5.474
6.218 5.107	6.218 5.143	6.218 5.304	6.218 5.715	

A
B

A : Initial Control (10^{-6})
B : Converged Control (10^{-6})

Figure 4.5: Initial and optimal BP number densities for Case A

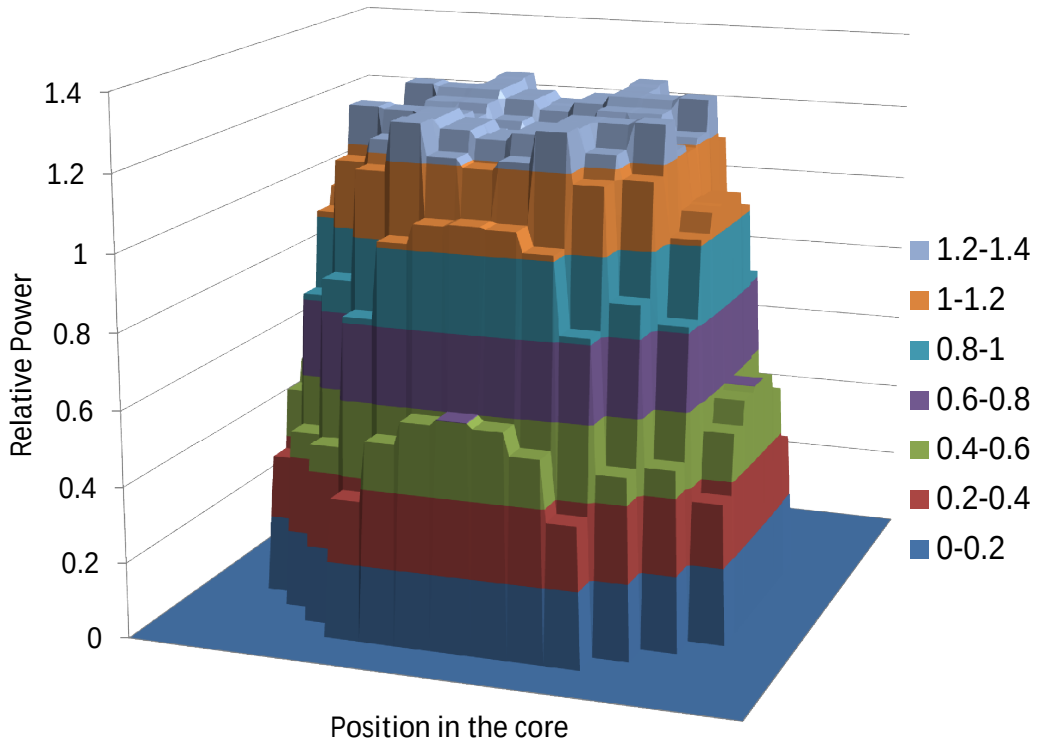

Figure 4.6: Optimal relative power distribution with peaking factor 1.299 for Case A

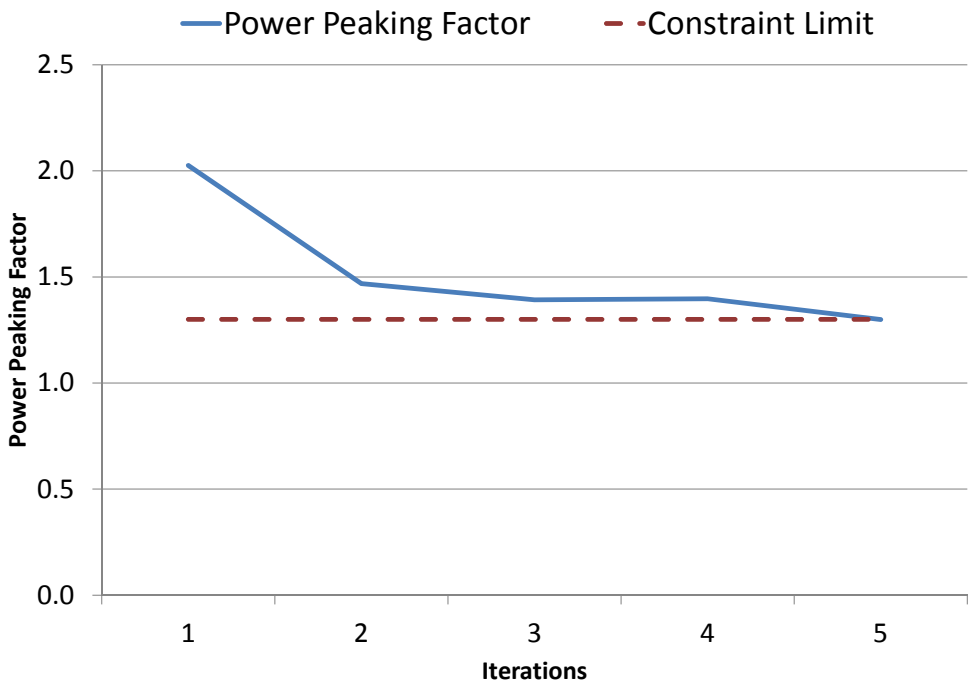

Figure 4.7: Power peaking factor and constraint limit p_{max}=1.3 for Case A

calculate the search direction with the gradient $\partial H/\partial u$ to find the suggested control for the next iteration.

To test this method, we perform two test cases beginning from the same initial loading. Case B demonstrates the power peaking control during depletion as described in the depletion optimal control flowchart in Figure 2.3. Case C demonstrates a regular forward depletion calculation followed by the backwards adjoint depletion calculation, without using the additional quasi-steady state power peaking control as in Case B. The results from both test cases are compared to illustrate the effects of our depletion control approach, particularly on the search direction, maximum power peaking factor and the optimal control.

For these two test cases, we choose to use the fissile U^{235} number densities as the control and begin with a fuel loading that does not have a power peaking violation at the BOC. Instead the power peaking violations occur somewhere in the middle of the cycle. The reason for this is to show the capability of controlling power peaking

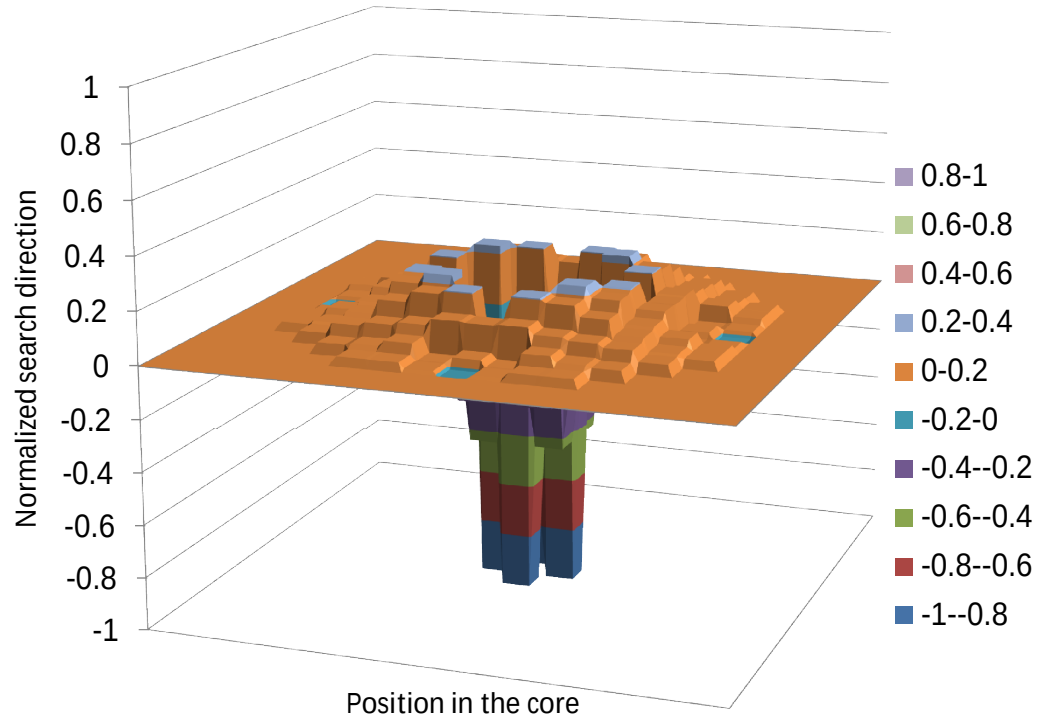

Figure 4.8: Normalized search direction for Case B

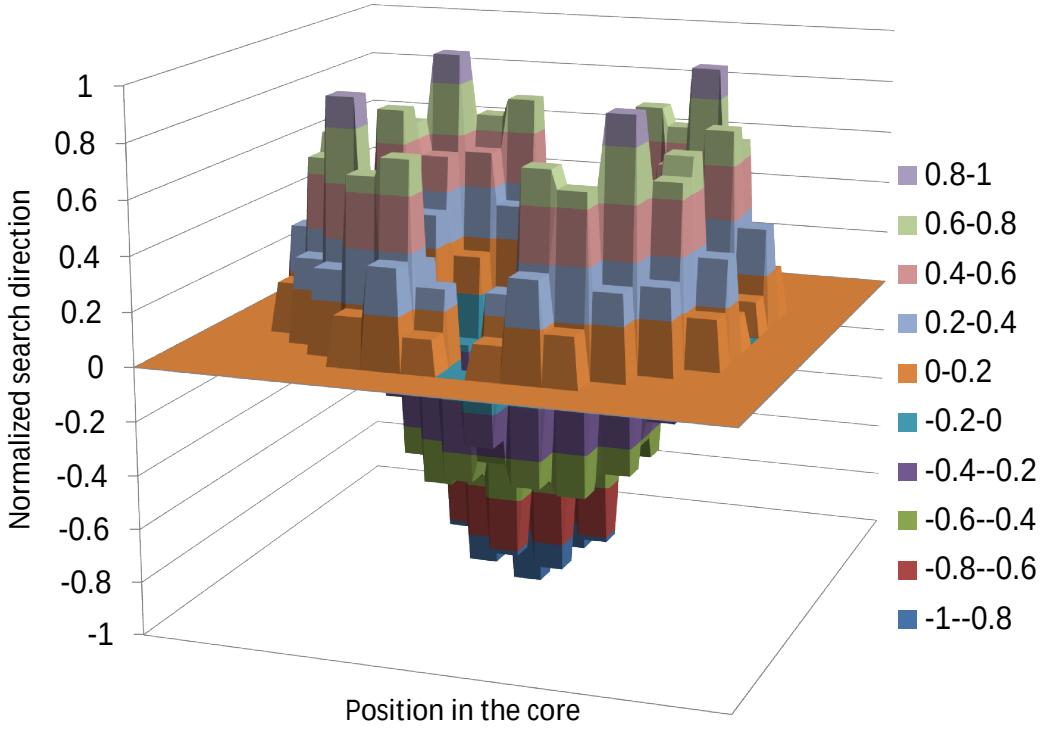

Figure 4.9: Normalized search direction for Case C

Table 4.1: Objective function comparison for Cases B and C

	Objective Function
Initial	11757
Case B	10833
Case C	11290

during later part in the cycle. After performing the forward and adjoint calculations for both cases, the search direction is calculated for both cases and presented in a 3-D plot in Figures 4.9 and 4.8 to give a qualitative understanding of the differences between the two cases. The most significant difference between the two cases is higher positive values in the periphery of the core for Case C, representing the test case without depletion control. In terms of fissile enrichment control, this translates to adding more fuel in the periphery of the core whereas Case B with the depletion control suggests adding less fissile enrichment in that region. Case B also has larger negative values in the central region of the core, leading to larger removal of the fissile material in that region as compared to Case C.

To examine if this is a good recommendation for controlling the power peaking during the middle of the cycle, we perform a forward depletion run on the suggested new controls in both test cases and plot their maximum power peaking factor over the fuel cycle in Figure 4.10. The maximum power peaking factor reduces the most for Case B, with a large reduction in the power peaking factor at 9 MWd/kgHM to 1.264. This is much lower than Case C which only managed to reduce the power peaking factor at the same burnup step to 1.314. These results confirm that the control suggestions from the search direction in Case B promote better control of the power peaking factor during the depletion as compared to Case C.

We also summarize in Table 4.1 the EOC objective function of Eq. (2.10) for both test cases, which indicates a lower value of 10,833 in Case B as compared to 11,290 in Case C. This shows that the objective function is minimized together with the power peaking factor, which is the ultimate goal of the optimization. The initial and new

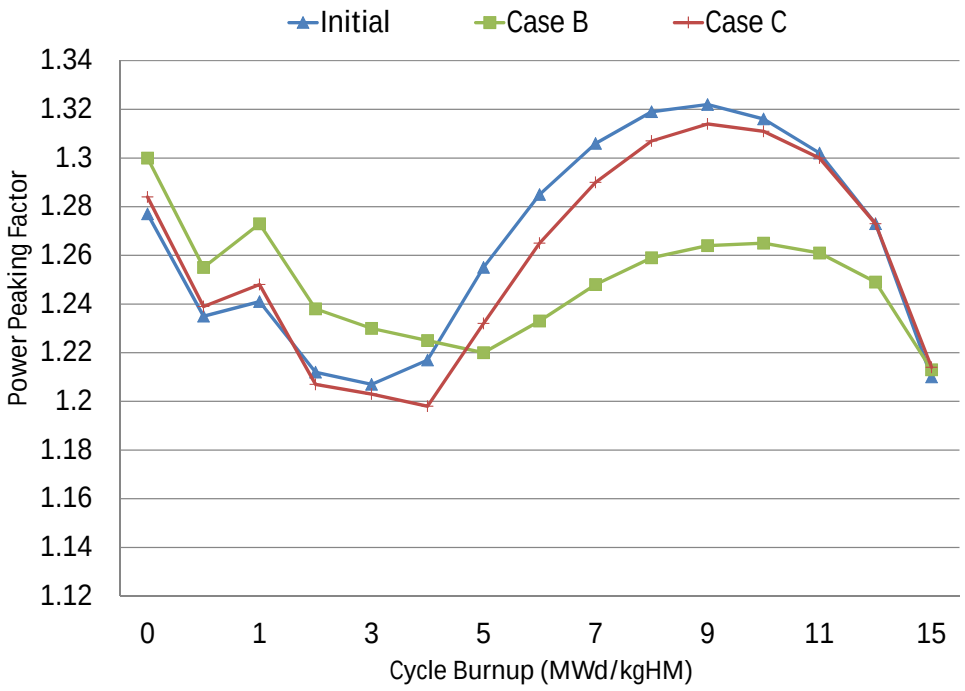

Figure 4.10: Comparison of power peaking factor Cases B and C

control loading for both test cases are presented in Figure 4.11 where we can verify that indeed less fissile enrichment was added in Case B compared to Case C in the periphery of the core, which means as a result there is less fissile material in that region for Case B. Likewise there is less fissile material in the central region of the core for Case B compared to Case C.

4.3 BP Optimal Control Problem (Case D)

We begin our multi-control optimization by disabling the fissile enrichment control and selecting the number of BP rods as the control, represented by the BP number densities to optimize the EOC burnup distribution for a flatter profile. The aim of Case D is to eventually benchmark the performance of our optimal BP control formulation with the AP600 first cycle loading. So we choose an average fissile enrichment distribution in our loading that is the same as the AP600 first cycle loading arranged in a general checkerboard distribution. We arrive at the general checkerboard distri-

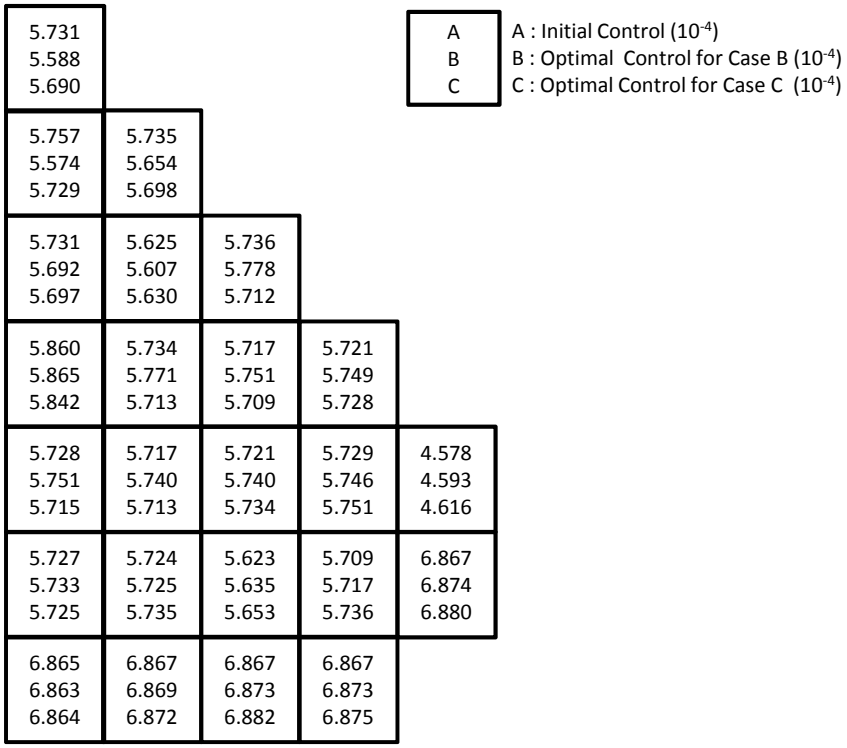

Figure 4.11: Initial and optimal fissile U^{235} number densities for Cases B and C

bution by first distributing fuel assemblies with 2.0wt% and 2.5wt% fissile enrichment in the middle part of the core with a checkerboard design. Then the remaining fuel assemblies in the periphery is loaded with 3.0wt% fissile enrichment such that the average fissile enrichment in the core is 2.5wt%, which is the same as in the AP600 first cycle loading. The reason we select a general checkerboard design for the fissile control distribution is to search the decision space for a checkerboard-like loading design, which would be comparable to the AP600 loading, which is a modified checkerboard design. As for the BP control distribution that will be optimized in this test case, we begin without any BP rods in the core, so that we begin from an unbiased initial control position. The initial fissile enrichment distribution is presented in Figure 4.12 and the EOC burnup distribution for this initial loading design is shown in Figure 4.13.

To summarize the evolution of the depletion optimization iterations for Case D,

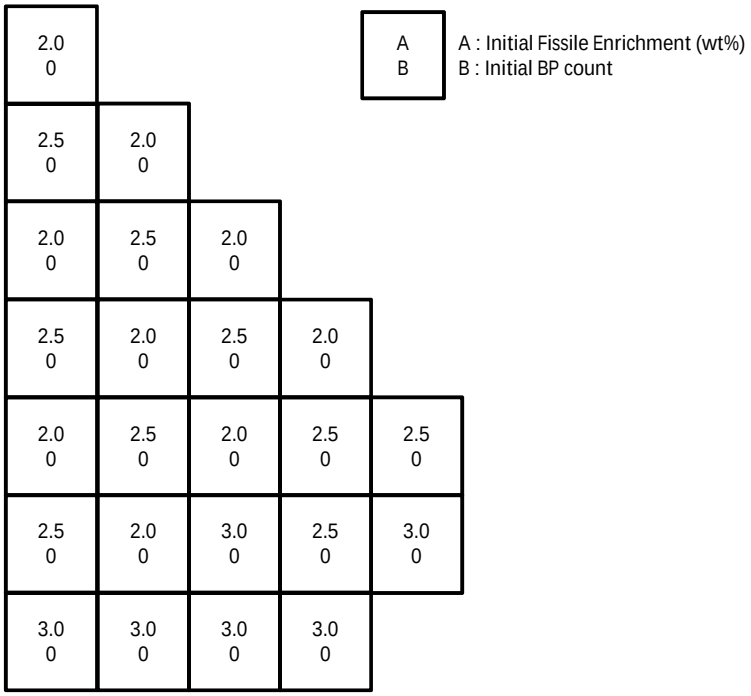

Figure 4.12: Initial controls for Case D

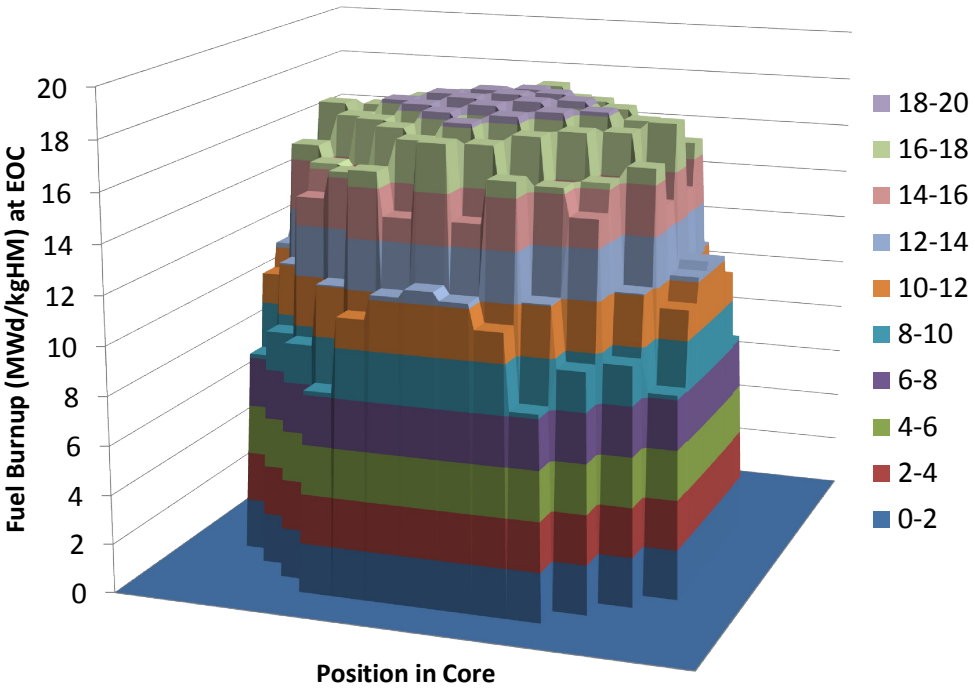

Figure 4.13: Initial fuel burnup distribution at EOC for Case D

we present in Table 4.2 the following significant results:

- maximum power peaking factor,
- EOC flat burnup objective function,
- BOC critical boron concentration,
- EOC burnup peaking factor, and
- cycle length in equivalent full power days (EFPDs).

After performing eight depletion optimization iterations, we arrived at an optimal fuel loading design in the 7^{th} iteration that satisfied the power peaking constraint of 1.3 and improved the objective function from 147 in the first iteration to 135. The cycle length also reached a maximum of 530.6 EFPDs on the optimal iteration. The optimization iterations showed a general improvement of the objective function until the 8^{th} iteration when the value started going up. This was the point where we stopped the optimization iterations as we have reached a local minimum for the objective function. Any further progress in the iterations would also point to a lower BOC critical boron value, which may not be desirable since effectively more BP rods are being added into the core. The optimal EOC burnup distribution in the 7^{th} iteration is presented in Figure 4.14 which shows a flatter profile compared with the initial burnup distribution in Figure 4.13. We note that the EOC burnup peaking factor tracks closely with the objective function in Table 4.2, although not exactly. As we would expect, the EOC burnup peaking factor is never greater than the maximum power peaking factor.

The optimal BP distribution that is obtained after the 7^{th} iteration is not readily applicable because it appears in various fractional values. For practical applications, such a control solution is not meaningful because we would need to design many fuel assemblies to closely match the various BP control fractions. Instead BP designs in

Table 4.2: Evolution of key parameters in Case D

Iteration Number	Maximum Power Peaking Factor	Objective Function	BOC Critical Boron Concentration (ppm)	EOC Burnup Peaking Factor	Cycle Length (EFPD)
1	1.261	147	1567	1.153	425.7
2	1.232	136	1549	1.154	430.0
3	1.261	142	1339	1.158	459.1
4	1.267	152	1160	1.158	486.3
5	1.235	157	1134	1.165	495.8
6	1.228	142	1088	1.158	506.6
7	1.218	135	942	1.146	530.6
8	1.275	244	827	1.190	391.5

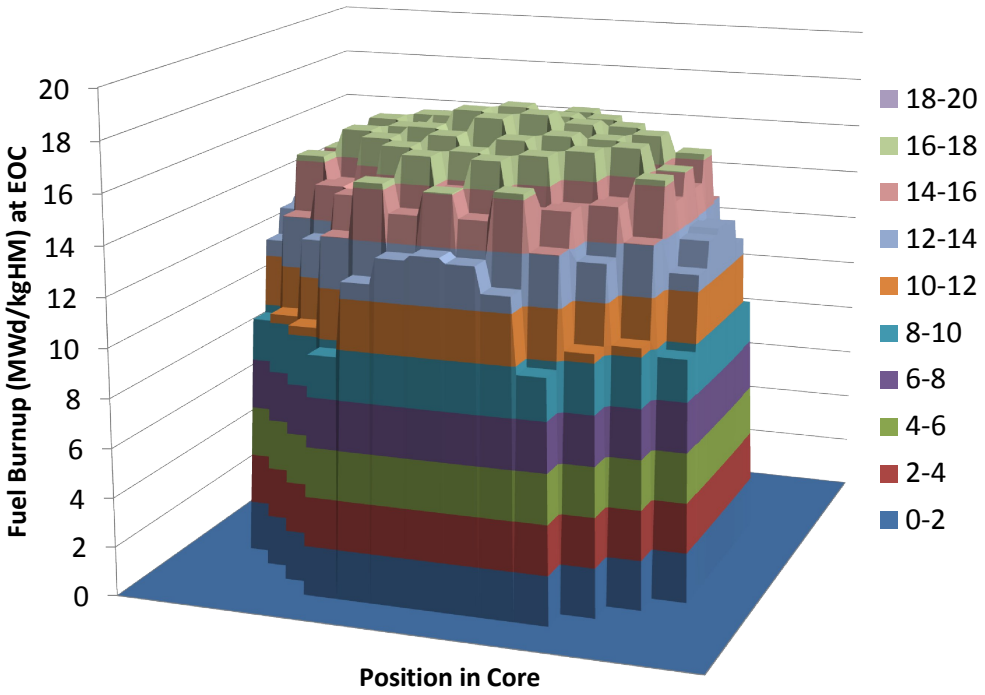

Figure 4.14: Optimal fuel burnup distribution at EOC for Case D

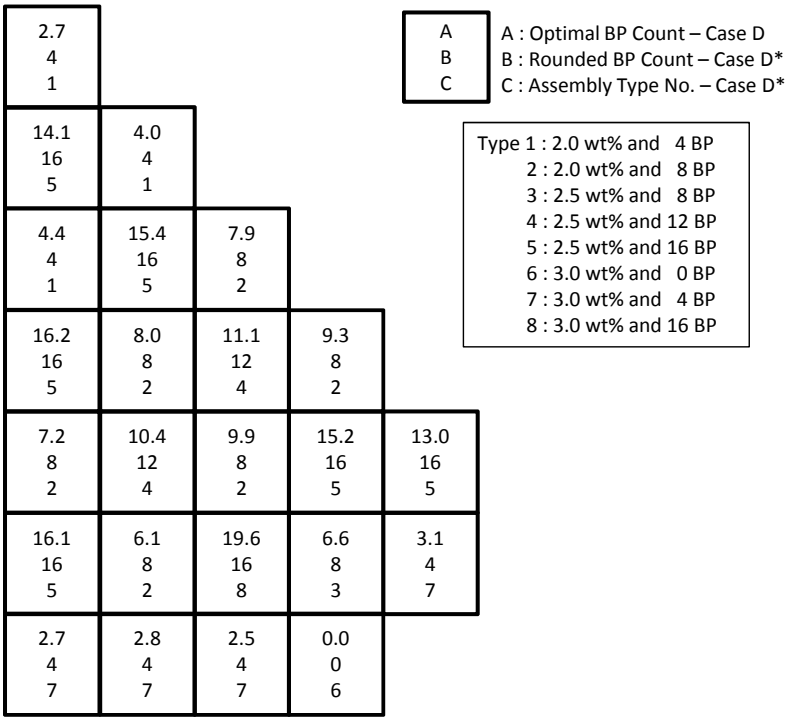

Figure 4.15: Optimal controls for Cases D and D*

fuel assemblies are created in incremental values such as 0, 4, 8 BP rods per assembly so that we minimize the number of BP designs actually manufactured. With this in mind, we round off the control solution from our optimization scheme to the nearest whole numbered BP design available and strive to use as few fuel assembly types as possible. We present our rounded off solution for the optimal BP control in Figure 4.15 with 8 types of fuel assemblies as Case D*, which is the same number of fuel type assemblies in the first cycle AP600 loading.

This rounding off is the only heuristics we applied to our optimal control selection, after we completed our optimization scheme without any heuristics. To verify our optimal control design with BP control, we simulate the fuel loading design for Case D* that has been rounded off, in the APA code using the same operating conditions that was used to benchmark the first cycle AP600 loading. The APA power peaking factor for Case D* plotted in Figure 4.16 verifies that the DMCO power peaking factor is below the desired 1.3 limit throughout the fuel cycle.

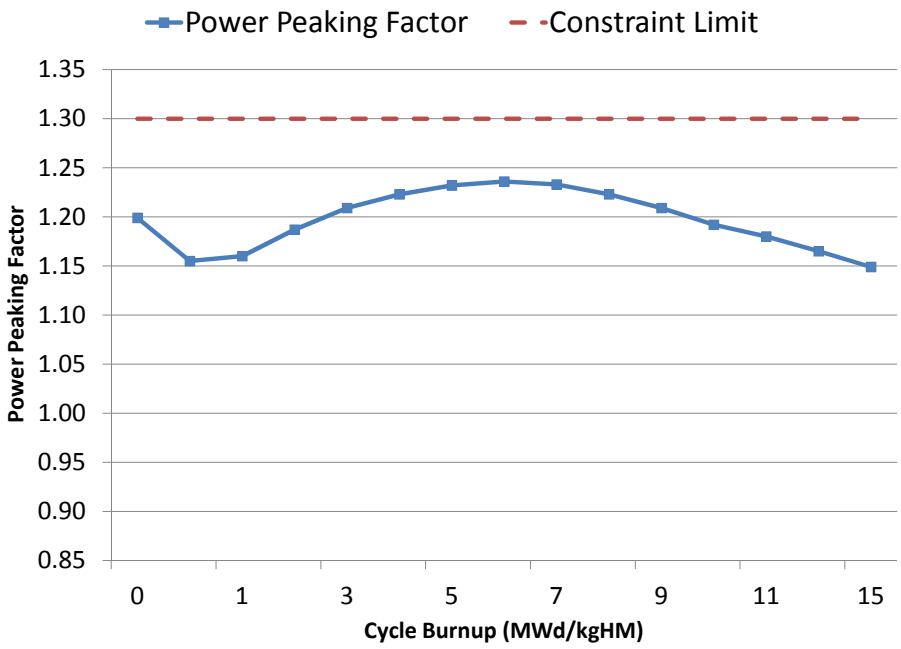

Figure 4.16: Maximum power peaking verified in APA for Case D*

4.4 Fissile Enrichment Optimal Control Problem (Case E)

We present our final Case E by selecting the fissile enrichment as the control and disabling the control for the number of BP rods. We use the same objective function as in Case D to find a flat fuel burnup profile at the EOC. For the BP control distribution in this test case, we use the rounded optimal BP controls that were obtained from Case D*. So finding the optimal fissile enrichment distribution in this test case will represent our solution for the multi-control optimization problem by developing our own BP and fissile enrichment loading design based on a general checkerboard loading pattern as the initial loading in Case D. For the initial fissile enrichment distribution, we select a flat distribution of 2.5wt% fissile enrichment. Again we emphasize our approach of starting from an unbiased control estimate like we did in Case D with a flat distribution in the control. The initial fuel loading for this test case is presented in Figure 4.17 and the initial burnup distribution at the EOC is presented in Figure 4.18.

After performing eleven depletion optimization iterations, we select the optimal

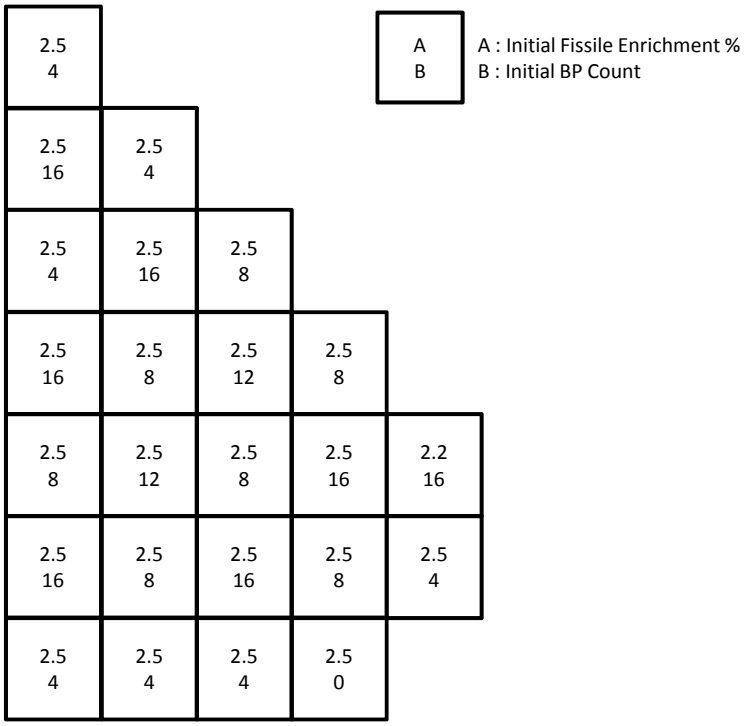

Figure 4.17: Initial fuel loading for Case E

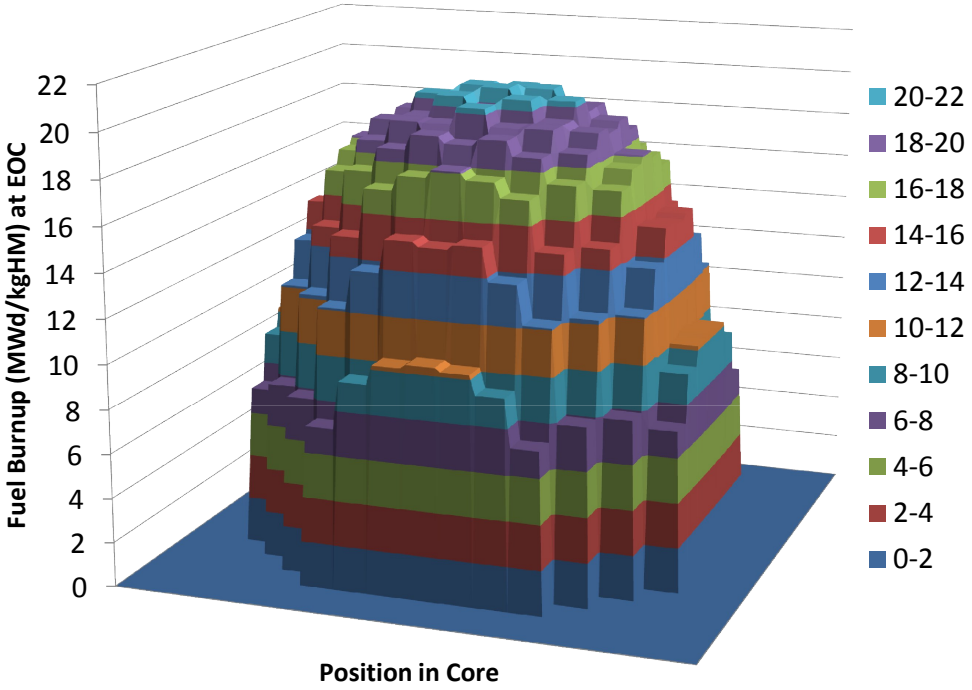

Figure 4.18: Initial fuel burnup distribution at EOC for Case E

control results on the 10^{th} iteration. A similar table as presented earlier in Case D is presented here for Case E to summarize the evolution of the depletion optimization iterations in Table 4.3. The objective function generally trended lower from a high value of 202 to 90 over ten iterations before starting to show signs of increase in the following few iterations. The cycle length on the 10^{th} iteration was also the highest value among other iterations that had an acceptable BOC critical boron concentration. For reference, the BOC critical boron concentration in the AP600 reactor is 1020 ppm and concentrations much higher than this are undesirable due to the possibility of the moderator temperature feedback turning positive. We plot the optimal EOC fuel burnup distribution in Figure 4.19 which shows a much flatter profile compared to the initial distribution of Figure 4.18.

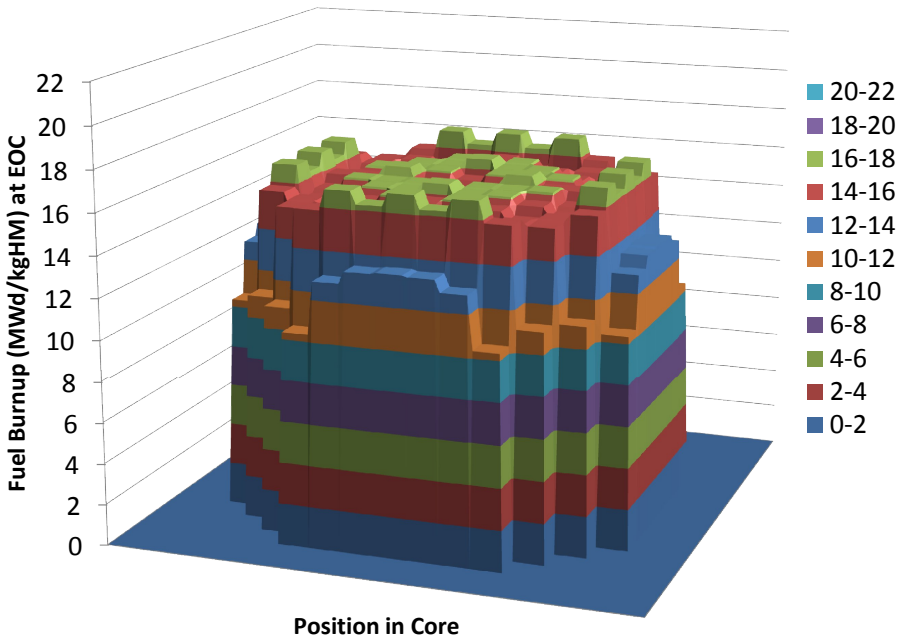

Figure 4.19: Optimal burnup distribution at EOC for Case E

The optimal fissile enrichment before and after rounding off is presented in Figure 4.20 as Cases E and E* respectively. The rounding of enrichment values was performed by matching our optimal controls in Case E with one of the three possible enrichment of 2.0wt%, 2.5wt% or 3.0wt% that are used in the AP600 reactor. During

Table 4.3: Evolution of key parameters in Case E

Iteration Number	Maximum Power Peaking Factor	Objective Function	BOC Critical Boron Concentration (ppm)	EOC Burnup Peaking Factor	Cycle Length (EFPD)
1	1.275	202	1289	1.143	653.1
2	1.274	212	629	1.148	364.1
3	1.255	181	864	1.123	504.7
4	1.175	166	850	1.136	498.8
5	1.244	141	820	1.115	484.5
6	1.234	132	692	1.174	412.4
7	1.279	93	760	1.129	454.1
8	1.241	103	972	1.113	558.5
9	1.242	128	971	1.162	558.0
10	1.251	90	971	1.110	558.3
11	1.254	119	1025	1.142	580.0

this rounding process, we also managed to match the average fissile enrichment in the rounded control design in Case E* with the AP600 value of 2.5wt%. This is done so that we can attribute any fuel cycle extension to the optimal design of the fuel loading, and not due to any difference in the fissile enrichment in the core. To verify this final fuel loading design, which represents our multi-control fuel loading design in Case E*, it was simulated in the APA code. The results showed that the power peaking constraint throughout the fuel cycle stayed below the 1.3 constraint limit as shown in Figure 4.21.

4.5 Benchmarking Test Cases

As a final exercise, we compare all the fuel loading design that we obtained in our test cases and compare them with the AP600 first cycle performance in Table 4.4. This includes the BP and fissile enrichment control problems performed in DMCO (Cases D and E), and their respective rounded BP and fissile enrichment fuel loading designs that were verified in APA (Cases D* and E*). These four cases are compared with the AP600 first cycle results obtained with the APA code.

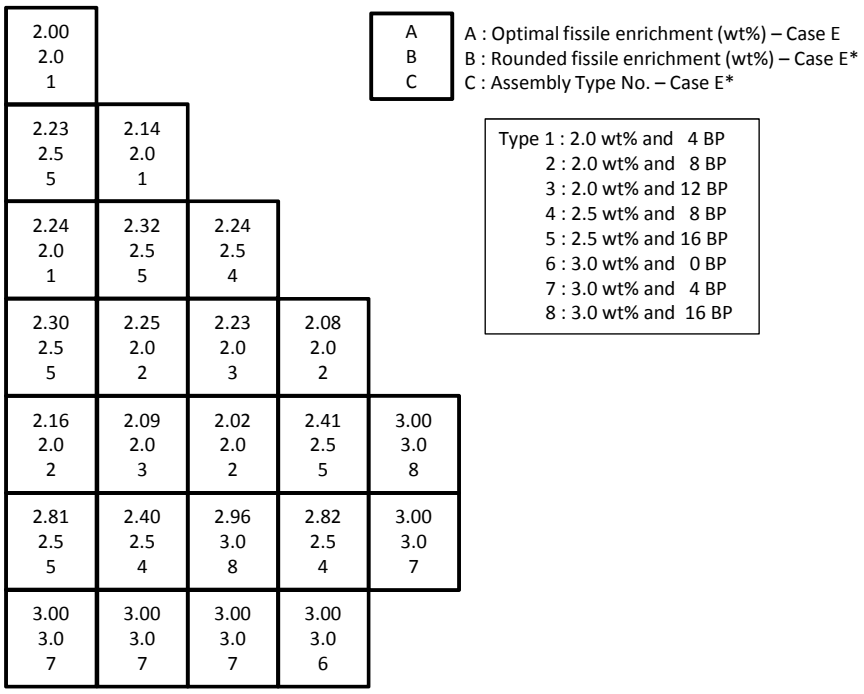

Figure 4.20: Optimal control distribution for Cases E and E*

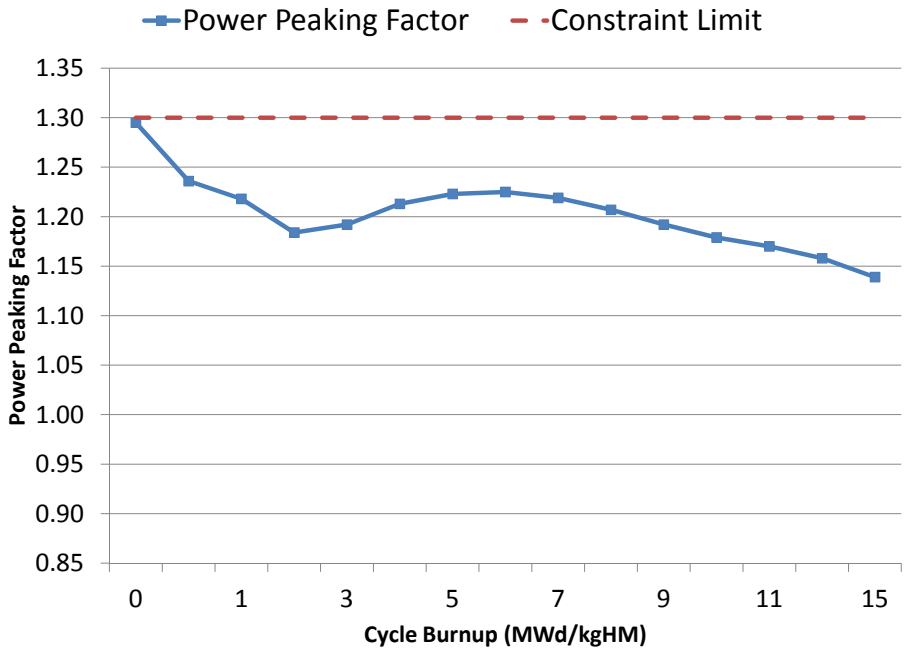

Figure 4.21: Power peaking factor verified in APA for Case E*

Table 4.4: Benchmarking test cases with AP600

	BP control		Fissile enrichment control		AP600
Test Case	D	D*	E	E*	APA
Cycle Length (EFPD)	530.6	526.7	558.3	525.2	517.4
Max Power Peaking Factor	1.218	1.210	1.251	1.295	1.294
Critical Boron Conc. (ppm)	942	934	971	932	962
Ave. Fissile Enrichment (wt%)	2.50	2.50	2.54	2.50	2.50
Total No. of BP Rods	1,269	1,332	1,332	1,332	1,424
No. of Assembly Types	N/A	8	N/A	8	8

* Controls have been rounded and simulated in APA.

Overall, the results from cases D* and E* show that our fuel loading designs for the BP and fissile enrichment control problems have longer fuel cycles than the AP600 which was the main goal in our study. We are able to extend the cycle length by 9.3 EFPDs in the fuel loading design for Case D*, and 7.8 EFPDs in the fissile enrichment control problem of case E*, which represents our final multi-control fuel loading design. Although our original optimal fuel loadings for Cases D and E had longer cycle lengths, they are not benchmarked against the AP600 result. This is because Cases D and E were not simulated in the APA code, and Case E had a higher average fissile enrichment than the AP600 design. Table 4.4 also shows that our fuel loading designs in all cases used fewer BP rods than the AP600 design, which interestingly did not result in a higher BOC critical boron concentration as would be expected with a minor exception in Case E. The configurations resulting in fewer BPs and lower BOC critical boron concentrations could be attributed to a more efficient distribution of the BP rods in our optimal designs.

CHAPTER V

Summary and Future Work

5.1 Summary of Work

The main contribution of our study is developing an overall optimization scheme that employs adjoint information through the optimality conditions derived from Lagrange multipliers and calculus of variation. Through this formulation, we are able to minimize the Hamiltonian and achieve our objective to maximize the fuel cycle length.

1. The overall structure is formulated harmoniously with the satisfaction of the inequality power peaking constraint via the direct adjoining method. The method of selecting the junction distribution developed was equally important in making it possible to use the direct adjoining method to avoid convergence problem. The role of the adjoint burnup and adjoint flux during the adjoint depletion solution was very important to propagate the desired burnup distribution from EOC to BOC to provide a means of finding the control through the optimality conditions.

2. To complete the overall optimization scheme in providing the optimal control, a key contribution in our study was to develop a Newton method approach in obtaining the optimal control in the constrained region together with the

optimal multiplication factor. Without this component, the suggested control is suboptimal because the multiplication factor is not updated with the latest adjoint information and control information from the unconstrained region. Based on the test case results, the two-region control formulation has proven to be very effective in controlling the power peaking constraint and optimizing the Hamiltonian at the same time.

3. Another significant contribution of our study is in formulating our optimality conditions with multi-controls that are more realistic in terms of number densities rather than macroscopic cross sections. Our formulation also generalizes the control variable so that either the fissile enrichment or number of BP rods could be used interchangeably within all the formulations. Our formulation has not required almost any form of approximation or assumption that may deter the use of either of the controls. The only approximation that was made was a minor one for the flux ratio by neglecting the thermal leakage. This was done for formulation convenience since the effect of the thermal leakage is almost insignificant on the effective multiplication factor.

In terms of key results, we have been successful in applying the flat burnup distribution objective for the depletion problems. Our test cases D* and E* with rounded control values achieved an extended fuel cycle of 9.3 and 7.8 EFPDs respectively compared with the AP600 first cycle performance. Power peaking constraints were satisfied in both cases. This was accomplished with fewer BP rods in the core which did not lead to an increase in BOC critical boron concentration. We recall that we arrived at our final multi-control fuel loading design in Case E* resembling a modified checkerboard design, starting from an initial general checkerboard fissile enrichment distribution and flat control estimates. The DMCO results with the UM2DB code for Cases D and E showed an even longer fuel cycle with an additional 13.2 and 40.9 EFPDs, respectively, for the BP and fissile enrichment control problem. To be

fair, Case E had a slightly higher average fissile enrichment in the core of 2.54wt% compared to 2.5wt% in the AP600 reactor, which contributed partially to the longer fuel cycle. Finally, although we were not focused on optimizing the run time of the optimization code, the estimated total CPU time for both our fissile enrichment and BP control problems with 19 iterations was 4.1 hours. This is based on an average run time of 13 minutes for each depletion optimization iteration described in Figure 2.3.

At the beginning of our study, we explored the idea of applying Newton's method as a numerical approach to solving the complete set of optimality conditions. A lot of time and effort was put into exploring this approach, but it came to an end because of two reasons. First, application of the Newton step on the control optimality condition did not produce the control which we initially thought was possible. This could have potentially resolved a big issue with the missing control variable from the control optimality condition. However, it would have involved taking a variation on the microscopic cross section, which would not be meaningful in our optimization problem. Second, we found that we could not solve the set of optimality conditions in an alternate way by using the control optimality condition to derive other system variables instead of the control variable. On the bright side of this, we are able to use the Newton method in an efficient manner for the forward system equation to provide a means of solving for the optimal control and optimal multiplication factor simultaneously in our iterative numerical approach.

5.2 Future Work

1. A natural progression of our work would be to develop fuel loading designs for either an equilibrium fuel cycle or a reload core. This would extend the application of our optimization method to different situations where both these cases may involve some form of integer programming or heuristic applications to

limit the possible selection of the fuel loading controls to the available inventory. In our study, we applied a simple heuristic application by rounding and matching our fractional optimal control solutions to arrive at fuel assembly types similar to the AP600. Our basic formulation involving a continuous form of optimization may not interface effectively with the heuristic matching of fuel assembly types. This could be a starting point for applications to the equilibrium fuel cycle or reload core by matching to only the assembly types available in the inventory. However, it may be necessary to incorporate the heuristic matching during the optimization iteration to achieve good results, but this will require care in handling the convergence of the problem whenever heuristics are applied during the optimization process.

2. Another possible future work is to extend our study to a three-dimensional optimal control problem and develop intra-assembly fuel loading designs. So instead of optimizing the location of fuel assemblies within the core with homogenized fuel assembly cross sections, the optimization is performed by controlling the positions of fuel pins and BP rods within a fuel assembly itself. The power peaking constraints would now be pin-to-pin power peaking factors instead of averaged power peaking factors in a fuel assembly. It may also make sense for this optimization problem, albeit challenging, to consider the third dimension of the problem and account for F_q which is the ratio of the power density of the pin divided by the power density of the core. The optimization code will need to be applied to the lattice physics code combined with the global code.

3. Another area of study that could be performed is to extend our sequential multi-control optimization scheme to a simultaneous multi-control optimization scheme. Modifications would need to be made on the control optimality condition as it would involve taking a vector derivative of the control vector u

on the matrix L in the δL expression in Eq. (2.27). Theoretically we may have as many control variables in the control vector and turn the problem into a 2, 3 or 4 multi-control problem. Possible additional controls could be BP boron content, or other isotopes such as plutonium or thorium which could be applied for a reload fuel cycle. In addition to a systematic way to relate the operator variation δL to various controls, secondary effects between the controls need further attention. δL needs to be evaluated for a control vector and additional equations may be required to relate the control variables to each other to avoid an underdetermined system.

4. Further work could also develop a different method of determining the junction distributions iteratively. The junction distribution search was implemented as an outer iteration in our optimization scheme, which was performed manually by selecting a scalar value representing the desired fraction of constrained and unconstrained region in the core based on the relative power. A more sophisticated approach is to bring the junction distribution search into the optimization iteration by defining a new variable for the jump locations. For example in a one-dimensional problem, the junction distributions could be represented by variables z_1, z_2, etc. This would yield additional optimality conditions due to the additional variables, that could yield a method for finding the optimal values for z_1 and z_2.

5. Finally, another proposed future work could develop methods for producing checkerboard type of loadings from completely flat fissile enrichment and BP distribution. In our study, we began from an initial loading with some form of general checkerboard design, for one control that was not active. This allowed our fuel designs to look for optimal distributions with similar checkerboard designs. It may be possible to promote a checkerboard design by developing

a new selection method of the junction distributions since the constrained regions would have a significantly different control from the unconstrained regions. Along the same lines, perhaps the bang-bang control could be used to achieve more checkerboard fuel loading designs. However, care needs to be given when applying any large stepwise change to the controls so that convergence problems does not arise during the iterations. Another option could use heuristics in a colorset fashion to assign different control values within a cluster of fuel assemblies such that the average control in that cluster is the desired control.

APPENDIX

APPENDIX A

Newton's Method

Newton's method (also known as Newton-Raphson method) is a popular tool in numerical analysis. It is a method of successively finding better solutions to the roots (or zeroes) of a function by using the slope of the function. The general idea behind Newtons method is to begin with an initial guess x_0 that is reasonably close to the true root (refer to Figure A.1). Then the function is approximated by its tangent line and the x-intercept of this tangent line is found. This x-intercept will typically be a better approximation to the function's root than the original guess, and the method is iterated upon until the true root is found.

The general formulation for Newton's method or often referred to as taking a Newton step, is represented as

$$x_{n+1} = x_n - \frac{f(x_n)}{f'(x_n)}. \tag{A.1}$$

so that x_{n+1} will be an improved root of $f(x)$.

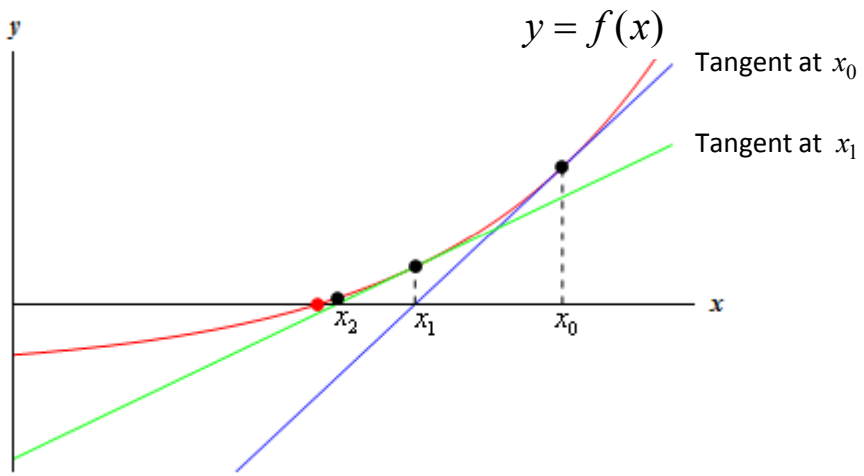

Figure A.1: Newton's Method to find the root of f(x)

In our research, the form of Newton step is in terms of δx:

$$\delta x = -\frac{f(x_n)}{f'(x_n)}. \tag{A.2}$$

BIBLIOGRAPHY

BIBLIOGRAPHY

[1] S. Levine, "In-Core Fuel Management of Four Reactor Types," in *Handbook of Nuclear Reactor Calculation*, vol. II, CRC Press, 1987.

[2] J. G. Steven, K. S. Smith, K. R. Rempe, and T. J. Downar, "Optimization of Pressurized Water Reactor Shuffling by Simulated Annealing with Heuristics," *Nucl. Sci. Eng.*, vol. 121, pp. 67–88, 1995.

[3] P. Turinsky, "Nuclear Fuel Management Optimization: A Work in Progress," *Nucl. Tech.*, vol. 110, July 2005.

[4] T. Rogers, J. Ragusa, S. Schultz, and R. S. Clair, "Optimization of PWR fuel assembly radial enrichment and burnable poison location based on adaptive simulated annealing," *Nucl. Eng. Des.*, vol. 239, pp. 1019–1029, 2009.

[5] T. K. Park, H. G. Joo, and C. H. Kim, "Multiobjective Loading Pattern Optimization by Simulated Annealing Employing Discontinuous Penalty Function and Screening Technique," *Nucl. Sci. Eng.*, vol. 162, pp. 134–147, 2009.

[6] R. Hays and P. Turinsky, "BWR in-core fuel management optimization using parallel simulated annealing in FORMOSA-B," *Prog. Nucl. Energy*, vol. 53, pp. 600–606, 2011.

[7] S. Yilmaz, K. Ivanov, and S. Levine, "Genetic Algorithm to Optimize the UO2/GD2O3 Fuel Pin Designs in a Pressurized Water Reactor," *Nucl. Tech.*, vol. 156, pp. 168–179, 2006.

[8] F. Khoshahval and A. H. Fadaei, "Application of a Hybrid Method Based on the Combination of Genetic Algorithm and Hopfield Neural Network for Burnable Poison Placement," *Annals of Nucl. Energy*, vol. 47, pp. 62–68, 2012.

[9] T. J. Kwon and J. K. Kim, "Application of a genetic algorithm for the optimization of enrichment zoning and gadolinia fuel (UO2/GD2O3) rod designs in OPR1000s," *Nucl. Eng. Tech.*, vol. 44, pp. 273–282, 2012.

[10] A. Castillo, J. J. Ortiz, J. L. Montes, and R. Perusquia, "Fuel loading and control rod patterns optimization in a BWR using tabu search," *Annals of Nucl. Energy*, vol. 34, pp. 207–212, 2007.

[11] E. F. Faria and C. Pereira, "Nuclear fuel loading pattern optimisation using a neural network," *Annals of Nucl. Energy*, vol. 30, pp. 603–613, 2003.

[12] J. J. Ortiz and I. Requena, "Using a multi-state recurrent neural network to optimize loading patters in BWRs," *Annals of Nucl. Energy*, vol. 31, pp. 789–803, 2004.

[13] A. H. Fadaei and S. Setayeshi, "LONSA as a tool for loading pattern optimization for VVER-1000 using synergy of a neural network and simulated annealing," *Annals of Nucl. Energy*, vol. 35, pp. 1968–1973, 2008.

[14] J. J. Ortiz-Servin, J. A. Castillo, and D. A. Pelta, "BWR Fuel Cycle Optimization Using Neural Networks," *Nucl. Eng. Des.*, vol. 241, pp. 3729–3735, 2011.

[15] G. Goertzel, "Minimum critical mass and flat flux," *Nucl. Energy*, vol. 2, p. 193, 1956.

[16] R. A. Axford, "Constrained Optimal Programming Problems in Reactor Statics," LA-4267, Los Alamos Scientific Laboratory, 1970.

[17] P. Goldschmidt and J. Quenon, "Minimum Critical Mass in Fast Reactors with Bounded Power Density," *Nucl. Sci. Eng.*, vol. 39, no. 3, p. 311, 1970.

[18] D. C. Wade and W. B. Terney, "Optimal Control of Nuclear Reactor Depletion," *Nucl. Sci. Eng.*, vol. 45, no. 2, pp. 199–217, 1971.

[19] R. K. Haling, "Operating Strategy for Maintaining An Optimum Power Distribution Throughout Life," in *Proc. Topl. Mtg., Nuclear Performance of Power Reactor Cores*, American Nuclear Society, 1963.

[20] R. L. Crowther, "Methods of Fuel Management Analysis - An Overview," in *Proc. Topl. Mtg., Mathematical Models and Computational Techniques for Analysis of Nuclear Systems*, American Nuclear Society, 1973.

[21] Y.-A. Chao, C.-W. Hu, and C.-A. Suo, "A Theory of Fuel Management via Backward Diffusion Calculation," *Nucl. Sci. Eng.*, vol. 93, no. 1, pp. 78–87, 1986.

[22] C. R. Drumm and J. C. Lee, "Gadolinium Burnable Absorbers Optimization by the Method of Conjugate Gradients," *Nucl. Sci. Eng.*, vol. 96, p. 17, 1987.

[23] L. S. Lasdon, A. D. Waren, and R. K. Rice, "An Interior Penalty Method for Inequality Constrained Optimal Control Problems," *IEEE Trans. Auto. Cont.*, p. 388, 1967.

[24] H. J. Kelley, "Method of Gradients on Optimization Techniques," in *Optimization Techniques with Application to Aerospace Systems* (G. Leitman, ed.), New York: Academic Press, 1962.

[25] L. M. Wu, *Optimal Burnable Loading Strategy.* PhD thesis, University of Michigan, 1990.

[26] R. T. Sorenson, *Systematic Method for Optimizing Plutonium Transmutation in LWRs*. PhD thesis, University of Michigan, 2006.

[27] D. H. Jacobson and M. M. Lele, "New Necessary Condition of Optimality for Control Problems with State-Variable Inequality Constraints," *Journal of Mathematical Analysis and Applications*, vol. 35, pp. 255–284, 1971.

[28] "AP600 Standard Safety Analysis Report," DE-AC03-90SF18495, Westinghouse Electric Company, 1992.

[29] T. Q. Nguyen, "Qualification of the PHOENIX-P/ANC Nuclear Design System for Pressurized Water Reactor Cores," WCAP-11597-A, Westinghouse Electric Company, 1988.

[30] R. F. Hartl, S. P. Sethi, and R. G. Vickson, "A Survey of the Maximum Principles for Optimal Control Problems with State Constraints," *Society for Industrial and Applied Mathematics*, vol. 37, pp. 181–218, 1995.

[31] A. E. Bryson, W. F. Denham, and S. E. Dreyfus, "Optimal Programming Problems with Inequality Constraints I: Necessary Conditions for Extremal Solution," *AIAA Journal*, vol. 1, p. 2544, 1963.

[32] D. G. Leunberger, *Optimization by Vector Space Methods*. New York: John Wiley & Sons, 1969.

[33] W. M. Stacey, "Variational Estimates and Generalized Perturbation Theory for the Ratios of Linear and Bilinear Functionals," *J. Math. Phys.*, vol. 13, no. 8, pp. 1119–1125, 1972.

[34] P. Lowdin, "On the Nonorthogonality Problem," *Adv. Quant. Chem.*, vol. 5, p. 185, 1970.

[35] W. W. Little and R. W. Hardie, "2DB - A Two-Dimensional Fast Reactor Burnup Code," *Nucl. Sci. Eng.*, vol. 32, p. 275, 1968.

[36] M. Edenius, K. Ekberg, F. B. H., and K. D., "CASMO-4, A Fuel Assembly Burnup Program, User's Manual," SOA-95/1, Studsvik, 1995.

[37] J. J. Duderstadt and L. J. Hamilton, *Nuclear Reactor Analysis*. John Wiley & Sons, 1976.

[38] E. M. Oblow, "Reactor Cross Section Sensitivity Studies Using Transport Theory," ORNL-TM-4437, Oak Ridge National Laboratory, 1974.

[39] H. Maurer, "On Optimal Control Problems with Bounded State Variables and Control Appearing Linearly," *J. Contr. and Opt.*, vol. 15, p. 3, 1977.